

**Development of a New Shock Capturing
Formula for Pressure Correction Methods**

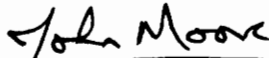
by

Ajay K. Gupta

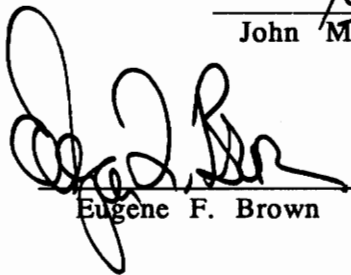
Thesis submitted to the Faculty of the
Virginia Polytechnic Institute and State University
in partial fulfillment of the requirements for the degree of

**Master of Science
in
Mechanical Engineering**

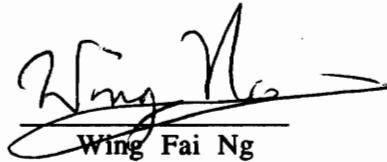
APPROVED:



John Moore, Chairman



Eugene F. Brown



Wing Fai Ng

December 1993

Blacksburg, Virginia

C.2

LD
5655
V855
1993
G867
C.2

**Development of a New Shock Capturing
Formula for Pressure Correction Methods**

by

Ajay K. Gupta

John Moore, Chairman
Mechanical Engineering

(Abstract)

Several methods have been developed to capture shock waves in turbomachinery flows, such as Moore's pressure correction procedure and Denton's time marching procedure. The time marching procedure is traditionally used for transonic flow calculations, whereas the pressure correction method is better suited for incompressible and subsonic flows. However, the focus of this research is on the Moore pressure correction flow code, the Moore Elliptical Flow Program (MEFP), to calculate shock waves in transonic compressor fans.

A new pressure interpolation method, the 2M formula, is developed to improve the shock capturing capabilities of the MEFP flow code. The 2M formula is a two Mach number dependent formula, with Mach numbers M_i and M_{i+1} . The previously used pressure interpolation method, the M&M formula, is a one Mach number dependent formula, using the maximum of M_i and M_{i+1} . In the development of the 2M formula, J.G. Moore's stability criterion is applied to the pressure correction equation such that the center point coefficient is greater than the sum of the other positive coefficients.

The 2M method is compared with the M&M formula for three test cases, 1-D flow in a converging-diverging nozzle, 2-D supersonic flow in a cascade of wedges, and choked flow in a 2-D L030-4 compressor blade row. Both formulae are tested for capturing normal shocks in the nozzle case and oblique shocks in the cascade of wedges. The flow in the L030-4 compressor cascade exhibits a weak bow shock and a strong normal shock in the passage.

In order to compare the 2M formula and the M&M formula for the nozzle case, a Fortran program is written for 1-D inviscid flow such that the solution procedure is similar to the MEFP flow code. The supersonic cascade of wedges is tested with the inviscid 3-D MEFP code, while the L030-4 compressor blade case uses the 3-D MEFP code with the full momentum equation for turbulent flow.

Acknowledgments

I owe great thanks to both Dr. John Moore and Joan Moore for their guidance throughout the whole research project. Dr. Moore did an excellent job in playing the "manager's" role, where he kept the group focused and the research moving in the right direction. I thank Joan for familiarizing me with the UNIX workstation and helping me understand and use the MEFP flow code. This research could not have been accomplished without the assistance of both Dr. Moore and Joan Moore. I would also like to thank my committee members, Dr. Eugene F. Brown and Dr. Wing Ng, for their participation in this work. Special thanks is due to Rolls-Royce for sponsoring this research. Finally, I would like to thank my family and friends, particularly the close friends made at Clemson and Virginia Tech, for all of their support in helping me achieve my goals.

TABLE OF CONTENTS

	<u>page#</u>
1.0 Introduction	1
2.0 Literature Review	5
2.1 Pressure Correction Methods	5
2.2 Shock Capturing Methods	8
3.0 Summary of 1-D version of MEFP	17
4.0 Development of New Shock Capturing Formula	21
4.1 Stability Analysis for a_0 and a_1 coefficients	26
4.2 Summary of Stability Equations	36
5.0 Normal Shock Capturing in a 1-D Nozzle	52
6.0 Oblique Shock Capturing in a Cascade of Wedges	70
7.0 L030-4 Compressor Blade	93
8.0 Conclusions	97
Appendix A. Denton's Pressure-Density Schemes	100
Appendix B. Truncation Error of Pressure Interpolation Equation	103
Appendix C. Moore and Moore Pressure Interpolation Schemes	104
Appendix D. 1-D Fortran version of the MEFP code	105
REFERENCES	116
Vita	117

List of Figures

	<u>page#</u>
Fig. 1.1 CFD's relation with pure experiment and pure theory	2
Fig. 2.1a Denton's control volume i to $i+1$, density change sent downwind	9
Fig. 2.1b Moore/Moore's control volume i to $i+1$, pressure change sent upwind	9
Fig. 2.2 Denton's calculation of Effective Pressure	12
Fig. 2.3 M&M Mach number dependent values for a_0 , a_1 and a_2	15
Fig. 3.1 1-D Converging-Diverging Nozzle	18
Fig. 4.1 $A=0$ from equation 21, where $A=f(M_i, M_{i+1})$	27
Fig. 4.2 $B=0$ from equation 28, where $B=f(M_i, M_{i+1})$	31
Fig. 4.3 $A=0$ curve, $B=0$ curve, $M_{i+1} = M_i$, and $M_{i+1} = \text{normal shock}(M_i)$	32
Fig. 4.4 Stability Limits for a_0 with $M_{i+1} = M_i$, Equations 22 & 29	38
Fig. 4.5 Stability Limit for a_1 with $M_{i+1} = M_i$, Equation 30	39
Fig. 4.6 a_{0i+1} with $M_i > M_{i+1}$ (Deceleration), Equation 29	41
Fig. 4.7 a_{0i+1} with $M_{i+1} > M_i$ (Acceleration), Equation 29	42
Fig. 4.8 a_{0i+1} with $M_{i+1} = \text{normal shock}(M_i)$, Equations 22, 29 and previous one Mach number limit	43
Fig. 4.9 $A > 0$ a_{1i+1} with $M_i > M_{i+1}$ (Deceleration), Equation 30	44
Fig. 4.10 $A > 0$ a_{1i+1} with $M_{i+1} > M_i$ (Acceleration), Equation 30	45
Fig. 4.11 $A < 0$ a_1 with $M_{i+1} = \text{normal shock}(M_i)$, Equations 23, 33 & 35	47
Fig. 4.12 a_0 & a_1 limits with $M_i = M_{i+1}$	48
Fig. 4.13 a_0 & a_1 limits with $M_{i+1} = \text{normal shock}(M_i)$	50
Fig. 4.14 Implementation of the 2M formula for 3-D flows	51
Fig. 5.1 1-D Converging-Diverging Nozzle	53

Fig. 5.2a	Theoretical Mach numbers versus nozzle position for $P_{\text{exit}}/P_{\text{to}} = 0.85, 0.80, \text{ and } 0.75$	55
Fig. 5.2b	Theoretical P/P_{to} versus nozzle position for $P_{\text{exit}}/P_{\text{to}} = 0.85, 0.80, \text{ and } 0.75$	56
Fig. 5.2c	Theoretical P_t/P_{to} versus nozzle position for $P_{\text{exit}}/P_{\text{to}} = 0.85, 0.80, \text{ and } 0.75$	57
Fig. 5.3a	2M formula Mach numbers versus nozzle position for $P_{\text{exit}}/P_{\text{to}} = 0.85, 0.80, \text{ and } 0.75$	58
Fig. 5.3b	2M formula P/P_{to} versus nozzle position for $P_{\text{exit}}/P_{\text{to}} = 0.85, 0.80, \text{ and } 0.75$	59
Fig. 5.3c	2M formula P_t/P_{to} versus nozzle position for $P_{\text{exit}}/P_{\text{to}} = 0.85, 0.80, \text{ and } 0.75$	60
Fig. 5.4	$M_{\text{shock}} = 1.1, P_{\text{exit}}/P_{\text{to}} = 0.86687$	62
Fig. 5.5	$M_{\text{shock}} = 1.267, P_{\text{exit}}/P_{\text{to}} = 0.85$	63
Fig. 5.6	$M_{\text{shock}} = 1.455, P_{\text{exit}}/P_{\text{to}} = 0.80$	64
Fig. 5.7	$M_{\text{shock}} = 1.578, P_{\text{exit}}/P_{\text{to}} = 0.75$	65
Fig. 5.8	$M_{\text{shock}} = 2.5, P_{\text{exit}}/P_{\text{to}} = 0.47101$	66
Fig. 5.9	$M_{\text{shock}} = 3.5, P_{\text{exit}}/P_{\text{to}} = 0.20285$	67
Fig. 6.1	Denton's Cascade of Wedges	71
Fig. 6.2	Full 43 x 22 grid	73
Fig. 6.3a	Enlarged oblique shocks region for 43 x 22 and 82 x 22 grids	75
Fig. 6.3b	Enlarged oblique shocks region for 82 x 42 and 123 x 42 grids	76
Fig. 6.4a	Mach number and P_t/P_{to} contours for 43 x 22 grid	77
Fig. 6.4b	Mach number and P_t/P_{to} contours for 82 x 22 grid	78
Fig. 6.4c	Mach number and P_t/P_{to} contours for 82 x 42 grid	79
Fig. 6.4d	Mach number and P_t/P_{to} contours for 123 x 42 grid	80
Fig. 6.5a	Repeating Boundary Mach number and P_t/P_{to} for 43 x 22 grid	82
Fig. 6.5b	Repeating Boundary Mach number and P_t/P_{to} for 82 x 22 grid	83
Fig. 6.5c	Repeating Boundary Mach number and P_t/P_{to} for 82 x 42 grid	84

Fig. 6.5d	Repeating Boundary Mach number and P_t/P_{t0} for 123 x 42 grid.	85
Fig. 6.6	Mass averaged P_t/P_{t0} in flow direction	87
Fig. 6.7	Comparison of a_0 at the repeating boundary calculated from .. M&M and 2M formulae for 82 x 22 grid	89
Fig. 6.8	m and dm/m versus iteration number	90
Fig. 6.9	p -max and p -rms changes versus iteration number.....	91
Fig. 6.10	u -max and u -rms changes versus iteration number	92
Fig. 7.1	74 x 23 grid for L030-4 compressor blade	94
Fig. 7.2	Mach number contours using 2M and M&M formulae	95
Fig. 7.3	Perfect gas comparison ($P/\rho RT$) of 2M and M&M formulae	96

Nomenclature

a_0, a_1, a_2	coefficients of pressure interpolation equation
A	area
A, B	variables defined for stability analysis of a_0, a_1 and a_2
c	speed of sound
CFP_i	pressure correction factor
ρ	density
ρ_{eff}	effective density
i	grid index in flow direction
M	Mach number
m	mass flowrate
dm	change in mass flowrate
$m_{e,i}, m_{error,i}$	continuity error
p, P	static pressure
P_{eff}	effective pressure
P_{exit}	exit pressure
P_t	total pressure
P_{to}	inlet total pressure
R	ideal gas constant
T	static temperature
δt	time step
u, U	x component of velocity vector
\underline{u}	velocity vector
δV	change in volume

α	constant to adjust effective pressure in region of high gradients
δ	small change
γ	ratio of specific heat capacities
μ	sum of the laminar and turbulent viscosities

1.0 Introduction

Computational Fluid Dynamics (CFD) codes have contributed significantly to the area of fluid dynamics for the past 25 years. These codes are used as powerful tools in predicting and analyzing fluid flows for engineering design. Today, computational fluid dynamics is viewed as a third dimension of fluid dynamics with pure experiment and pure theory as the other two dimensions, shown in Fig. 1.1 [1]. CFD codes basically provide a numerical description of the fluid flow of interest by solving governing equations of three fundamental principles: (1) conservation of mass; (2) Newton's second law (momentum); and (3) conservation of energy [1].

Turbomachinery and aerospace related industries use CFD codes to predict and analyze fluid flows over airfoils, around fuselages, and within components of a gas turbine engine. Wendt [1] describes some specific applications of CFD codes such as: (1) analyzing shock waves for flow fields over the space shuttle; (2) calculating unsteady, oscillating flows through supersonic engine inlets; (3) predicting the flow field over an automobile towing a trailer; and (4) studying flows through supersonic combustion ramjet engines. Thus, CFD codes are used in a variety of situations to predict flow phenomena such as shock waves, expansions, wakes or vortices in the fluid flow.

The work in this thesis focuses mainly on the finite volume approach, particularly the time marching and pressure correction methods, for solving the fundamental flow equations. Both of these finite volume methods are described in section 2.2. Typically, the time marching procedure is traditionally used for transonic flow calculations, whereas the pressure

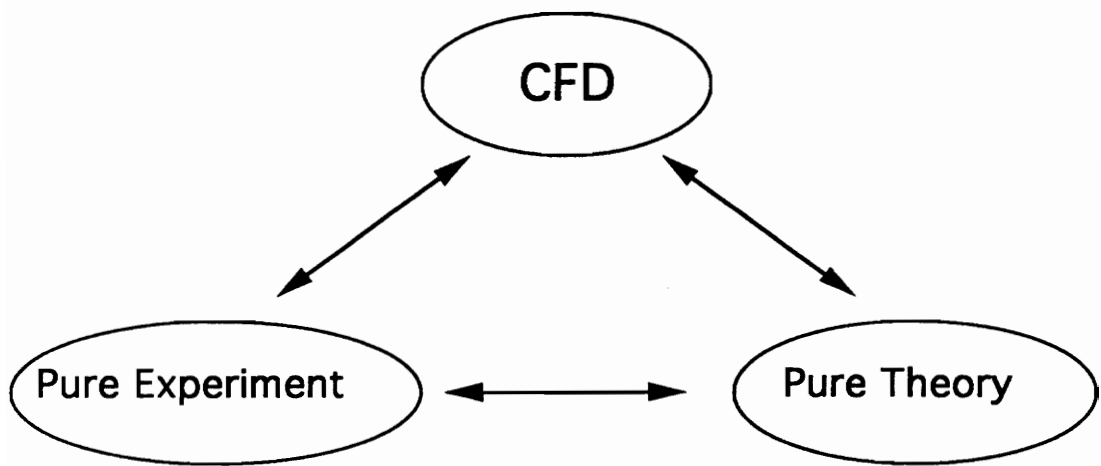


Fig. 1.1 The relationship of computation fluid dynamics with pure experiment and pure theory (1)

correction method is better suited for incompressible and subsonic flows [2]. However, the work presented here uses a pressure correction code to study flows in transonic fans.

The primary objective of this research is to demonstrate and improve the shock capturing capability of the Moore pressure correction flow code [3], Moore Elliptical Flow Program (MEFP). An application of this flow code is to analyze flows, specifically with shock waves, in transonic fans for several blade geometries. In order to calculate shock waves properly, special attention is placed on the shock location, losses, and sharpness. Along with shock capturing improvements, the new version of the MEFP code is tested.

A new shock capturing method, the 2M formula, is developed using a two Mach number dependent pressure interpolation formula, with Mach numbers M_i and M_{i+1} . The previously used pressure interpolation method, the M&M formula [3], is dependent on one Mach number, the maximum Mach number of M_i and M_{i+1} . This 2M formula, implemented in the MEFP code, is then tested on a 1-D converging-diverging nozzle (section 5.0), a 2-D cascade of wedges (section 6.0), and a 2-D L030-4 compressor blade (section 7.0). The 1-D nozzle test has subsonic flow in the inlet, choked flow of $M=1$ at the throat, and a normal shock wave in the diverging part of the nozzle. The cascade of wedges is a 2-D test where a supersonic flow of $M=1.6$ produces an oblique shock off the leading edge, a reflected second oblique shock, a Prandtl-Meyer expansion region, and a third oblique shock off the trailing edge of the blade. The L030 compressor blade is tested to study shock capturing and the stagnation region near the round leading edge, where large changes in Mach number occur in very few grid steps. For each test case, the results from the 2M method are compared with the previously used M&M formula. The

development and stability analysis of the 2M pressure interpolation method is described in section 4.0.

2.0 Literature Review

Since the focus of this research is improving shock capturing using a pressure interpolation procedure, a fundamental understanding of both pressure correction methods and shock capturing methods is necessary. The advantages and types of pressure correction methods are described in section 2.1. Section 2.2 then reviews two types of shock capturing methods, Denton's density update time marching procedure [4] and Moore and Moore's pressure correction procedure [3].

2.1 Pressure Correction Methods

In pressure correction methods [5], the pressure is calculated from the continuity equation and the ideal gas equation gives the density. Whereas, for time marching methods, the density is found from the unsteady continuity equation and the ideal gas equation gives the pressure. Pressure correction methods are considered to be efficient, accurate, and flexible. They require few iterations for low Mach number flows and can handle highly non-uniform grid spacing, both orthogonal and non-orthogonal. In addition, a wide range of cell aspect ratios can be used, thus allowing very complex geometries to be analyzed. Even though pressure correction methods are better suited for incompressible and subsonic flows, they are still very accurate in analyzing both incompressible and compressible flows for all Mach numbers. The compressible flow calculations however, require more iterations than incompressible flows to converge towards a solution.

There are three traditional pressure correction methods [5], which include parabolic, elliptic, and partially parabolic. The parabolic calculation procedure, the most limited of the three methods, is a one-pass space marching calculation where the pressure distribution in the primary flow direction is known to within a 1-D correction. This method is suitable for subsonic flows with no back flow. In contrast, the elliptic method, the most general of the three, can handle subsonic flow including back flow. The elliptic method calculates the velocity and pressure using the full 3-D solution of the momentum and pressure correction equations. The partially parabolic method, a combination of the other two, is a one-pass space marching calculation such that only the pressure is evaluated using the full 3-D pressure correction equation. This method can handle subsonic flows, however back flows are not possible.

These traditional pressure correction methods are basically limited to subsonic flows and need to be modified in order to solve transonic and supersonic flow problems. In the MEFP code, a transonic pressure correction procedure is used for shock capturing. This transonic method calculates the velocity and pressure using the full 3-D momentum and pressure correction equations, just as the elliptic method does. Several test cases for all four of these pressure correction methods are described in reference [5].

The equations used in the MEFP code for steady viscous compressible flow are shown below.

$$\text{continuity,} \quad \nabla \cdot \rho \underline{u} = 0 \quad (1)$$

$$\text{momentum,} \quad \rho \underline{u} \cdot \nabla \underline{u} - \nabla \cdot \mu \nabla \underline{u} = \nabla \cdot \mu \overline{\nabla \underline{u}}^T - \nabla p \quad (2)$$

$$\text{and equation of state,} \quad p = \rho RT \quad (3)$$

The 1-D converging-diverging nozzle and cascade of wedges tests use the inviscid part of the momentum equations. However, the L030-4 compressor blade case uses the full momentum equation with μ as the sum of the laminar and turbulent viscosities.

The basis of pressure correction methods is to turn the continuity equation into a pressure correction equation. This transformation involves satisfying the continuity equation with a current velocity, \underline{u} , and a correction to the velocity field, $\delta\underline{u}$, as shown in equation 4.

$$\nabla \cdot \rho(\underline{u} + \delta\underline{u}) = 0 \quad (4)$$

The correction to the velocity field is related to the pressure correction distribution, δp , through a momentum correction equation.

$$C \delta\underline{u} = -\nabla p \quad (5)$$

The coefficient C is usually taken from the full discretized momentum equations. For example, it might be the local mass flowrate per unit area divided by the grid spacing, $\rho u / \Delta x$. Combining equations 4 and 5 transforms the continuity equation into a pressure correction equation.

$$\nabla \cdot (\rho/C) \nabla p = -\nabla \cdot \rho \underline{u} = \text{continuity error} \quad (6)$$

2.2 Shock Capturing Methods

Several CFD methods have been developed in order to capture shock waves. Two of these codes are discussed here in detail: Denton's density update time marching method [4] and Moore and Moore's pressure correction method [3]. The main differences in the two codes are the sequence in which flow properties are updated and the direction in which the flow property changes are taken, either to the upstream node or downstream node. An outline of the two procedures is given below.

Density Update Time Marching Method

1. the density is updated from the continuity error and the density change is sent to the downstream node, $i+1$, as in Fig. 2.1a
2. the pressure is updated from the new density using the ideal gas equation
3. an effective pressure is calculated using an interpolation scheme with the new pressures
4. the velocity is updated from the momentum equation using the new effective pressure

Pressure Correction Method

1. the pressure is updated from the continuity error and the pressure change is sent to the upstream node, i , as in Fig 2.1b
2. the velocity is updated from the momentum equation using the new pressure

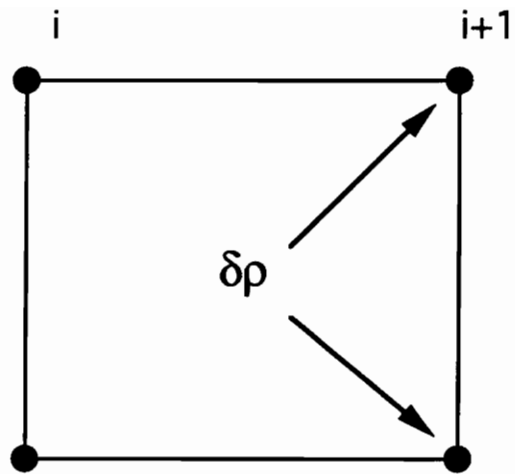


Fig. 2.1a Denton's control volume i to $i+1$, density change sent downwind

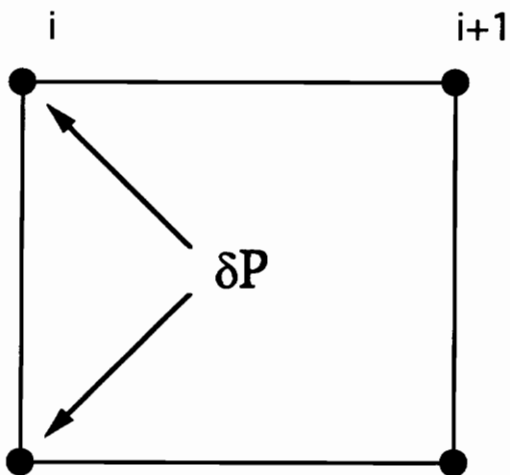


Fig. 2.1b Moore and Moore's control volume i to $i+1$, pressure change sent upwind

Fig. 2.1 Control volumes for Shock Capturing Methods

3. an effective pressure is calculated using an interpolation procedure with the new pressures
4. an effective density is updated from the new effective pressure using the ideal gas equation

For both methods, the direction of the property changes and the order in which the flow properties are updated are critical to maintaining stability in the code. Each code will now be discussed in further detail.

Density Update Time Marching Method

In Denton's [4] time marching code, the density change is sent to the downstream node as shown in Fig. 2.1a such that

$$\delta\rho_{i+1} = m_{e,i}\delta t/\delta V \quad (1)$$

where the continuity error, $m_{e,i}$, is calculated as

$$m_{e,i} = \rho_i u_i A_i - \rho_{i+1} u_{i+1} A_{i+1} \quad (2)$$

The pressure is then calculated from the ideal gas equation using the new density. For stability purposes, a correction factor, CFP_i , is used to correct the downwinded pressure to a value closer to the true pressure, P_i , as in equation 3. This correction factor is basically an approximation to the pressure difference between points i and $i+1$, thus the pressure used in the momentum equation is an approximation to the true pressure. An exact pressure difference using the true pressures would induce unstable results. It

should be noted that the pressure is the only flow property evaluated at the upstream point, i .

$$P_{eff,i} = P_{i+1} + CFP_i \quad (3)$$

Denton uses two methods to calculate the pressure correction factor, shown in Fig. 2.2 [6]. The first method, equation 4, is a simple average of the pressures at node points $i-1$ and $i+1$. Equation 5 is an alternate method where a parabolic interpolation is used on the pressures at node points $i-1$ and $i+2$.

$$CFP_i = \alpha(P_{i-1} - P_{i+1})/2 \quad (4)$$

$$\text{or} \quad CFP_i = \alpha(P_{i-1} - P_{i+2})/3 \quad (5)$$

Both correction factors, equations 4 and 5, are second order accurate when $\alpha = 1$ and first order accurate when $\alpha < 1$. It is desirable to make the value of α slightly lower than 1 to introduce numerical damping to the solution. This damping, with α typically between 0.8 to 0.9, is an attempt to reduce overshoots and undershoots across shock waves.

An alternative method is to calculate α based on the density gradient as in equation 6; however, this evaluation of α can only be used during an increase in density. Using equation 6, α will automatically decrease across a shock wave, i.e. sufficient damping will be introduced to the solution.

$$\alpha = 1 - (\rho_{i+1} - \rho_{i-1})/\rho_i \quad (6)$$

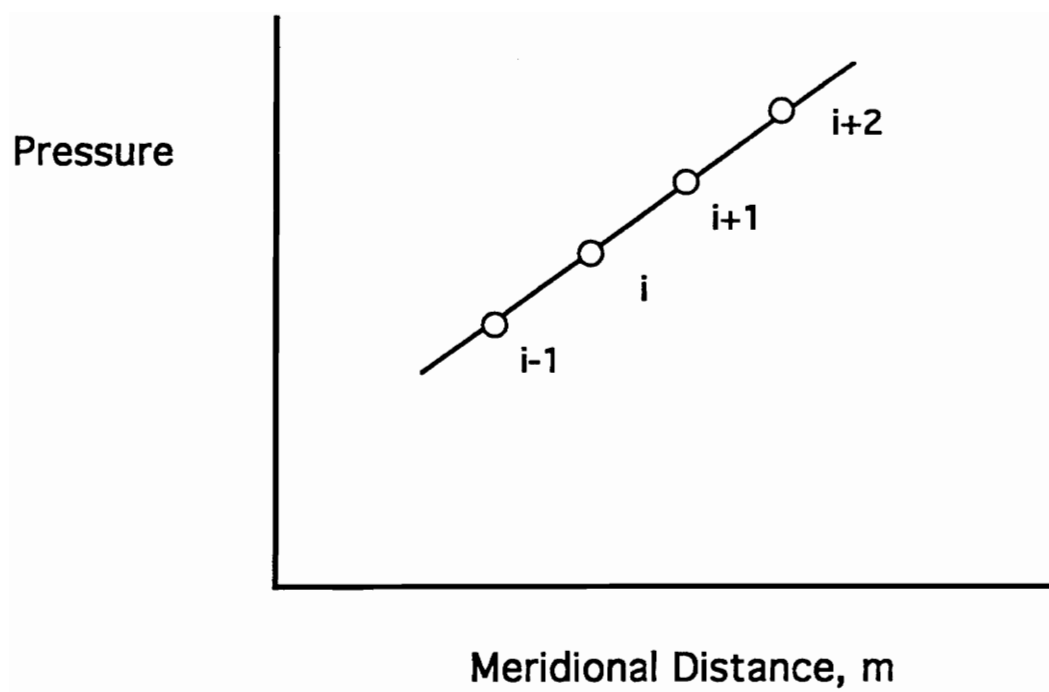


Fig. 2.2 Denton's Calculation of Effective Pressure [6]

Denton attempted several other pressure-density relationship schemes before developing his present time marching code. These pressure-density relations are briefly described in Appendix A. The main differences in the schemes are basically which direction the density change is taken and how the pressure is corrected. Scheme A is stable for supersonic flows, whereas scheme B is stable for subsonic flows and reverse flows. Combining these two methods, a discontinuity occurs in the solution around the transonic region, Mach = 1. Thus, a single method is desired which is stable for all Mach numbers and has good shock capturing capabilities.

Pressure Correction Method

In the pressure correction method, Moore and Moore [3] send the pressure change to the upstream node, as shown in Fig. 2.1b. Expressed in terms of an explicit pressure correction procedure [7],

$$\delta P_i = (m_{e,i} \delta t) R T_i / \delta V \quad (7)$$

Again, a correction factor is used to evaluate an effective pressure. The one point inconsistency in equation 8 is to assure stability.

$$P_{eff,i+1} = P_i + CFP_{i+1} \quad (8)$$

The pressure correction factor is calculated as

$$CFP_{i+1} = a_0(P_{i+1} - P_i) + a_1(P_{i+1} - P_{i-1})/2 + a_2(P_{i+1} - P_{i-2})/3 \quad (9)$$

where the interpolation equation (9) is second order accurate when $a_0 + a_1 + a_2 = 1$ (Appendix B). The Mach number dependent interpolation equations for a_0 , a_1 and a_2 are given below, such that the maximum Mach number of M_i and M_{i+1} is used. Equations 10 and 11, graphed in Fig. 2.3 [3], were chosen and are lower than the actual limiting stability criteria.

$$\text{For } M \leq 2.0 \quad (10)$$

$$a_0 = (0.8/3)(4/M^2 - 1)$$

$$a_1 = 1.0 - a_0$$

$$a_2 = 0.$$

$$\text{For } M > 2.0 \quad (11)$$

$$a_0 = 0.$$

$$a_1 = 4/M^2$$

$$a_2 = 1.0 - a_1$$

These Mach number dependent equations are referred to as the M&M formula [3]. Appendix C describes several other pressure interpolation attempts by Moore and Moore.

The density at node point $i+1$ can now be calculated with the new effective pressure at point $i+1$.

$$\rho_{i+1} = P_{\text{eff},i+1}/RT_{i+1} \quad (12)$$

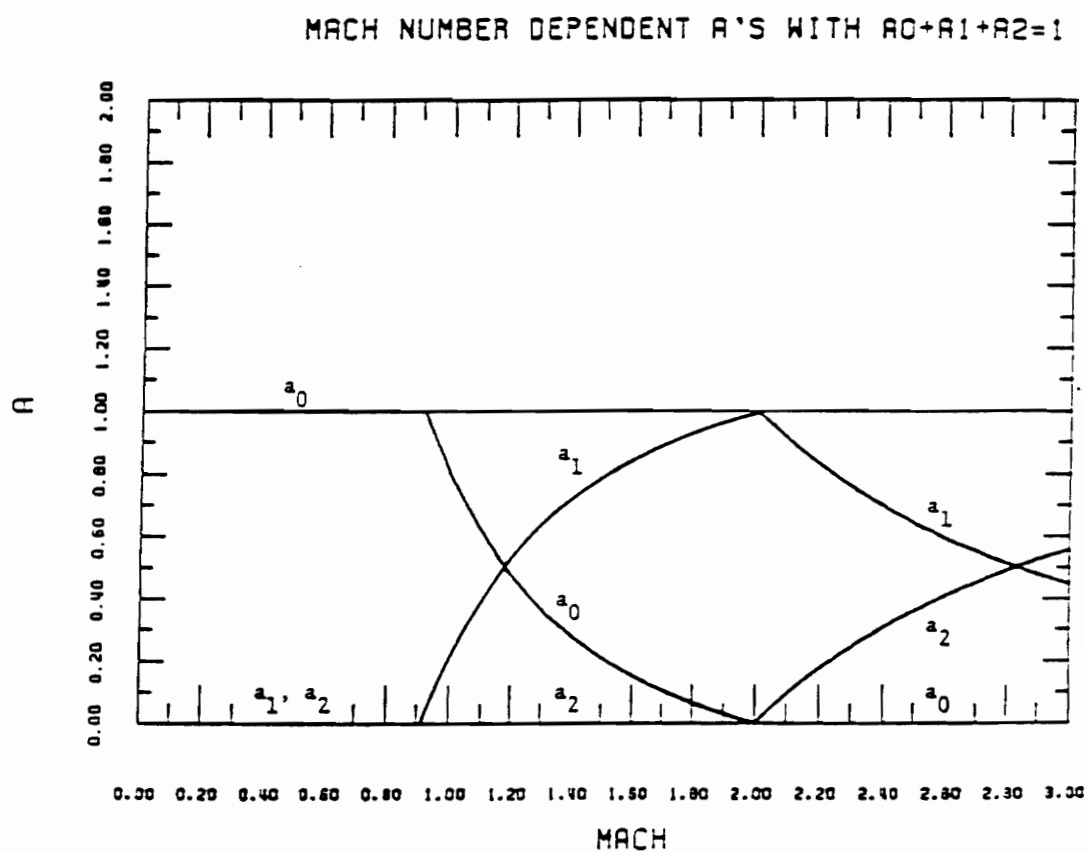


Fig. 2.3 M&M Mach number dependent values (equations 10 & 11) for the coefficients in equation 9, a_0 , a_1 , and a_2 [3]

Density Correction Method

Moore, J.G. [7] also developed a density correction method, such that the solution procedure is similar to the pressure correction method. However, the density correction method calculates an effective density instead of an effective pressure. For this method, the pressure at i is found using an upwind effective density.

$$P_i = \rho_{\text{eff},i} R T_i \quad (13)$$

The effective density is calculated as

$$\rho_{\text{eff},i} = \rho_{i+1} + a_0(\rho_i - \rho_{i+1}) + a_1(\rho_i - \rho_{i+2})/2 + a_2(\rho_i - \rho_{i+3})/3 \quad (14)$$

The coefficients a_0 , a_1 and a_2 are different from the ones used for the pressure correction method, but again the equation is second order accurate when $a_0 + a_1 + a_2 = 1$.

3.0 Summary of 1-D version of MEFP

In order to test the 2M formula on a 1-D converging-diverging nozzle, a Fortran program is written such that the solution procedure is similar to the MEFP transonic calculation method. Figure 3.1 shows the nozzle geometry and the grid in the flow direction, i. For this nozzle example, both pressure interpolation methods are used, the 2M formula and the M&M formula. Section 5.0 compares the results from both methods with theoretical values. The full procedure of this 1-D Fortran program, including the main equations used (written in Fortran coding), is provided in Appendix D.

The MEFP solution procedure basically satisfies the continuity and momentum equations using a perfect gas assumption with constant total temperature.

$$\text{continuity,} \quad \nabla \cdot \rho \underline{u} = 0 \quad (1)$$

$$\text{momentum,} \quad \rho \underline{u} \cdot \nabla \underline{u} = - \nabla p \quad (2)$$

When discretized in 1-D over a grid step from $i-1$ to i , equations 1 and 2 are expressed as the following.

$$\text{continuity,} \quad (\rho u A)_i - (\rho u A)_{i-1} = 0 \quad (3)$$

$$\text{momentum,} \quad (\rho u)_{i-1/2} (u_i - u_{i-1}) = - (p_i - p_{i-1}) \quad (4)$$

Summary of Solution Procedure

The input parameters for the Fortran code include a nozzle back pressure and Mach numbers to set up the nozzle geometry and grid. The areas along the nozzle are determined directly from isentropic relations and the

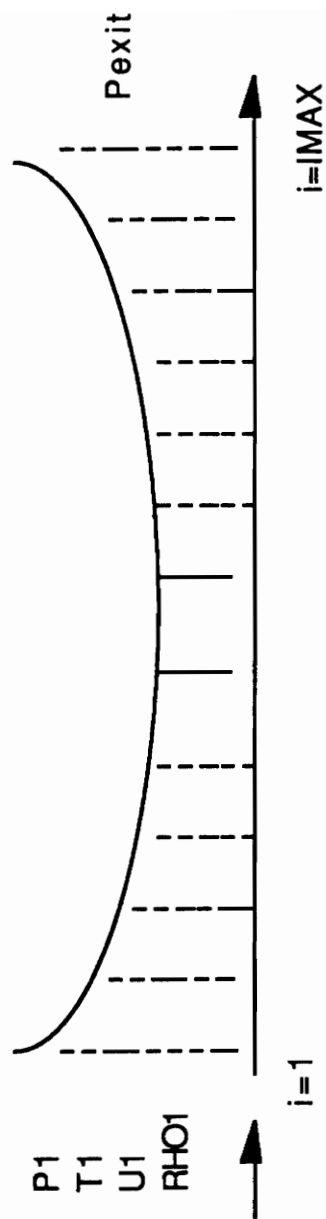


Fig. 3.1 1-D Converging-Diverging Nozzle

specified Mach numbers. Pressure, temperature, and velocity values at the nozzle inlet and exit are initialized using isentropic relations, except for the exit pressure which is specified. A linear relationship is then used to initialize the values along the nozzle. Density is calculated with the ideal gas equation. After initializing the variables, the solution procedure is as follows.

- (1). The mass flowrate, evaluated at the nozzle inlet, is used to update the velocity field from continuity with the density held fixed.
- (2). A discretized form of the one dimensional momentum equation is solved between node points $i-1$ and i to find the change in velocity at i , δU_i . For this evaluation, the change in velocity at $i-1$ is assumed to be zero, $\delta U_{i-1} = 0$.
- (3). Coefficients for the pressures in the transonic pressure correction equations are formed by substituting pressure correction expressions for δU_i and δp_i into the continuity equation.
- (4). An effective pressure is calculated using either the M&M formula or the 2M formula and the density is then evaluated from this effective pressure.
- (5). The pressure correction equations are solved using the continuity errors calculated from the velocity, updated from momentum in step 2, and the density, updated in step 4.
- (6). This pressure correction is then used to update the density, velocity, and pressure along the nozzle.
- (7). The inlet velocity is recalculated using the new inlet static pressure and isentropic relations.

(8). This new inlet velocity is then used as in step 1 to update the mass flowrate and velocities.

Thus, all the flow properties are updated and the program starts another iteration from step 2. At the end of every other iteration, the current density, velocity, and pressure are averaged with values from the previous iteration and then used for the next iteration. This procedure of averaging the properties helps the program converge to a solution.

4.0 Development of a New Shock Capturing Formula

A pressure interpolation method is used to determine the effective pressure at the point being evaluated, P_i . The interpolation formula previously used, the M&M formula, is dependent on one Mach number, the maximum Mach number of M_i and M_{i-1} . This section shows the development of the new 2M formula and compares it to the M&M formula previously used. The 2M formula uses two Mach numbers, M_i and M_{i-1} . The main idea for developing the new pressure interpolation formula was to sharpen the shock, which was previously captured over three to four grid points with the old pressure formula.

The continuity equation between grid points i and $i+1$ can be expressed in discretized form such that

$$[\rho_{i+1} + \delta\rho_{i+1}][U_{i+1} + \delta U_{i+1}]A_{i+1} - [\rho_i + \delta\rho_i][U_i + \delta U_i]A_i = 0 \quad (1)$$

Rearranging equation 1 gives the following

$$\begin{aligned} & \rho_{i+1}A_{i+1}\delta U_{i+1} - \rho_iA_i\delta U_i + U_{i+1}A_{i+1}\delta\rho_{i+1} - U_iA_i\delta\rho_i \\ & = \rho_iU_iA_i - \rho_{i+1}U_{i+1}A_{i+1} + \delta\rho_i\delta U_iA_i - \delta\rho_{i+1}\delta U_{i+1}A_{i+1} \end{aligned} \quad (2)$$

The first two terms on the right hand side of equation 2, $\rho_iU_iA_i$ and $\rho_{i+1}U_{i+1}A_{i+1}$, represent the current continuity error. The last two terms, $\delta\rho_i\delta U_iA_i$ and $\delta\rho_{i+1}\delta U_{i+1}A_{i+1}$, are of order δ^2 ; thus, these terms are negligible when the computation is nearly converged and $\delta\rho \ll \rho$ and $\delta U \ll U$. Therefore, equation 2 can be rewritten as

$$[\rho_{i+1}\delta U_{i+1} + U_{i+1}\delta\rho_{i+1}]A_{i+1} - [\rho_i\delta U_i + U_i\delta\rho_i]A_i = m_{\text{error},i} + \text{small} \quad (3)$$

The continuity error, $m_{\text{error},i}$, is the error at i for a control volume from i to $i+1$.

The change in velocity is found from the momentum correction equations as

$$\begin{aligned} \delta U_i &= (\delta P_{i-1} - \delta P_i) / [0.5(\rho_i U_i + \rho_{i-1} U_{i-1})] \quad \text{and} \\ \delta U_{i+1} &= (\delta P_i - \delta P_{i+1}) / [0.5(\rho_{i+1} U_{i+1} + \rho_i U_i)] \end{aligned} \quad (4)$$

Substituting δU_i and δU_{i+1} into equation 3 gives

$$\begin{aligned} &2\rho_{i+1}A_{i+1}[(\delta P_i - \delta P_{i+1})/(\rho_{i+1}U_{i+1} + \rho_i U_i)] \\ &- 2\rho_i A_i[(\delta P_{i-1} - \delta P_i)/(\rho_{i-1}U_{i-1} + \rho_i U_i)] \\ &+ U_{i+1}A_{i+1}\delta\rho_{i+1} - U_i A_i \delta\rho_i = m_{\text{error},i} + \text{small} \end{aligned} \quad (5)$$

Since $\rho_i U_i A_i = \rho_{i+1} U_{i+1} A_{i+1}$ from continuity and $\rho_{i+1} U_{i+1} + \rho_i U_i = \rho_{i+1} U_{i+1} [1 + \rho_i U_i / \rho_{i+1} U_{i+1}]$, the denominators in equation 5 can be expressed as

$$\rho_{i+1} U_{i+1} + \rho_i U_i = \rho_{i+1} U_{i+1} [1 + A_{i+1}/A_i] \quad (6)$$

$$\text{and } \rho_i U_i + \rho_{i-1} U_{i-1} = \rho_i U_i [1 + A_i/A_{i-1}] \quad (7)$$

Combining equations 6 and 7 with equation 5 gives

$$\begin{aligned}
& - 2A_i/U_i(1 + A_i/A_{i-1}) & \delta P_{i-1} \\
& + 2A_{i+1}/U_{i+1}(1 + A_{i+1}/A_i) + 2A_i/U_i(1 + A_i/A_{i-1}) & \delta P_i \\
& - 2A_{i+1}/U_{i+1}(1 + A_{i+1}/A_i) & \delta P_{i+1} \\
& - U_i A_i & \delta \rho_i \\
& + U_{i+1} A_{i+1} & \delta \rho_{i+1} \\
& = m_{\text{error},i} & (8)
\end{aligned}$$

Since the Mach number is $M = U/c$, where c is the speed of sound, equation 8 can be rewritten as

$$\begin{aligned}
& - 2A_i/M_i(1 + A_i/A_{i-1}) & \delta P_{i-1} \\
& + 2A_{i+1}/M_{i+1}(1 + A_{i+1}/A_i) + 2A_i/M_i(1 + A_i/A_{i-1}) & \delta P_i \\
& - 2A_{i+1}/M_{i+1}(1 + A_{i+1}/A_i) & \delta P_{i+1} \\
& - c^2 M_i A_i & \delta \rho_i \\
& + c^2 M_{i+1} A_{i+1} & \delta \rho_{i+1} \\
& = c m_{\text{error},i} & (9)
\end{aligned}$$

Equation 9 is the pressure correction equation for the pressure at point i . The assumption $A_{i-1} = A_i = A_{i+1}$ was made since we are interested in shock capturing and the areas directly before and after a normal shock are considered to be equal. This is a reasonable assumption because a shock wave is extremely thin, on the order of 10^{-6} meters. Equation 9 reduces to

$$\begin{aligned}
& - 1/M_i \delta P_{i-1} + (1/M_{i+1} + 1/M_i) \delta P_i - 1/M_{i+1} \delta P_{i+1} \\
& - c^2 M_i \delta \rho_i + c^2 M_{i+1} \delta \rho_{i+1} = c m_{\text{error},i} & (10)
\end{aligned}$$

A generalized pressure interpolation equation for the effective density is

$$\rho_i = P_{eff_i} / RT_i \quad (11)$$

with the effective pressure at i represented as

$$P_{eff_i} = P_{i-1} + a_{0_i}[P_i - P_{i-1}] + a_{1_i}[P_i - P_{i-2}]/2 \quad (12)$$

where a_{0_i} and a_{1_i} are coefficients. The only values considered for a_{0_i} and a_{1_i} are between 0 and 1 with $a_0 + a_1 \leq 1$. Equation 12 is a second order interpolation equation for uniform grids when $a_0 + a_1 = 1$ (Appendix B).

The change in density at points i and $i+1$ can be written as

$$\delta p_i = [(1-a_{0_i})\delta P_{i-1} + (a_{0_i} + a_{1_i}/2)\delta P_i - (a_{1_i}/2)\delta P_{i-2}] / RT_i \quad (13)$$

$$\delta p_{i+1} = [(1-a_{0_{i+1}})\delta P_i + (a_{0_{i+1}} + a_{1_{i+1}}/2)\delta P_{i+1} - (a_{1_{i+1}}/2)\delta P_{i-1}] / RT_{i+1} \quad (14)$$

Substituting equations 13 and 14 into equation 10 and using the relation $\gamma = c^2/RT$ gives

$$\begin{aligned} & (- 1/M_{i+1} + \gamma M_{i+1} a_{0_{i+1}} + \gamma M_{i+1} a_{1_{i+1}}/2) \delta P_{i+1} \\ & + (\gamma M_{i+1} + 1/M_{i+1} + 1/M_i - \gamma M_i a_{0_i} - \gamma M_{i+1} a_{0_{i+1}} - \gamma M_i a_{1_i}/2) \delta P_i \\ & + (-\gamma M_i - 1/M_i + \gamma M_i a_{0_i} - \gamma M_{i+1} a_{1_{i+1}}/2) \delta P_{i-1} \\ & + (+\gamma M_i a_{1_i}/2) \delta P_{i-2} \\ & = c m_{error,i} \end{aligned} \quad (15)$$

Since values for a_0 and a_1 must remain between 0 and 1, it is evident from equation 15 that the

coefficient of δP_{i+1} is either positive or negative,
coefficient of δP_{i-1} is always negative, and the
coefficient of δP_{i-2} is always positive or zero

In order to determine Mach number limitations for the coefficients a_0 and a_1 , a stability criterion is applied such that the coefficient of the center point must be greater than or equal to the sum of the other positive coefficients. The center point is δP_i .

$$\text{Coef}_{\text{center}} \geq \Sigma \text{ of all other positive Coef} \quad (16)$$

This criterion can be separated into two conditions:

$$\text{Coeff. } \delta P_i \geq \text{Coeff. } \delta P_{i-2} \quad (17)$$

$$\text{Coeff. } \delta P_i \geq \text{Coeff. } \delta P_{i-2} + \text{Coeff. } \delta P_{i+1} \quad (18)$$

4.1 Stability Analysis for a_0 & a_1

In order to determine the stability limits on a_0 and a_1 , both criteria, equations 17 and 18, have to be satisfied. Each criterion is applied to equation 15.

1st Criterion: **Coeff. $\delta P_i \geq$ Coeff. δP_{i-2}**

Applying Coeff. $\delta P_i \geq$ Coeff. δP_{i-2} to equation 15 gives

$$\gamma M_{i+1} + 1/M_{i+1} + 1/M_i - \gamma M_i a_{0i} - \gamma M_{i+1} a_{0i+1} - \gamma M_i a_{1i}/2 \geq \gamma M_i a_{1i}/2 \quad (19)$$

Rearranging and collecting terms,

$$\gamma M_i (a_{1i} + a_{0i}) + \gamma M_{i+1} a_{0i+1} \leq \gamma M_{i+1} + 1/M_{i+1} + 1/M_i$$

Subtracting γM_i from both sides gives

$$\gamma M_i (a_{1i} + a_{0i} - 1) + \gamma M_{i+1} a_{0i+1} \leq \gamma M_{i+1} + 1/M_{i+1} + 1/M_i - \gamma M_i \quad (20)$$

From this point on, the right hand side of equation 20 will be referred to as A , such that

$$A = \gamma M_{i+1} + 1/M_{i+1} + 1/M_i - \gamma M_i \quad (21)$$

The variable A is a function of M_i and M_{i+1} . Figure 4.1 displays a curve which represents $A=0$. A is positive everywhere to the left of the $A=0$ curve and negative everywhere to the right of the $A=0$ curve.

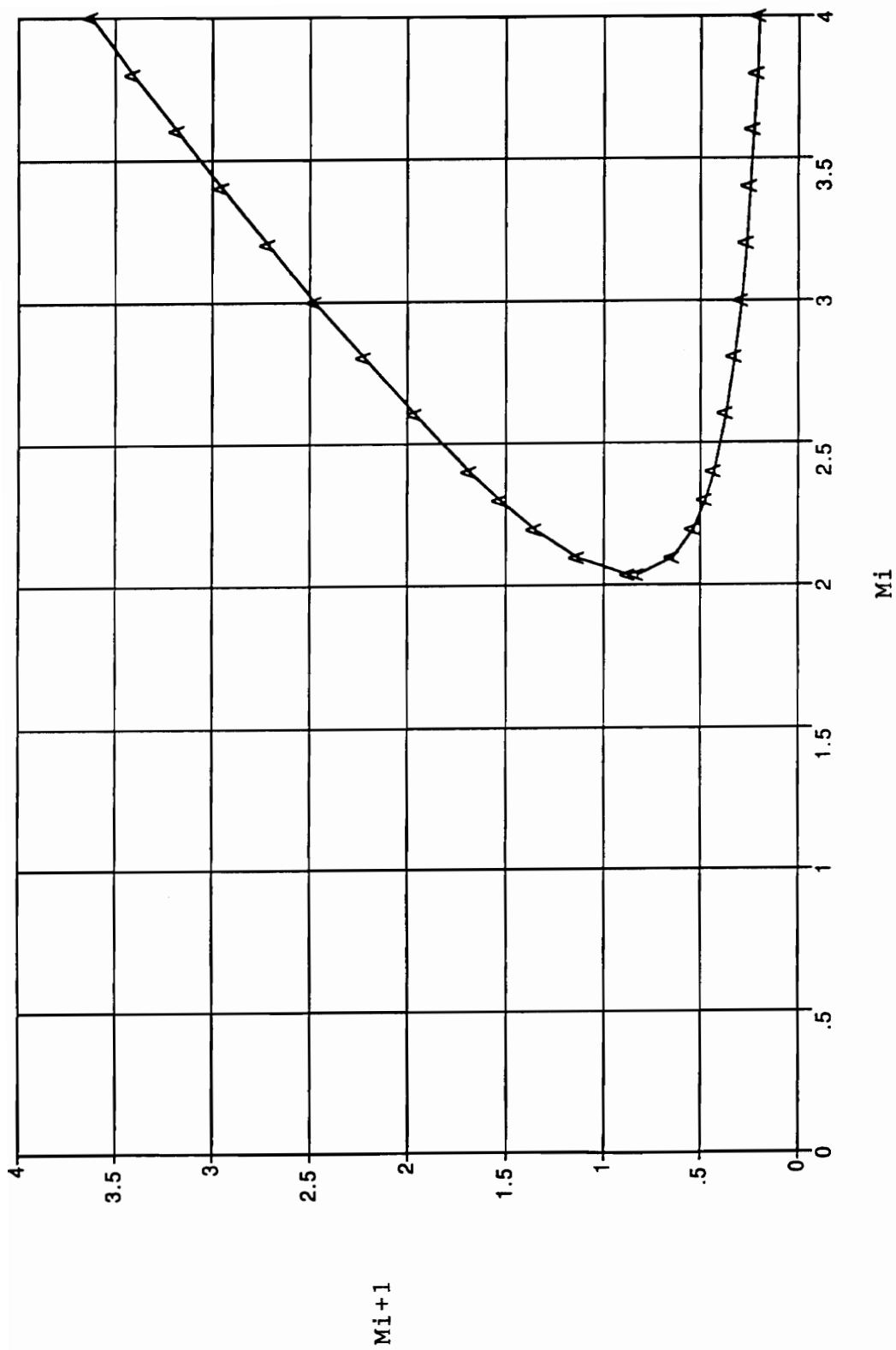


Fig. 4.1 $A=0$ from equation 21, where $A=f(M_i, M_{i+1})$

If $A > 0$

Noting that

$$a_{0i} + a_{1i} \leq 1$$

$$\text{i.e., } \gamma M_i (a_{1i} + a_{0i} - 1) \leq 0$$

the criterion represented by equation 20 is satisfied for $A > 0$

by choosing $\gamma M_{i+1} a_{0i+1} \leq \gamma M_{i+1} + 1/M_{i+1} + 1/M_i - \gamma M_i$

$$\text{Thus, } a_{0i+1} \leq 1 + 1/(\gamma M_{i+1}^2) + 1/(\gamma M_{i+1} M_i) - M_i/M_{i+1} \quad (22)$$

Equation 22 is a downstream stability limit on a_{0i+1} ; i.e., it is a limit on a_0 on the downstream side of the control volume being analyzed. This limit allows second order accuracy.

If $A < 0$

For the condition when $A \leq 0$, the criterion represented by equation 20 requires

$$a_{0i} + a_{1i} < 1$$

If values of a_{0i} and a_{0i+1} are set such that

$$a_{0i} = a_{0i+1} = 0$$

then $\gamma M_i a_{1i} \leq \gamma M_{i+1} + 1/M_{i+1} + 1/M_i$

Thus,
$$a_{1i} \leq M_{i+1}/M_i + 1/(\gamma M_{i+1} M_i) + 1/(\gamma M_i^2) \quad (23)$$

Equation 23 is an upstream stability limit on a_{1i} . This limit reduces the interpolation procedure to first order accuracy.

2nd Criterion: $\text{Coeff. } \delta P_i \geq \text{Coeff. } \delta P_{i-2} + \text{Coeff. } \delta P_{i+1}$

Applying equation 18, where $\text{Coeff. } \delta P_i \geq \text{Coeff. } \delta P_{i-2} + \text{Coeff. } \delta P_{i+1}$, to equation 15 gives

$$\begin{aligned} & \gamma M_{i+1} + 1/M_{i+1} + 1/M_i - \gamma M_i a_{0i} - \gamma M_{i+1} a_{0i+1} - \gamma M_i a_{1i}/2 \\ & \geq \gamma M_i a_{1i}/2 - 1/M_{i+1} + \gamma M_{i+1} a_{0i+1} + \gamma M_{i+1} a_{1i+1}/2 \end{aligned} \quad (24)$$

Rearranging and collecting terms,

$$\gamma M_i (a_{0i} + a_{1i}) + \gamma M_{i+1} (2a_{0i+1} + 0.5a_{1i+1}) \leq \gamma M_{i+1} + 2/M_{i+1} + 1/M_i$$

Again, subtracting γM_i from both sides gives

$$\gamma M_i (a_{0i} + a_{1i} - 1) + \gamma M_{i+1} (2a_{0i+1} + 0.5a_{1i+1}) \leq \gamma M_{i+1} + 2/M_{i+1} + 1/M_i - \gamma M_i \quad (25)$$

If $A > 0$

For the condition when $A > 0$, the right hand side of equation 25 must also be greater than zero since the RHS of equation 25 = $A + 1/M_{i+1}$. Therefore, again noting that

$$\gamma M_i (a_{1i} + a_{0i} - 1) \leq 0$$

equation 25 is satisfied by taking

$$\gamma M_{i+1}(2a_{0i+1} + 0.5a_{1i+1}) \leq \gamma M_{i+1} + 2/M_{i+1} + 1/M_i - \gamma M_i \quad (26)$$

If the condition $a_{1i+1} = 1 - a_{0i+1}$ is set, then equation 26 becomes

$$\gamma M_{i+1}(1.5a_{0i+1}) \leq 0.5\gamma M_{i+1} + 2/M_{i+1} + 1/M_i - \gamma M_i \quad (27)$$

From this point on, the right hand side of equation 27 will be referred to as B, such that

$$B = 0.5\gamma M_{i+1} + 2/M_{i+1} + 1/M_i - \gamma M_i \quad (28)$$

The variable B is a function of M_i and M_{i+1} , just as A was in the analysis above. Figure 4.2 displays a curve which represents $B=0$. B is positive everywhere to the left of the $B=0$ curve and negative everywhere to the right of the $B=0$ curve. Figure 4.3 shows the $A=0$ curve, $B=0$ curve, $M_{i+1} = M_i$ line, and $M_{i+1} = \text{normal shock}(M_i)$ curve. It is evident from Fig. 4.3 that both A and B are positive everywhere below Mach 2. For a normal shock, A is positive for an upstream Mach number up to $M_i = 2.2$ and B is positive up to $M_i=3.6$.

If $B > 0$

When $B > 0$, equation 27 reduces to

$$a_{0i+1} \leq 4/(3\gamma M_{i+1}^2) + 2/(3\gamma M_{i+1} M_i) - 2M_i/3M_{i+1} + 1/3 \quad (29)$$

using $a_{1i+1} = 1 - a_{0i+1}$

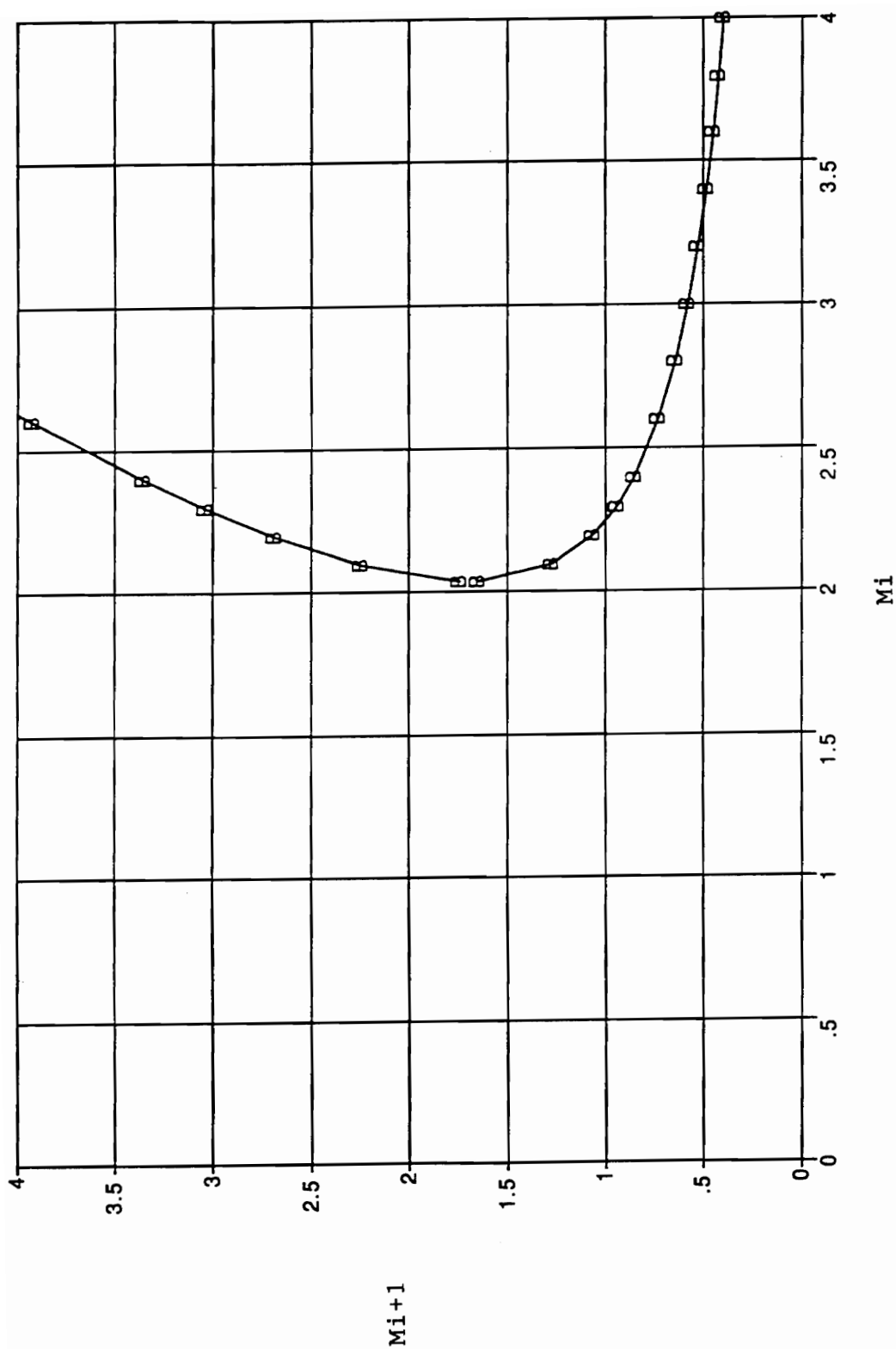


Fig. 4.2 $B=0$ from equation 28, where $B=f(M_i, M_{i+1})$

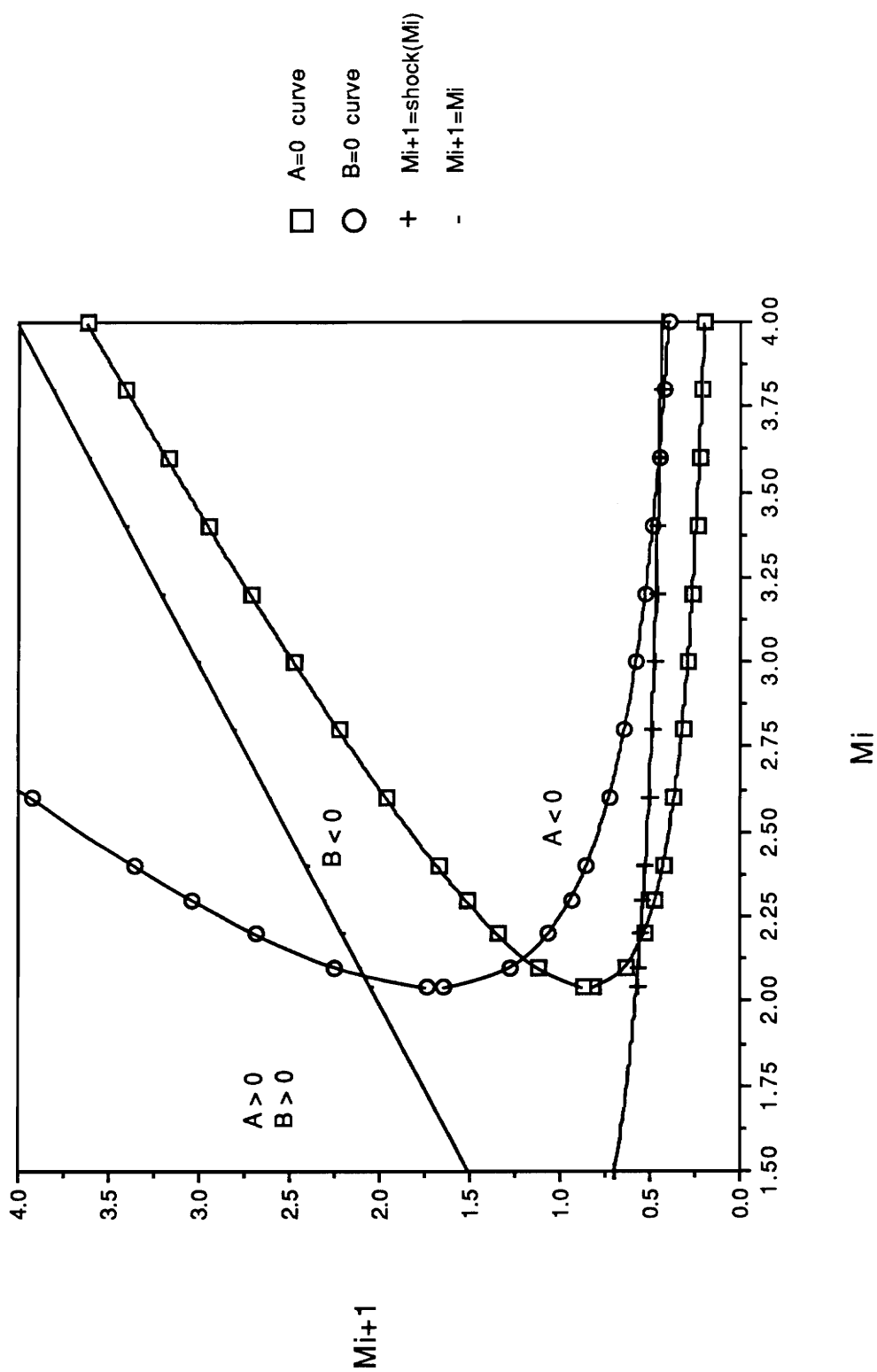


Fig. 4.3 $A=0$ curve, $B=0$ curve, $M_{i+1}=M_i$, and $M_{i+1}=\text{shock}(M_i)$

Equation 29 is a downstream stability limit on a_{0i+1} . This limit allows second order accurate interpolation.

If $B < 0$

When $B \leq 0$, the condition $a_{1i+1} = 1 - a_{0i+1}$ cannot be used. Instead equation 26 is satisfied by taking

$$a_{0i+1} = 0$$

and
$$a_{1i+1} \leq 2 + 4/\gamma M_{i+1}^2 + 2/(\gamma M_{i+1} M_i) - 2M_i/M_{i+1} \quad (30)$$

Equation 30 is a downstream stability limit on a_{1i+1} . The interpolation procedure is then first order accurate.

If $A < 0$

For the condition when $A \leq 0$,

$$a_{0i} = a_{0i+1} = 0$$

was set for the first criterion, equation 23.

Thus, from equation 25,

$$\gamma M_i a_{1i} + 0.5 \gamma M_{i+1} a_{1i+1} \leq \gamma M_{i+1} + 2/M_{i+1} + 1/M_i \quad (31)$$

Since equation 31 contains both a_{1i} and a_{1i+1} , two cases were considered:

$$a_{1i} < a_{1i+1} \quad \text{and} \quad a_{1i+1} < a_{1i}.$$

For $a_{1i} < a_{1i+1}$

In this case, $a_{1i} = a_{1i+1} - \epsilon$, where ϵ is positive. Therefore, equation 31 becomes

$$\gamma M_i a_{1i+1} + 0.5 \gamma M_{i+1} a_{1i+1} \leq \gamma M_{i+1} + 2/M_{i+1} + 1/M_i + \gamma M_i \epsilon \quad (32)$$

If the left hand side of equation 32 is less than the right hand side, then it is true that the left hand side is less than the right hand side minus the term $\gamma M_i \epsilon$, since $\gamma M_i \epsilon$ has a positive value. Therefore, $\gamma M_i \epsilon$ can be dropped and equation 32 reduces to

$$a_{1i+1} \leq (\gamma M_{i+1} + 2/M_{i+1} + 1/M_i) / [0.5 \gamma M_{i+1} + \gamma M_i] \quad (33)$$

Equation 33 is a downstream stability limit on a_{1i+1} .

For $a_{1i+1} < a_{1i}$

In this case, $a_{1i+1} = a_{1i} - \epsilon$, where ϵ is positive. Therefore, equation 31 becomes

$$\gamma M_i a_{1i} + 0.5 \gamma M_{i+1} a_{1i} \leq \gamma M_{i+1} + 2/M_{i+1} + 1/M_i + 0.5 \gamma M_{i+1} \epsilon \quad (34)$$

Again, the term $0.5\gamma M_i \epsilon$ in equation 34 can be dropped.

Thus,
$$a_{1i} \leq (\gamma M_{i+1} + 2/M_{i+1} + 1/M_i)/[0.5\gamma M_{i+1} + \gamma M_i] \quad (35)$$

Equation 35 is an upstream stability limit on a_{1i} . Equations 33 and 35 result in first order accuracy.

4.2 Summary of Stability Limits for a_0 & a_1

From the 1st criterion, $\text{Coeff. } \delta P_i \geq \text{Coeff. } \delta P_{i-2}$, the following equations were obtained.

$$\text{For } A > 0 \quad a_{0i+1} \leq 1 + 1/(\gamma M_{i+1}^2) + 1/(\gamma M_{i+1} M_i) - M_i/M_{i+1} \quad (22)$$

$$\begin{aligned} \text{For } A \leq 0 \quad a_{1i} &\leq M_{i+1}/M_i + 1/(\gamma M_{i+1} M_i) + 1/(\gamma M_i^2) \\ \text{and } a_{0i} &= a_{0i+1} = 0 \end{aligned} \quad (23)$$

From the 2nd criterion, $\text{Coeff. } \delta P_i \geq \text{Coeff. } \delta P_{i-2} + \text{Coeff. } \delta P_{i+1}$, the following equations were obtained.

For $A > 0$

$$B > 0 \quad a_{0i+1} \leq 4/(3\gamma M_{i+1}^2) + 2/(3\gamma M_{i+1} M_i) - 2M_i/3M_{i+1} + 1/3 \quad (29)$$

$$\begin{aligned} B \leq 0 \quad a_{1i+1} &\leq 2 + 4/\gamma M_{i+1}^2 + 2/(\gamma M_{i+1} M_i) - 2M_i/M_{i+1} \\ \text{and } a_{0i+1} &= 0 \end{aligned} \quad (30)$$

For $A \leq 0$

$$a_{1i+1} \leq (\gamma M_{i+1} + 2/M_{i+1} + 1/M_i)/[0.5\gamma M_{i+1} + \gamma M_i] \quad (33)$$

$$\text{and } a_{1i} \leq (\gamma M_{i+1} + 2/M_{i+1} + 1/M_i)/[0.5\gamma M_{i+1} + \gamma M_i] \quad (35)$$

$$\text{and } a_{0i} = a_{0i+1} = 0$$

The regions of A and B are determined by

$$A = \gamma M_{i+1} + 1/M_{i+1} + 1/M_i - \gamma M_i \quad (21)$$

$$B = 0.5\gamma M_{i+1} + 2/M_{i+1} + 1/M_i - \gamma M_i \quad (28)$$

Cases where $M_i = M_{i+1}$

For a_0

For the case when $M_i = M_{i+1}$, Fig. 4.4 shows two curves of a_{0i+1} as a function of Mach number. These curves are based on the stability criteria used for equations 22 and 29. The lower curve, corresponding to equation 29, is equivalent to the stability limit resulting from the previous stability analysis [3]. Thus, in the limit that $M_i = M_{i+1}$, the stability analysis for the 2M formula gives the same results as the M&M formula. Valid values of the downstream limit on a_{0i+1} are represented by the shaded region in Fig. 4.4.

For a_1

For the case when $M_i = M_{i+1}$, A is always positive; thus, a_1 stability equations 23, 33, and 35 are not considered. Figure 4.5 shows a_{1i+1} as a function of Mach number from equation 30. Valid values of the downstream limit on a_{1i+1} are represented by the shaded region in Fig. 4.5.

Cases where M_{i+1} is not equal to M_i

In any analysis of nozzles, M_{i+1} will not be equal to M_i . Arbitrary values of 0.2 and 0.5 were used as the change in Mach number, $|M_{i+1} - M_i|$, to determine how a_0 and a_1 vary. The variation in a_0 due to the 2M formulation is then compared to the a_0 obtained from the M&M formulation.

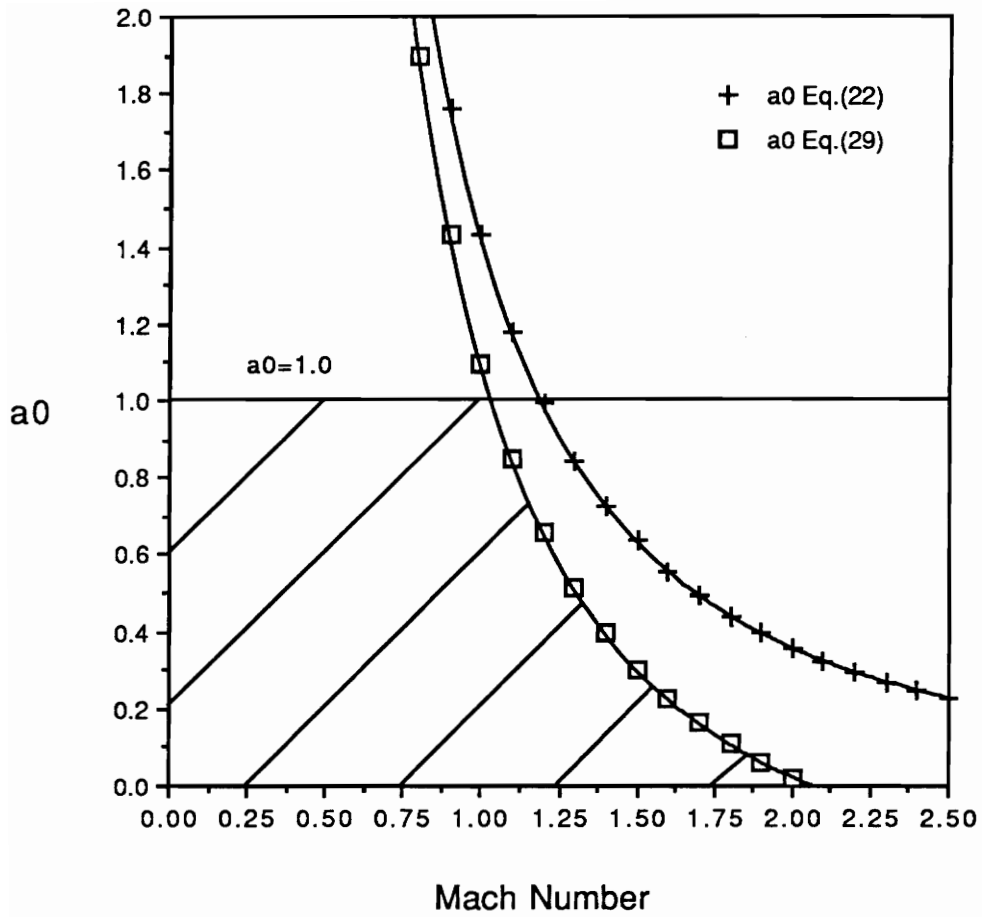


Fig. 4.4 Stability Limits for a_0 with $M_{i+1}=M_i$, Equations 22 & 29

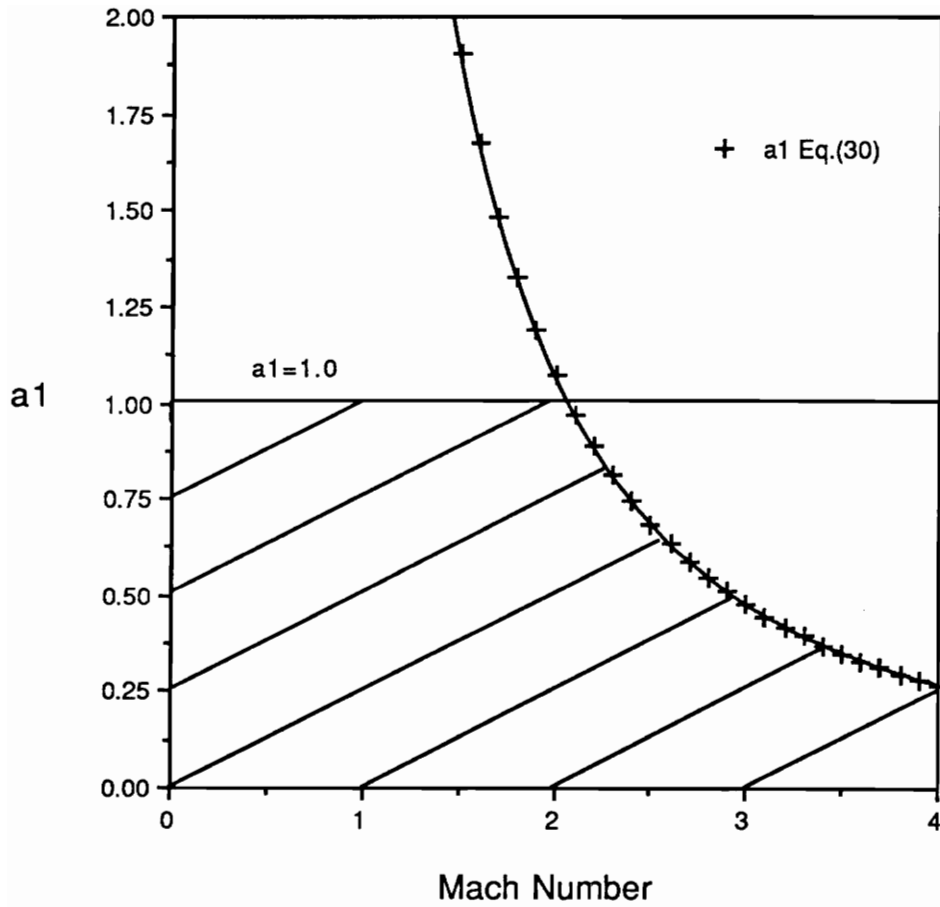


Fig. 4.5 Stability Limit for a_1 with $M_{i+1}=M_i$, Equation 30

For a_0

Figure 4.6 displays the variation in a_{0i+1} for a deceleration in Mach number, such that the upstream Mach number is greater than the downstream Mach number, $M_i > M_{i+1}$. Figure 4.7 shows a_{0i+1} for an acceleration, $M_{i+1} > M_i$. Only equation 29 was plotted in Fig. 4.6 and 4.7 because it is the limiting criterion. Figure 4.8 has $M_{i+1} = \text{normal shock}(M_i)$ for both a_{0i+1} stability limits, equations 22 and 29, along with the a_{0i+1} limit from the M&M formulation. Again, the shaded region represents valid a_{0i+1} values. From Figure 4.8, it is evident that equation 22 is the limiting criterion for the case of a shock. Thus the criterion switches from being equation 29 for equal or small changes in Mach number, to equation 22 for the larger Mach number changes corresponding to a normal shock. Figures 4.6, 4.7, and 4.8 show that a_{0i+1} can be significantly increased by using two Mach numbers instead of one. The larger values of a_{0i+1} will give a better approximation of the pressure distribution and should sharpen the shock.

For a_1

$A > 0$

For the deceleration and acceleration cases considered above, $\delta M = 0.2$ and 0.5 , A is always positive; thus, a_1 equations 23, 33, and 35 are not considered. Figure 4.9 shows the variation in a_1 for a deceleration in Mach number, $M_i > M_{i+1}$. Figure 4.10 shows a_{1i+1} for an acceleration, $M_{i+1} > M_i$. Only equation 30 is plotted in Figs. 4.9 and 4.10. Thus, using two Mach numbers decreases a_{1i+1} during a deceleration in Mach number and increases a_{1i+1} for

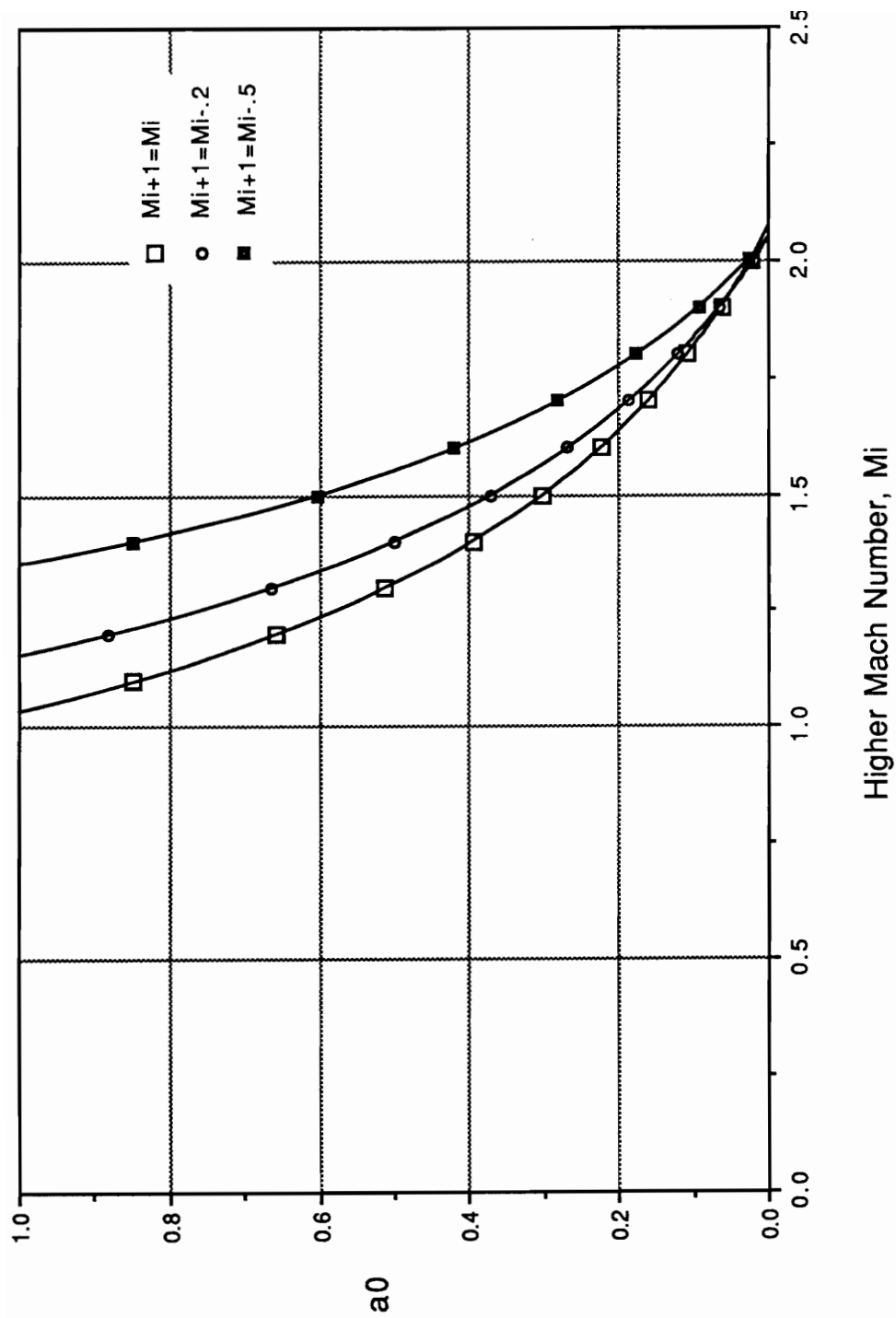


Fig. 4.6 $a_0(i+1)$ with $M_i > M_{i+1}$ (Deceleration),
Equation 29

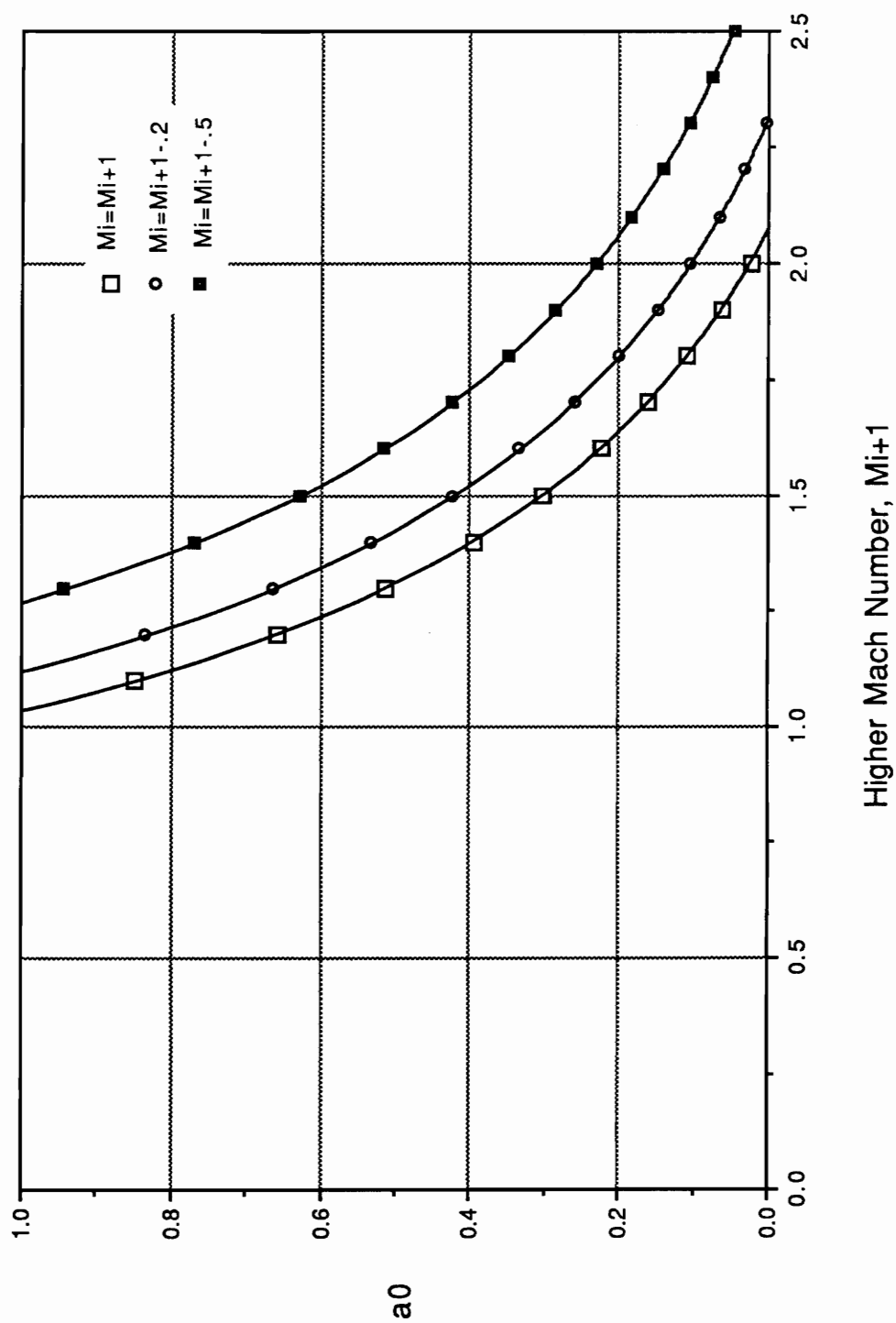


Fig. 4.7 $a_0(i+1)$ with $M_{i+1} > M_i$ (Acceleration),
Equation 29

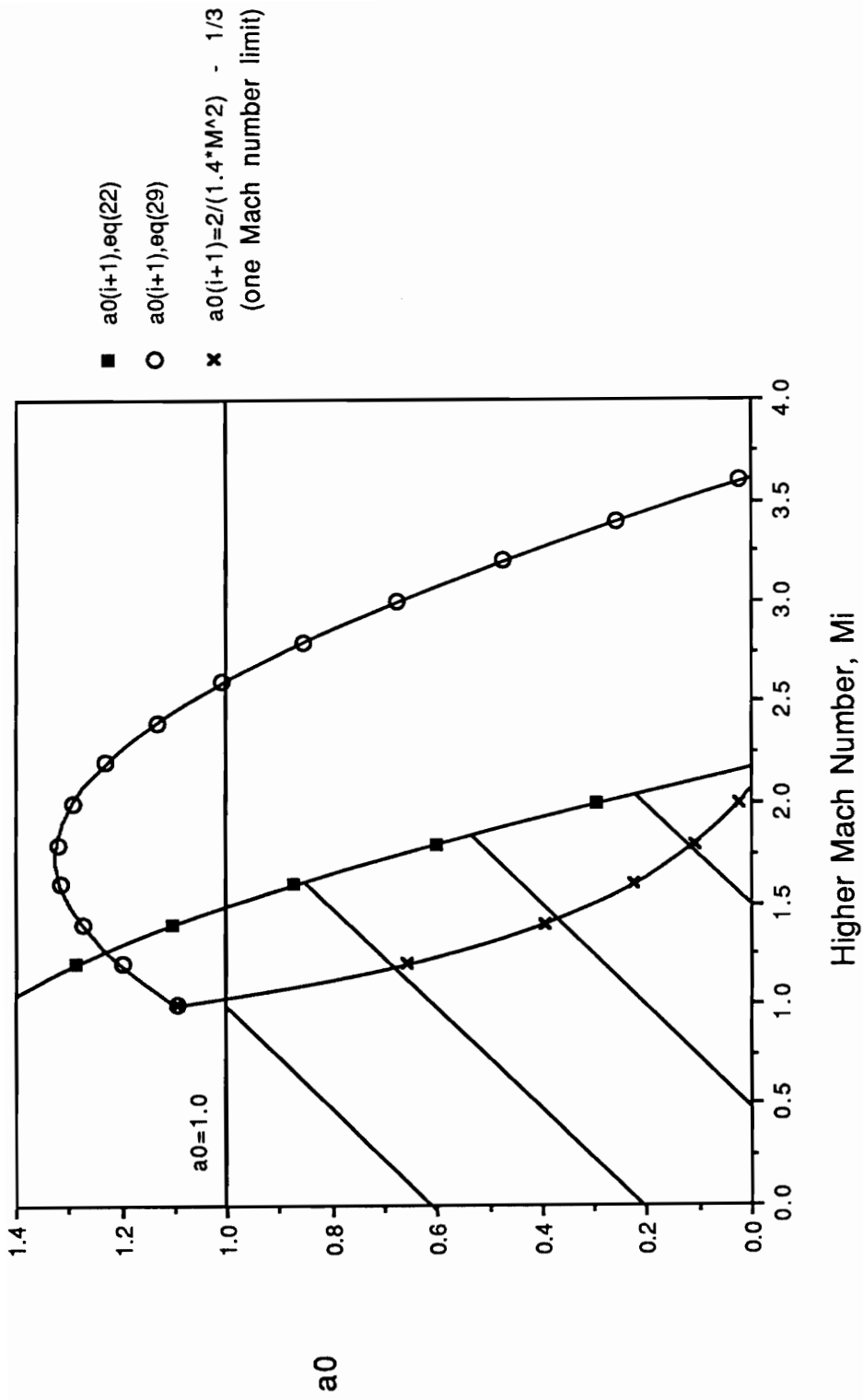


Fig. 4.8 $a_0(i+1)$ with M_{i+1} = normal shock(M_i),
Equations 22, 29 & previous one Mach
number limit

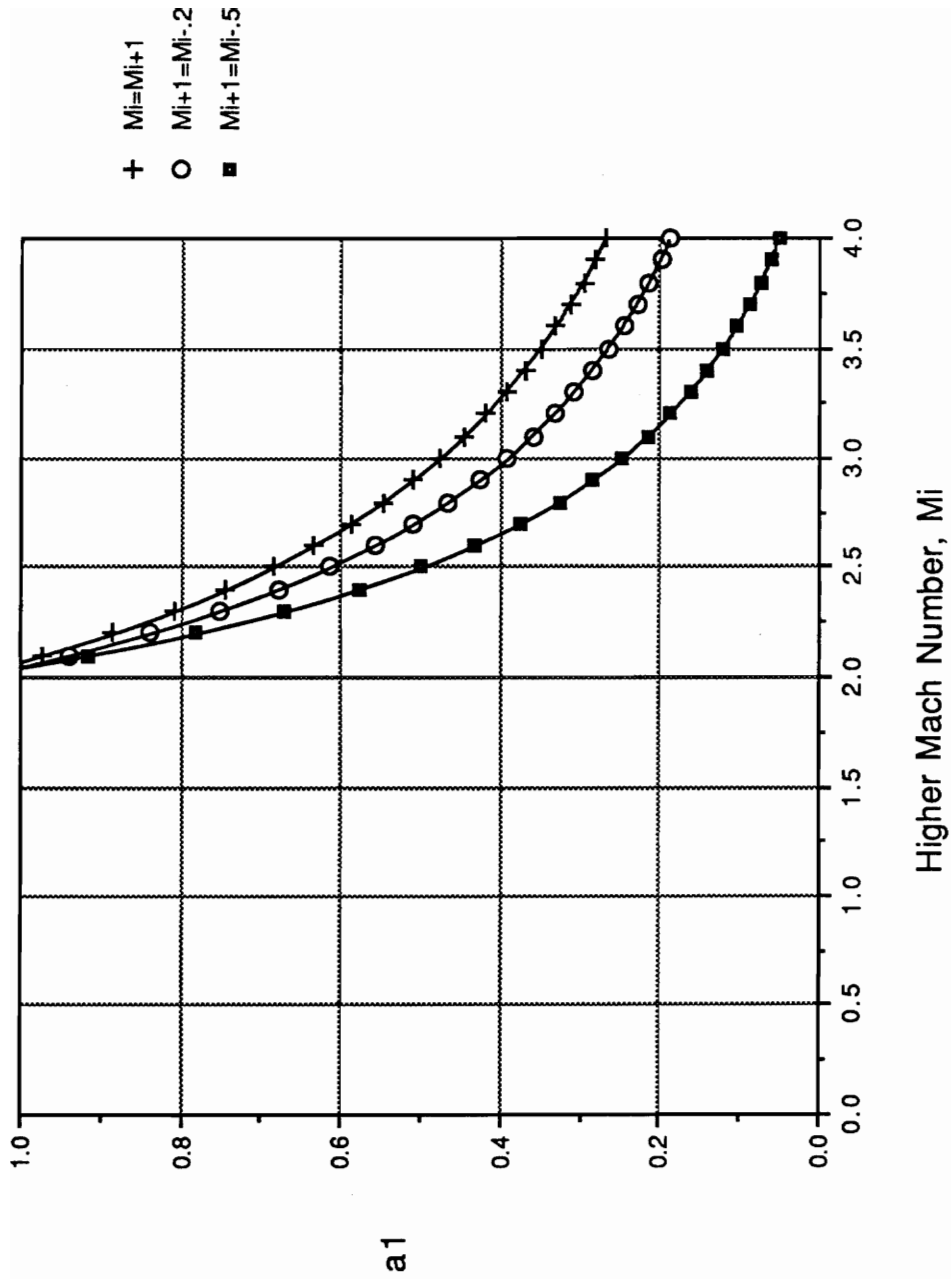


Fig. 4.9 $A > 0$ $a_1(i+1)$ with $M_i > M_{i+1}$ (Deceleration),
Equation 30

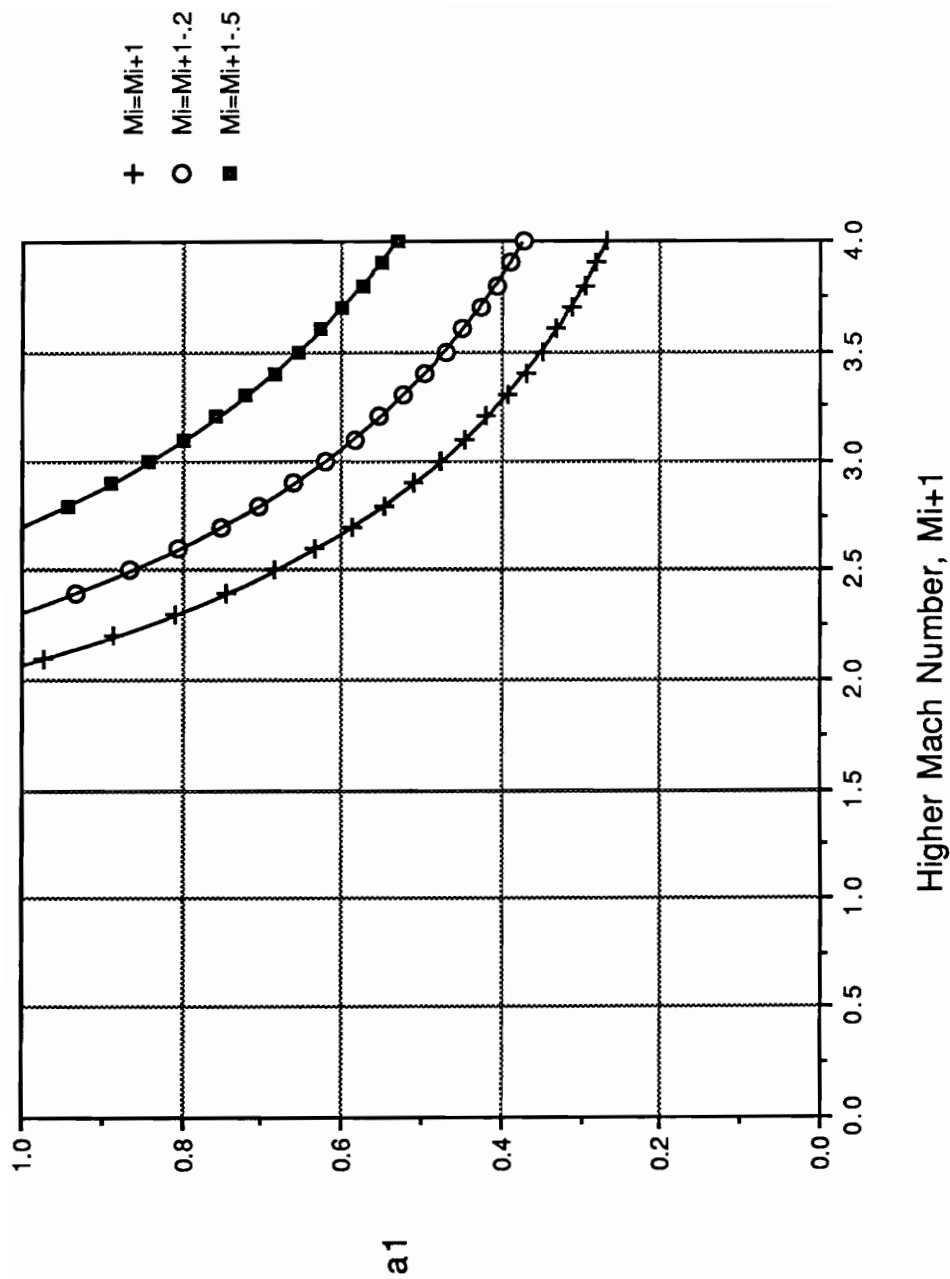


Fig. 4.10 $A > 0$ $a_1(i+1)$ with $M_{i+1} > M_i$ (Acceleration),
Equation 30

an acceleration. Since equation 30 is only valid when $A > 0$ and $B < 0$, it is evident from Fig. 4.3 that equation 30 does not apply for a shock case.

$A \leq 0$

For a shock case, A is negative when the upstream Mach number is greater than $M_i = 2.2$. Figure 4.11 shows equations 23, 33 and 35 for $M_{i+1} = \text{normal shock}(M_i)$. It should be noted that the right hand side of equations 33 and 35 are identical, thus in Fig. 4.11, the line with the filled squares is both a limit for a_{1i+1} (equation 33) and for a_{1i} (equation 35). Even though the a_1 curves with $M_i = M_{i+1}$ are not valid limits, they are plotted for comparison purposes only. Since the curve for equation 23 lies below that for equation 35, equation 23 is the limit for a_{1i} . Thus, for a shock, the limit for the upstream side, a_{1i} , is equation 23 and the limit for the downstream side, a_{1i+1} , is equation 33. Again, the criterion switches from being equation 30 for equal Mach numbers to equation 23 for a shock, thus from being a criterion on a_{1i+1} to being a criterion on a_{1i} . This switching of limiting a_1 curves corresponds to the switching of the limiting a_0 curves described above. Each a_0 curve corresponds to an a_1 curve because both come from the same stability criteria.

Combination of a_0 and a_1

When $M_i = M_{i+1}$, Fig. 4.12 shows the stability limits of a_0 and a_1 . Up to a Mach number of $M_i = 2.05$, equation 29 is the a_0 limit and $1-a_0$ is the a_1 limit at $i+1$; thus, the interpolation gives second order accuracy. Above $M_i = 2.05$, $a_0 = 0$ and equation 30 is the a_1 limit; thus, providing first order accuracy. It should be noticed that as a_0 goes to zero, a_1 goes to one. In addition, at the point where

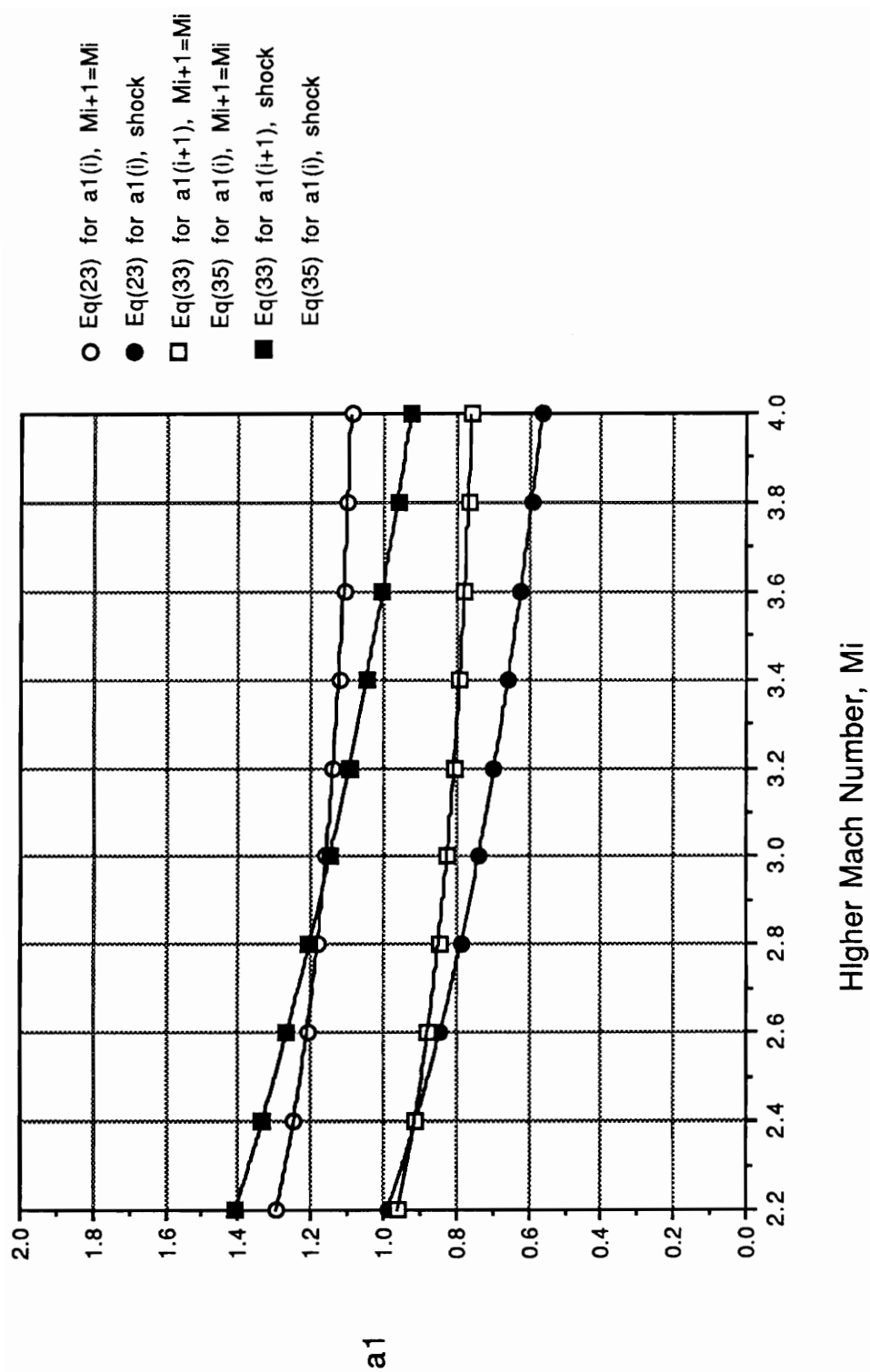


Fig. 4.11 $A < 0$ a_1 with $M_{i+1} = \text{normal shock}(M_i)$,
Equations 23, 33 & 35

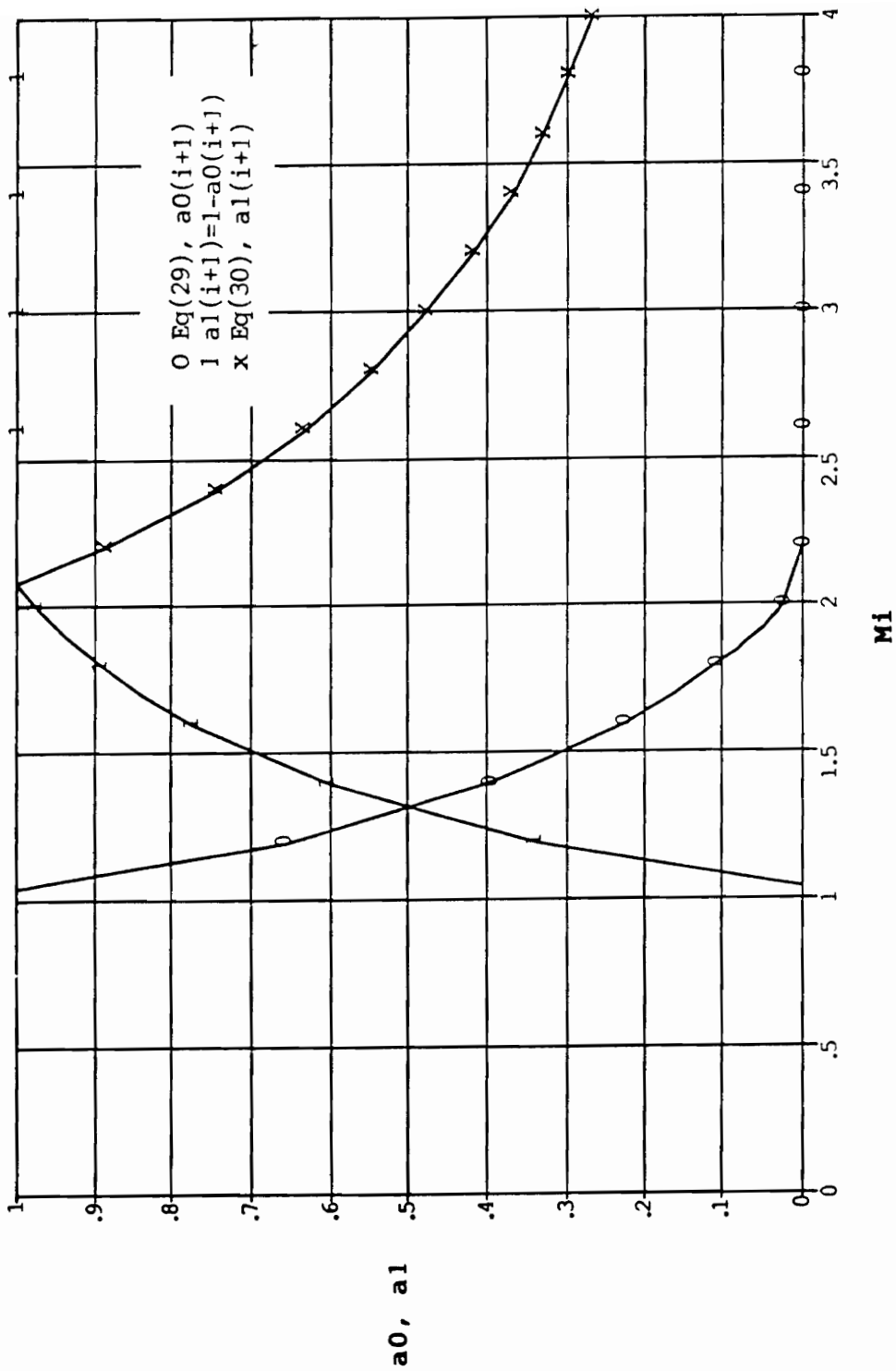


Fig. 4.12 a_0 & a_1 limits with $M_i=M_i+1$

a_0 equals zero the a_1 limit, equation 30, is introduced. Figure 4.13 shows the limits for a shock case. Up to a Mach number of $M_i = 2.2$, equation 22 is the a_0 limit and $1-a_0$ is the a_1 limit at $i+1$. Above $M_i = 2.2$, $a_{0i} = a_{0i+1} = 0$ and equation 23 is the limit on a_{1i} .

Implementation

The 2M pressure interpolation method replaces the M&M formulation in the MEFP code. The equations summarized on page 36 are used in the new coding (Appendix D). The value of 0.075 was added to all Mach numbers, M_i and M_{i+1} , in order to drop a_0 below 1 at Mach 1 and keep the a_1 curves continuous. This addition to the Mach numbers basically shifts the stability curves slightly to the left; thus, providing a margin of safety in stability.

To implement the 2M formula in the 3-D MEFP code, upstream and downstream Mach numbers corresponding to each grid point are needed. These are found by interpolation, at the intersections of the streamline (through the point) with the upstream and downstream grid surfaces, as shown in Fig. 4.14.

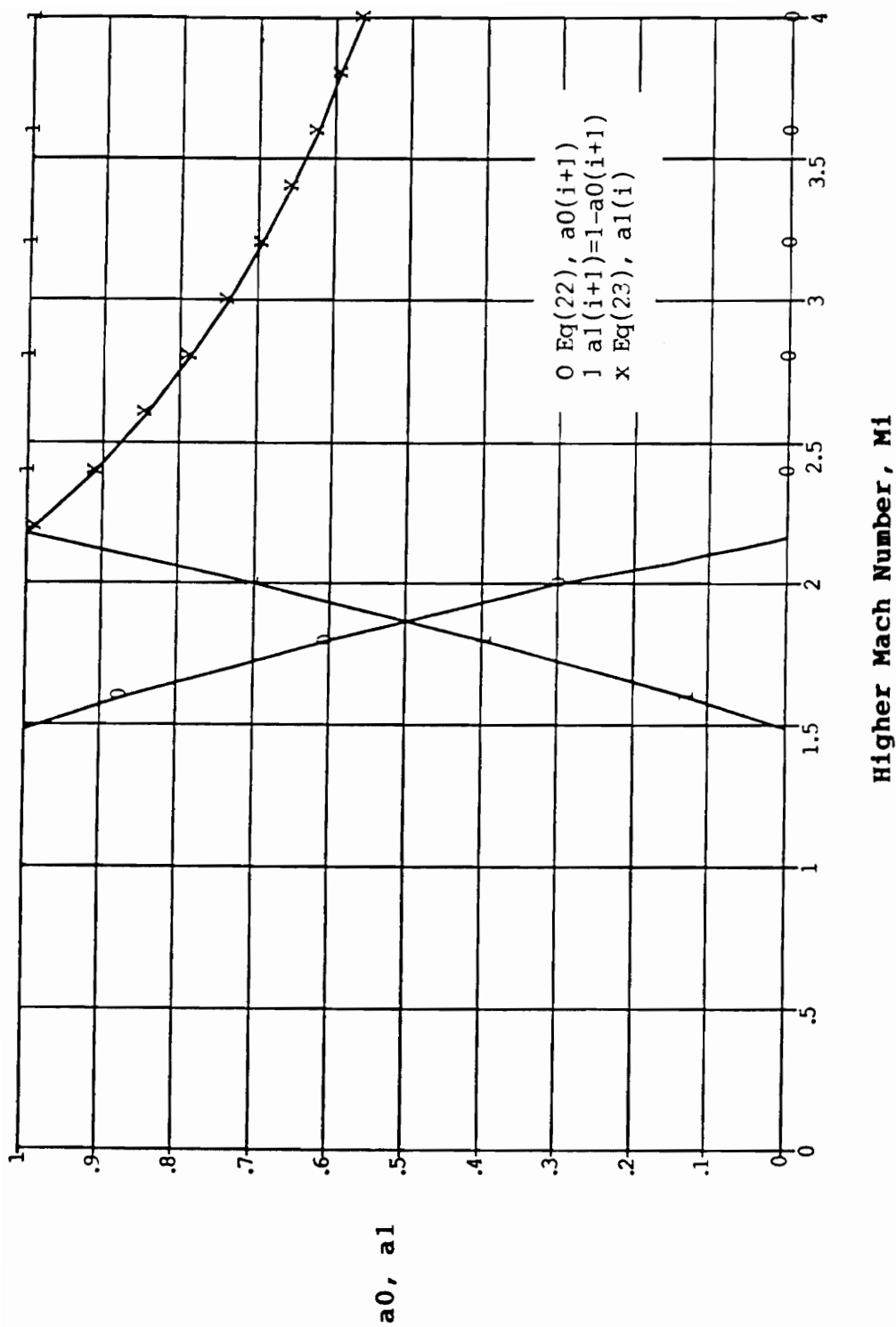


Fig. 4.13 a_0 & a_1 limits with M_{i+1} =normal shock(M_i)

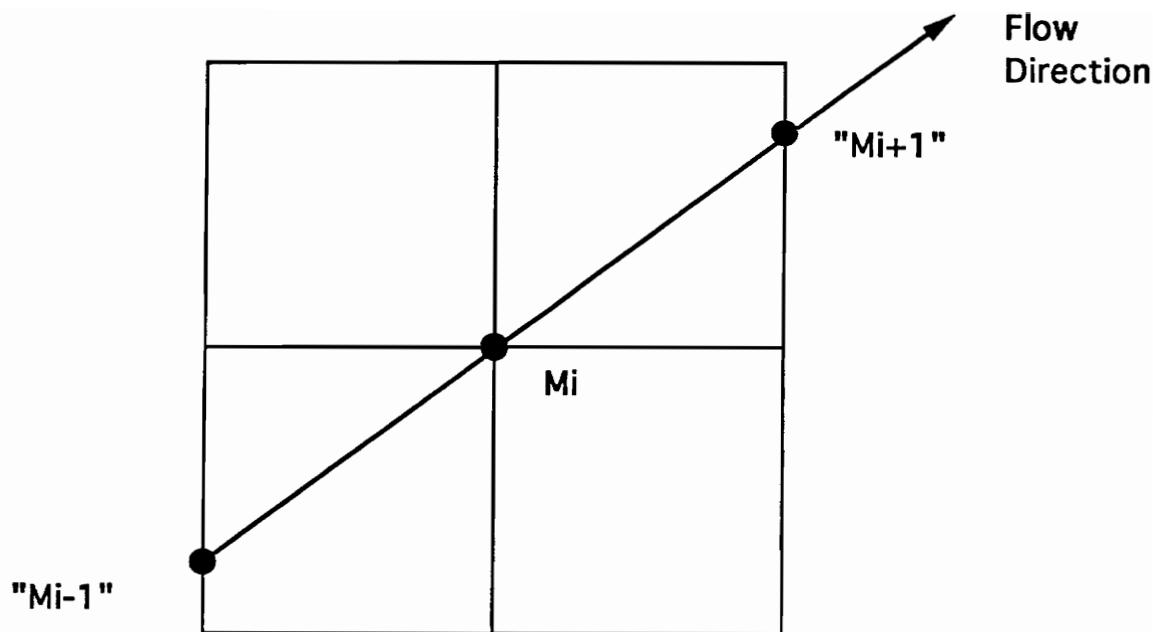


Fig. 4.14 Locations for evaluation of upstream and downstream Mach Numbers in 3-D flows

5.0 Normal Shock Capturing in a 1-D Nozzle

One-dimensional flow in a converging-diverging nozzle, shown in Fig. 5.1, is calculated to test the Fortran program summarized in section 3.0. A grid in the flow direction is used such that $i=1$ at the nozzle inlet and $i=IMAX$ at the nozzle exit. The main purpose of this test is to determine the normal shock capturing capabilities of the MEFP code using both pressure interpolation methods, the M&M formula and the 2M formula. This section then compares the results obtained using both methods with theoretical values. Several back pressure ratios, P_{exit}/P_{to} , are used: 0.85, 0.80, and 0.75, giving shock strengths of 1.267, 1.455, and 1.578, respectively. The term "shock strength" refers to the Mach number directly upstream of the shock. These three shock strengths are typical for turbomachinery flows. To check the 1-D code over a wide range of Mach numbers, shock strengths of 1.1, 2.5, and 3.5 are also tested. The input values for each test case and grid geometry are given below.

Calculation Details

All calculations are for air with $\gamma = 1.4$. The area at each grid point is determined from the isentropic Mach number.

1. For $P_{exit}/P_{to} = 0.75, 0.80, \text{ and } 0.85$ cases

Number of Axial Grid Points = 41

Grid Setup, $\delta M = 0.025$, where

at inlet	$i=1;$	$M=0.8$
at exit	$i=41;$	$M=1.8$

2. For $M_{shock} = 1.1$ case

Number of Axial Grid Points = 41

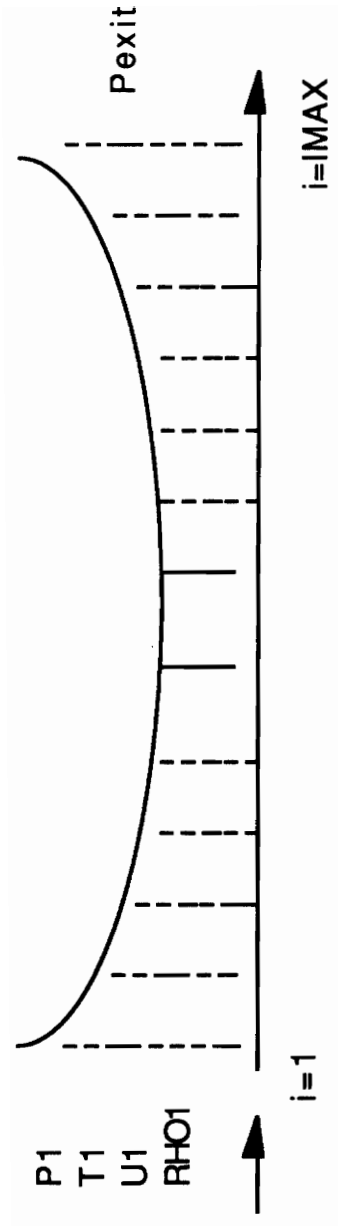


Fig. 5.1 1-D Converging-Diverging Nozzle

Grid Setup, $\delta M = 0.025$, where

at inlet	$i = 1;$	$M = 0.8$
at exit	$i = 41;$	$M = 1.8$

$$P_{\text{exit}}/P_{\text{to}} = 0.86687$$

3. For $M_{\text{shock}} = 2.5$ case

Number of Axial Grid Points = 45

Grid Setup, $\delta M = 0.05$, where

at inlet	$i = 1;$	$M = 0.8$
at exit	$i = 45;$	$M = 3.0$

$$P_{\text{exit}}/P_{\text{to}} = 0.47101$$

4. For $M_{\text{shock}} = 3.5$ case

Number of Axial Grid Points = 65

Grid Setup, $\delta M = 0.05$, where

at inlet	$i = 1;$	$M = 0.8$
at exit	$i = 65;$	$M = 4.0$

$$P_{\text{exit}}/P_{\text{to}} = 0.20285$$

The change in Mach number, δM , was doubled to 0.05 for the $M_{\text{shock}} = 2.5$ and 3.5 cases in order to keep the number of grid points low.

Results

Figures 5.2a, 5.2b, and 5.2c show the theoretical Mach number, pressure, and total pressure ratio values versus nozzle position for back pressure ratios of 0.85, 0.80, and 0.75. The Mach number increases linearly, while the pressure decreases according to the isentropic flow relations, up to the shock. The total pressure is 1.0 up to the shock, decreases at the shock due to shock losses, and then remains constant. Corresponding plots for the 2M formula results are given in Figs. 5.3a, 5.3b, and 5.3c. The calculated Mach number and pressure distributions are similar to the theoretical plots, except for the 0.75 and 0.85 cases, where a slight overshoot in the Mach number directly upstream of the shock occurs. This overshoot in Mach number is due to the

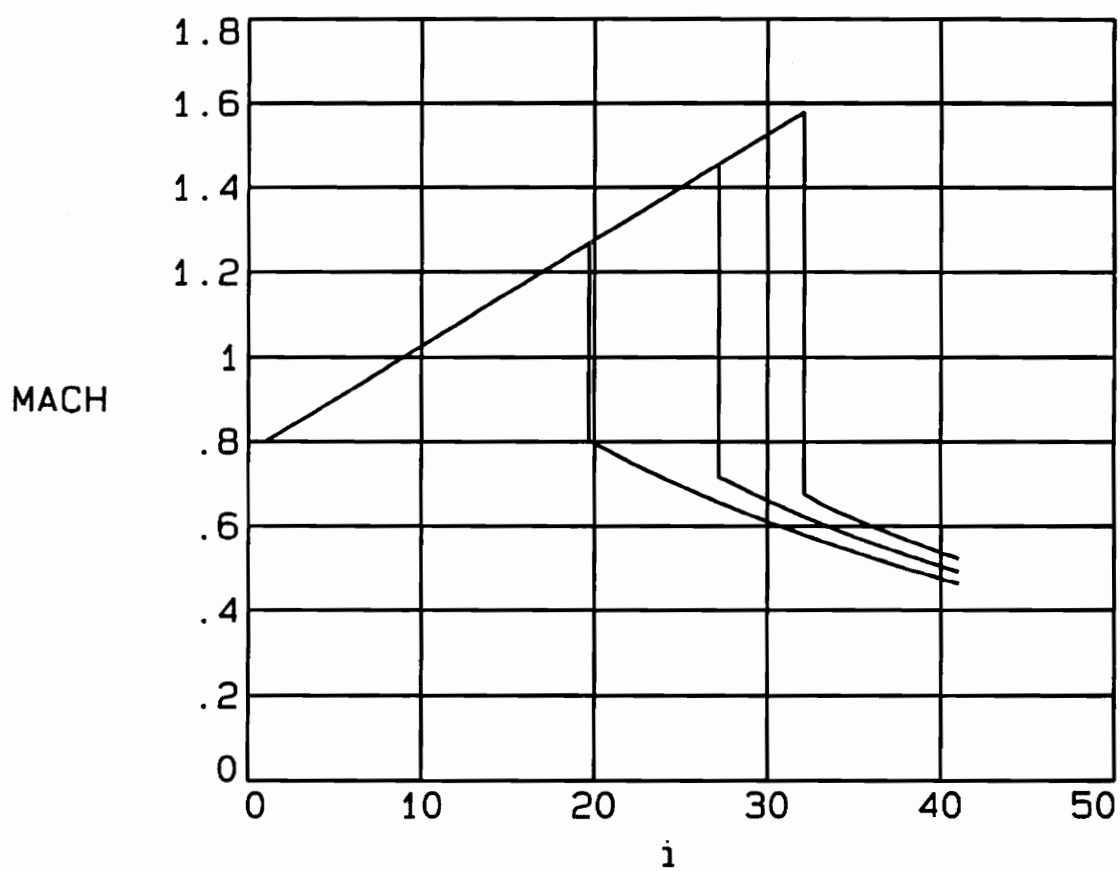


Fig. 5.2a Theoretical Mach numbers versus nozzle position for $P_{exit}/P_{to} = 0.85, 0.80$, and 0.75

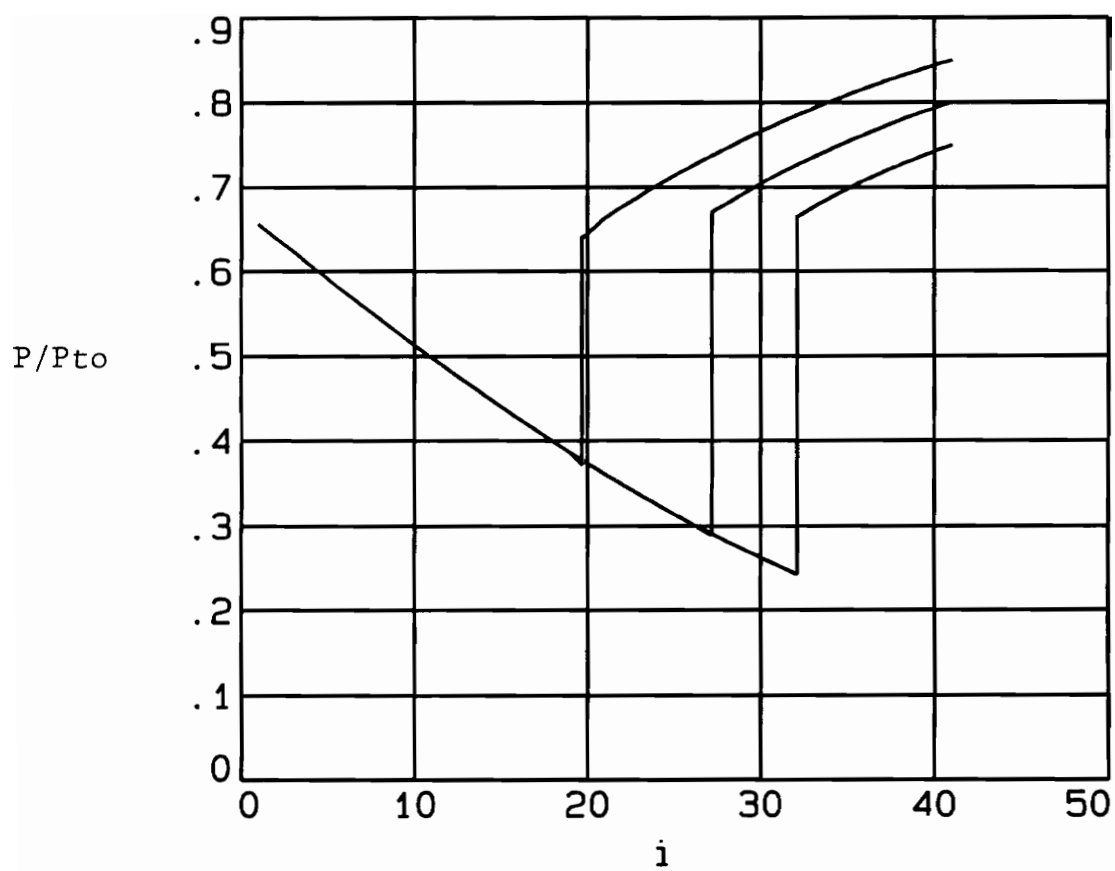


Fig. 5.2b Theoretical Pressure ratio values versus nozzle position for $P_{exit}/P_{to} = 0.85, 0.80, \text{ and } 0.75$

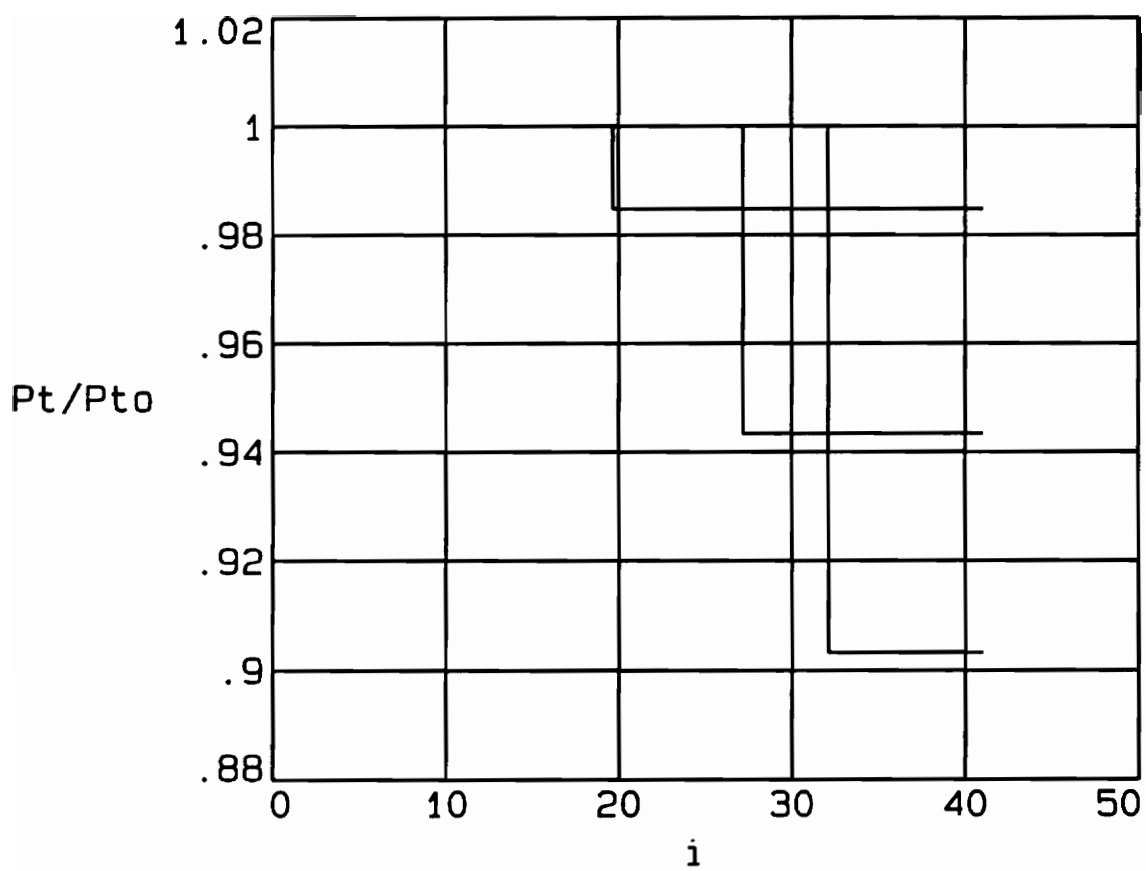


Fig. 5.2c Theoretical Total Pressure ratio values versus nozzle position for $P_{exit}/P_{t0} = 0.85, 0.80, \text{ and } 0.75$

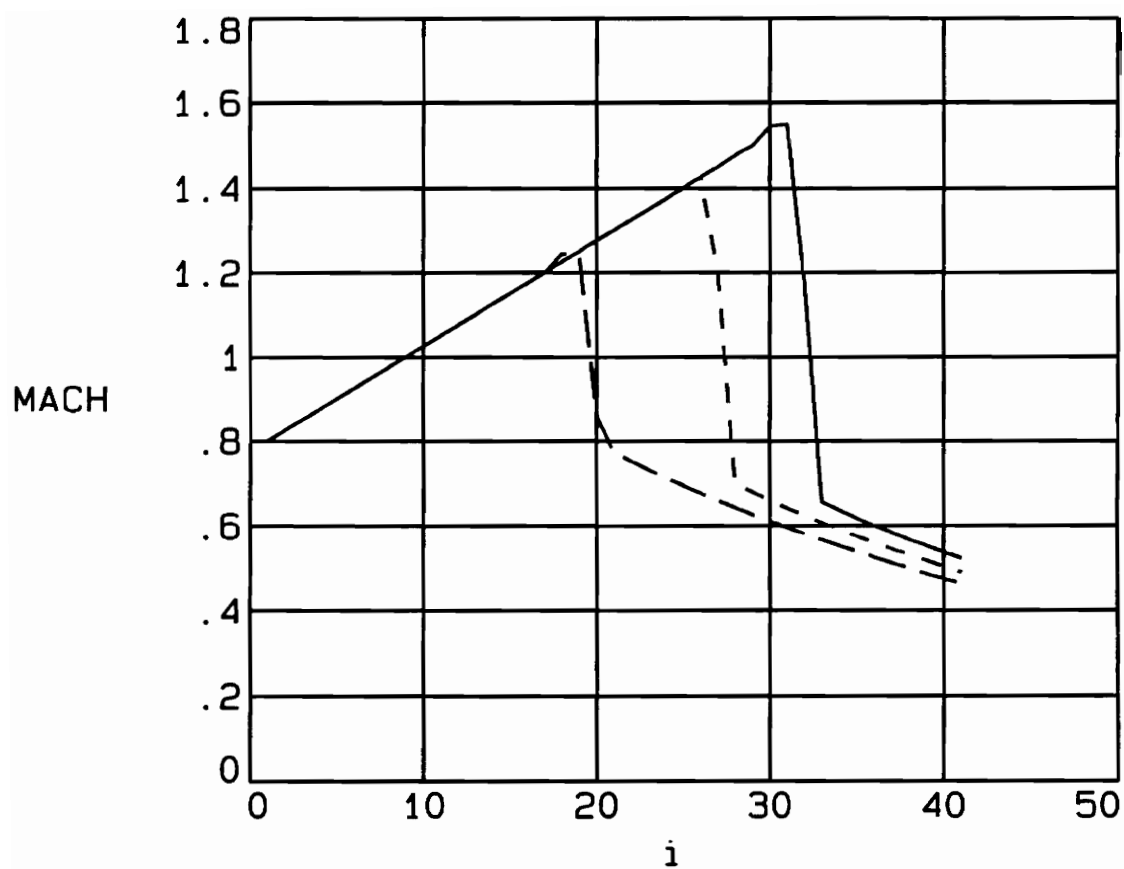


Fig. 5.3a 2M calculated Mach numbers versus nozzle position for $P_{exit}/P_{to} = 0.85, 0.80$, and 0.75

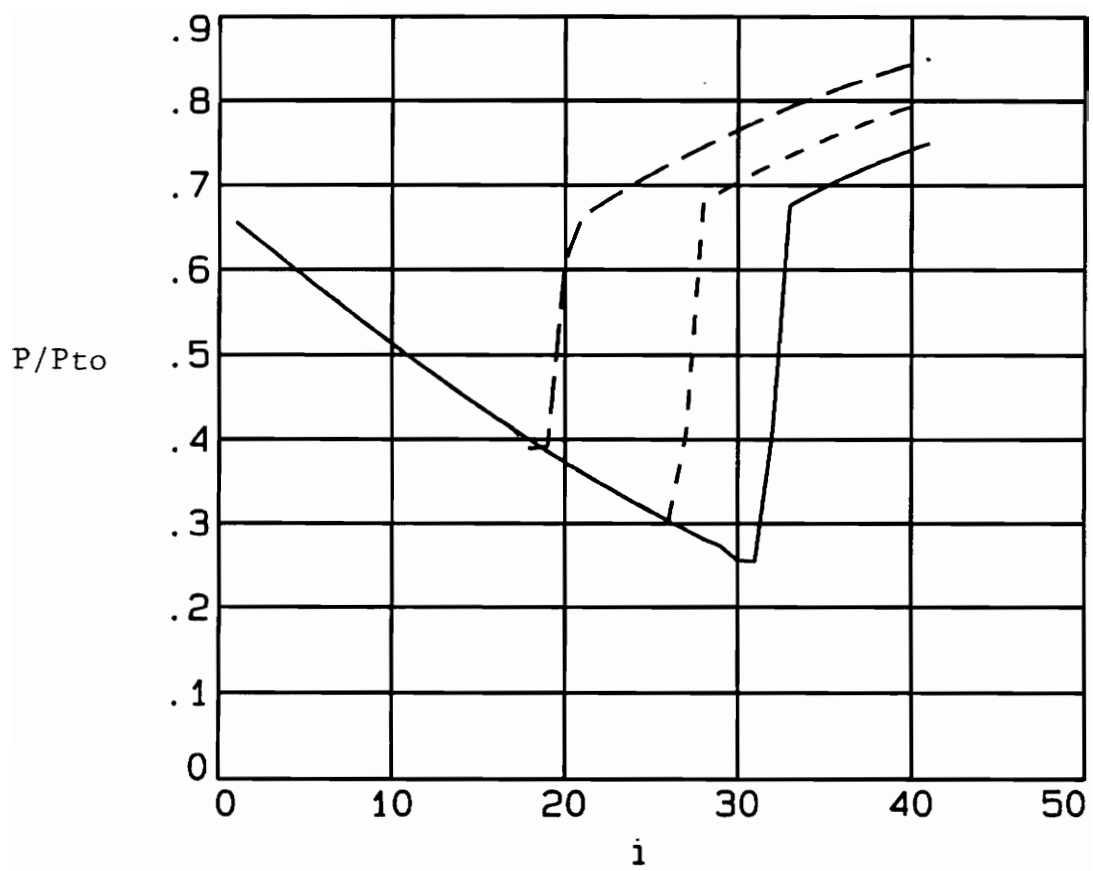


Fig. 5.3b 2M calculated Pressure ratio values versus nozzle position for $P_{exit}/P_{to} = 0.85, 0.80, 0.75$

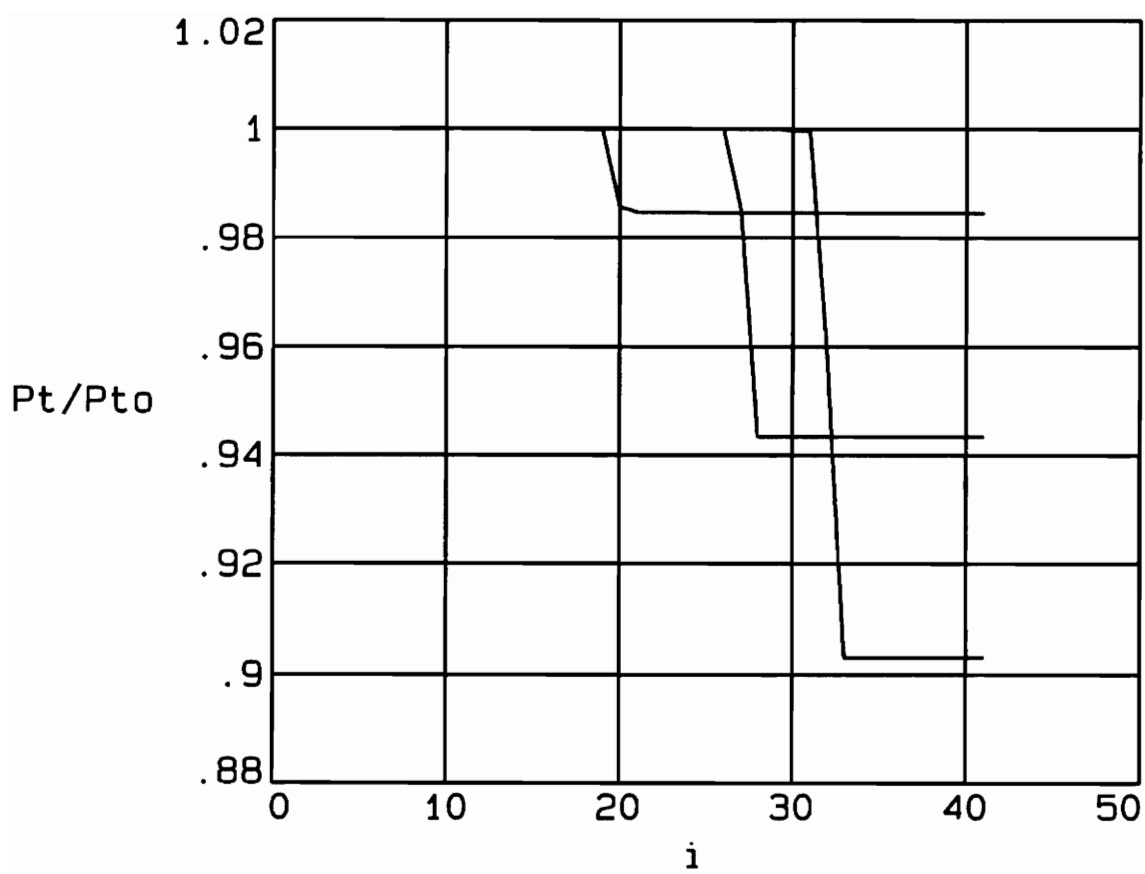


Fig. 5.3c 2M calculated Total Pressure ratio values versus nozzle position for $P_{exit}/P_{to} = 0.85, 0.80, \text{ and } 0.75$

slight undershoot in pressure, shown in Fig. 5.3b. The calculated total pressures across the shock, in Fig. 5.3c, closely match the theoretical total pressures, in Fig. 5.2c.

For each of the shock strengths tested, 1.1, 1.267, 1.455, 1.578, 2.5, and 3.5, the Mach numbers calculated using the M&M formula and the 2M formula are plotted versus nozzle position, and compared with the theoretical values. Figure 5.4 is an enlarged plot of the $M_{\text{shock}} = 1.1$ captured over 4 grid points. The 2M formula, shown as dashes in Fig. 5.4, sharpens the shock and gives an overshoot upstream of the shock. A significant improvement is noticed in Fig. 5.5 for the $M_{\text{shock}} = 1.267$ case. Figures 5.6 and 5.7 are the corresponding plots for the $M_{\text{shock}} = 1.455$ and $M_{\text{shock}} = 1.578$ cases. In all of these examples, the 2M formula captures a sharper shock than the M&M formula.

For the 2.5 shock case, both formulae give similar results, shown in Fig. 5.8. Figure 5.9 shows the 3.5 shock case, where the M&M formula gives a better estimate of the shock wave. This is due to the M&M formula being second order accurate for all Mach numbers, while the two Mach number formula is only second order accurate up to a Mach number of 2.2 (section 4.0). Thus, from this 1-D flow analysis, it can be concluded that the new method improves the shock capturing of the MEFP code for weaker shocks (say 1.0 to 2.0), but does not for stronger shocks (say > 2.5).

Table 5.1 summarizes the results of this 1-D nozzle test. For each case, the Mach number directly upstream and downstream of the shock and the total pressure ratio across the shock are recorded. The maximum Mach number upstream of the shock and the downstream Mach number that matches closely to the theoretical curve are chosen as the Mach numbers directly upstream and downstream of the shock.

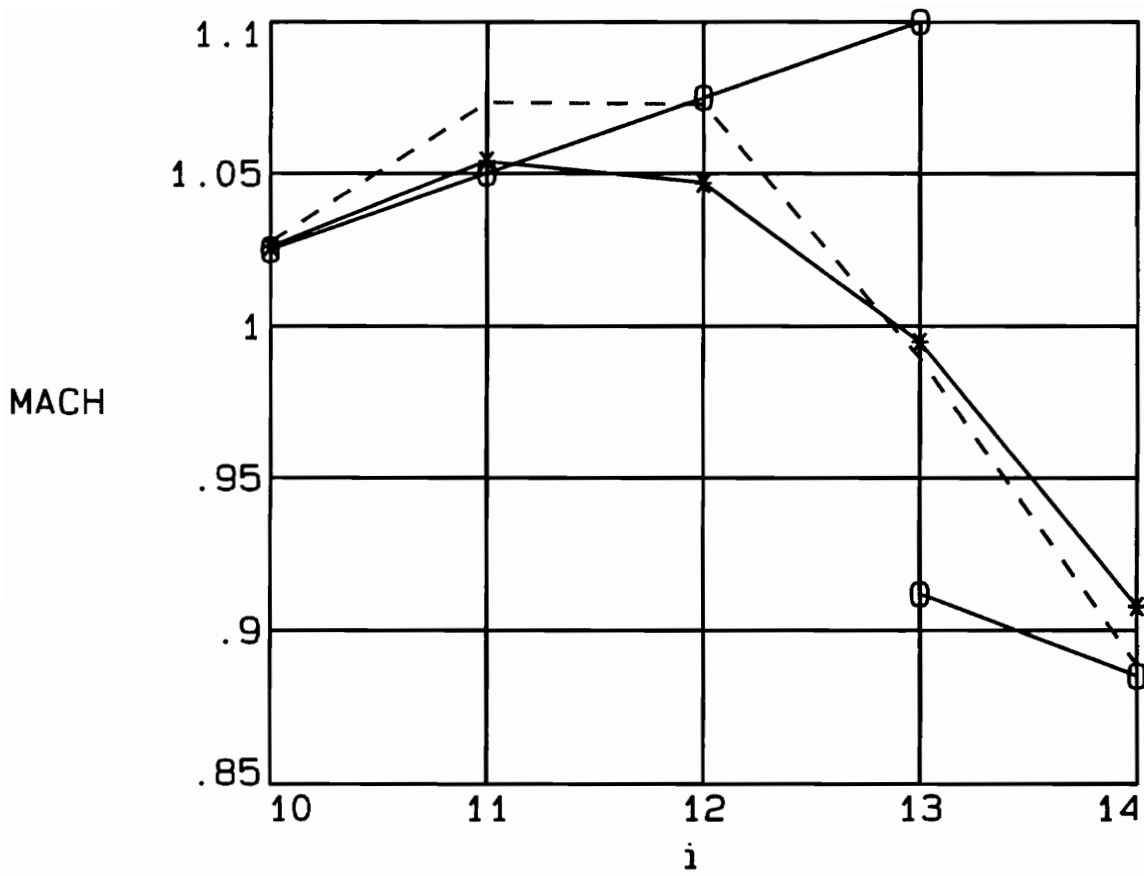


Fig. 5.4 Enlarged shock region for $M_{shock}=1.1$, $P_{exit}/P_{to} = 0.86687$

O theoretical
 - 2M formula
 * M&M formula

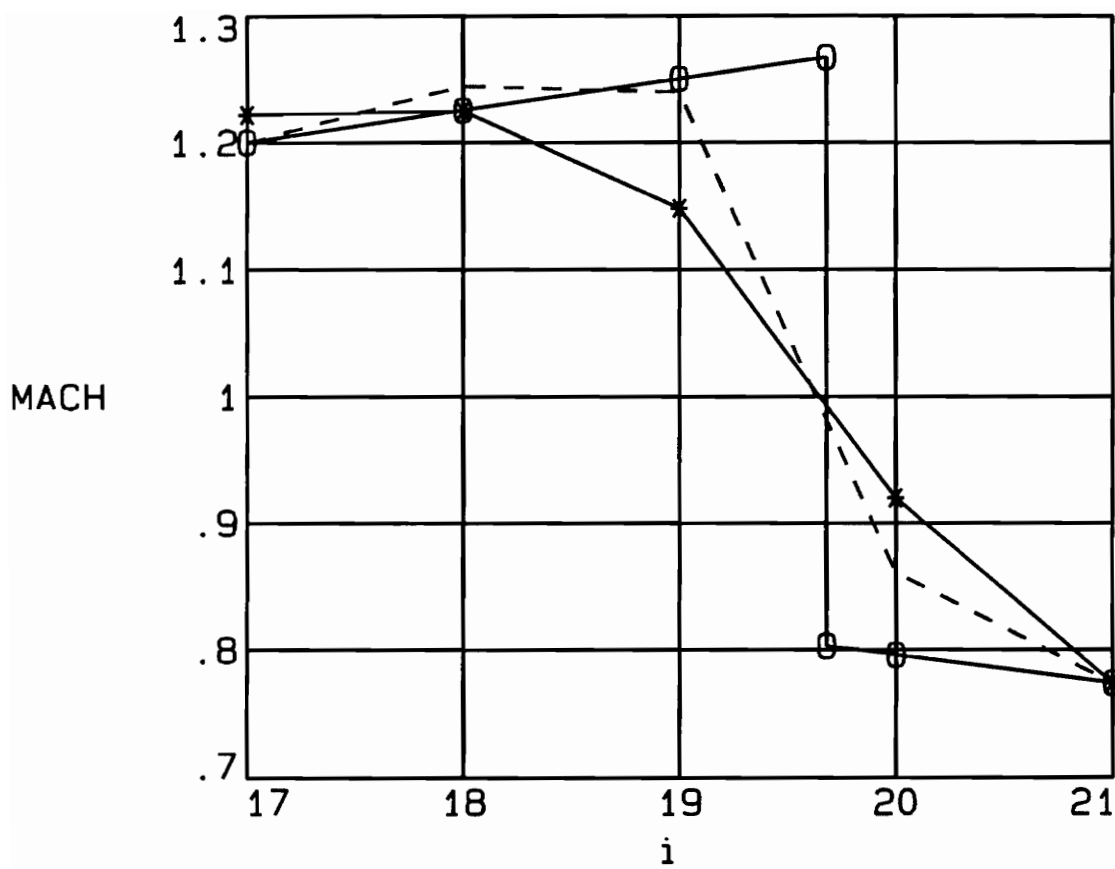


Fig. 5.5 Enlarged shock region for $M_{\text{shock}} = 1.267$, $P_{\text{exit}}/P_{\text{to}} = 0.85$

0 theoretical
 - 2M formula
 * M&M formula

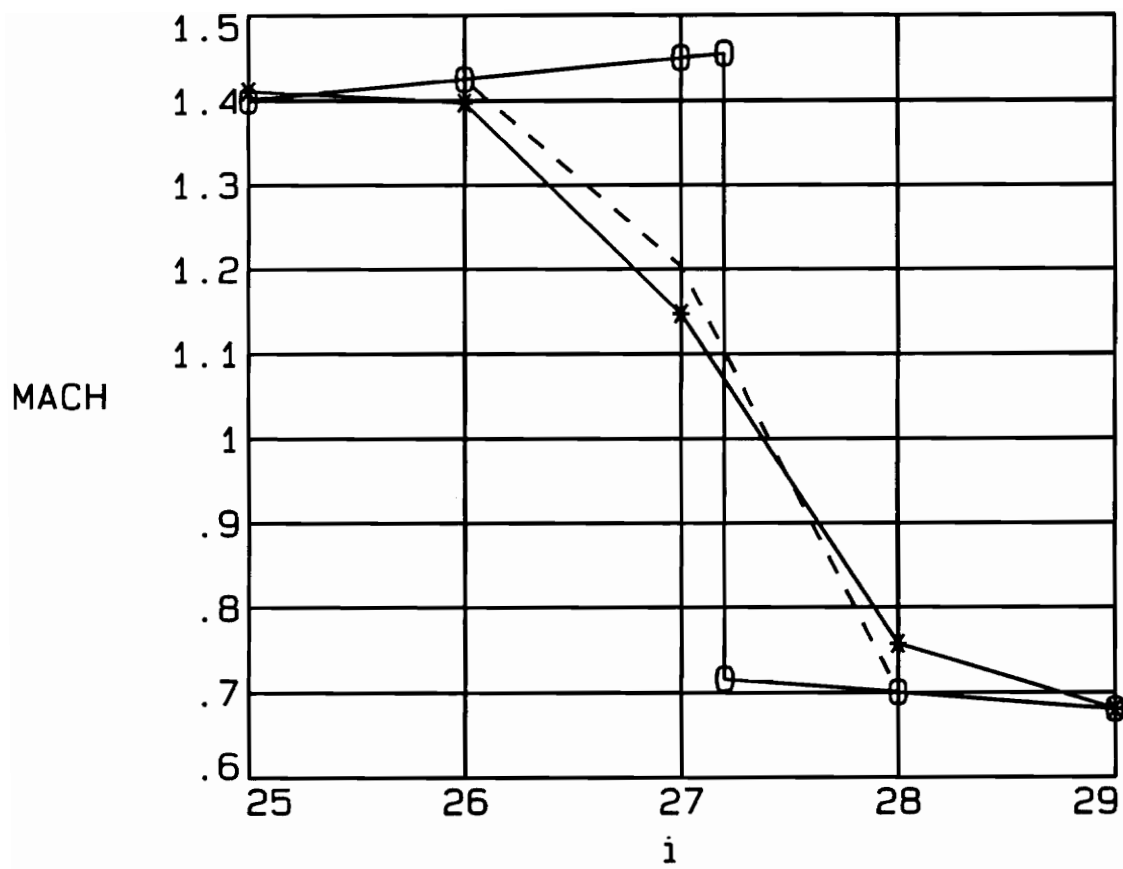


Fig. 5.6 Enlarged shock region for $M_{shock} = 1.455$, $P_{exit}/P_{to} = 0.80$

0 theoretical
 - 2M formula
 * M&M formula

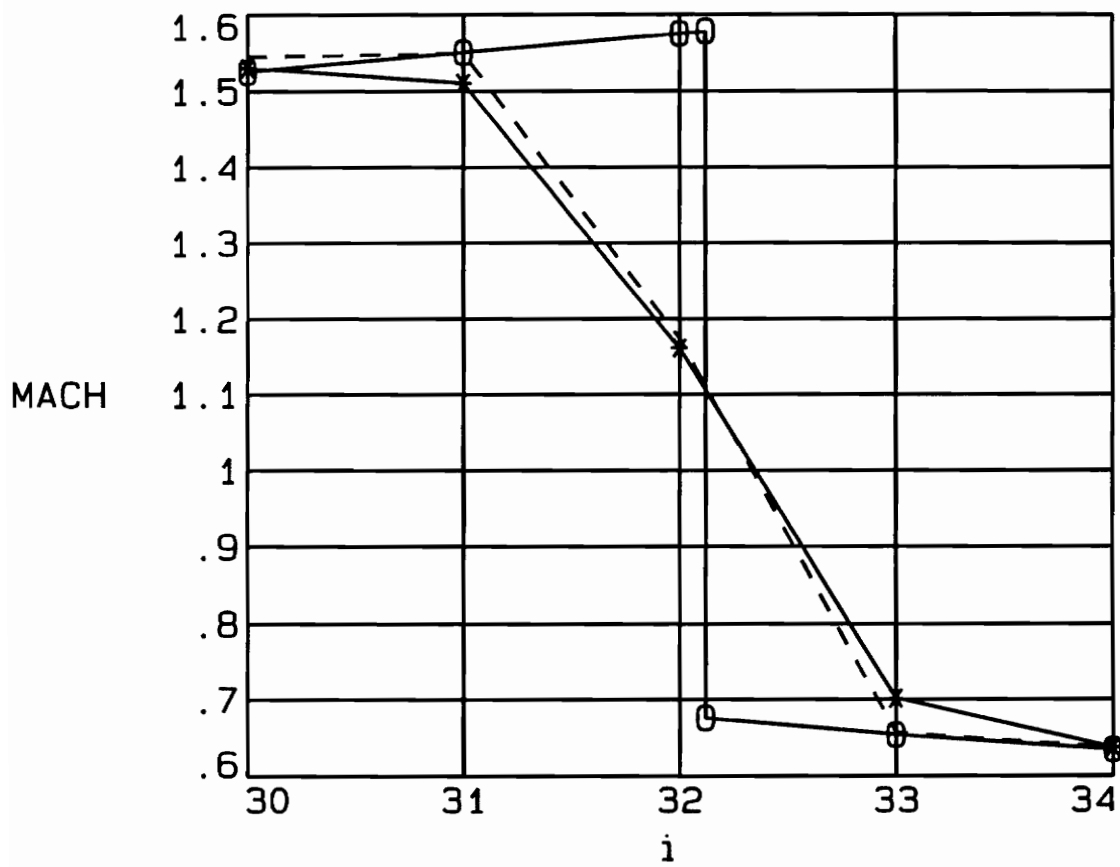


Fig. 5.7 Enlarged shock region for $M_{\text{shock}} = 1.578$, $P_{\text{exit}}/P_{\text{to}} = 0.75$

0 theoretical
 - 2M formula
 * M&M formula

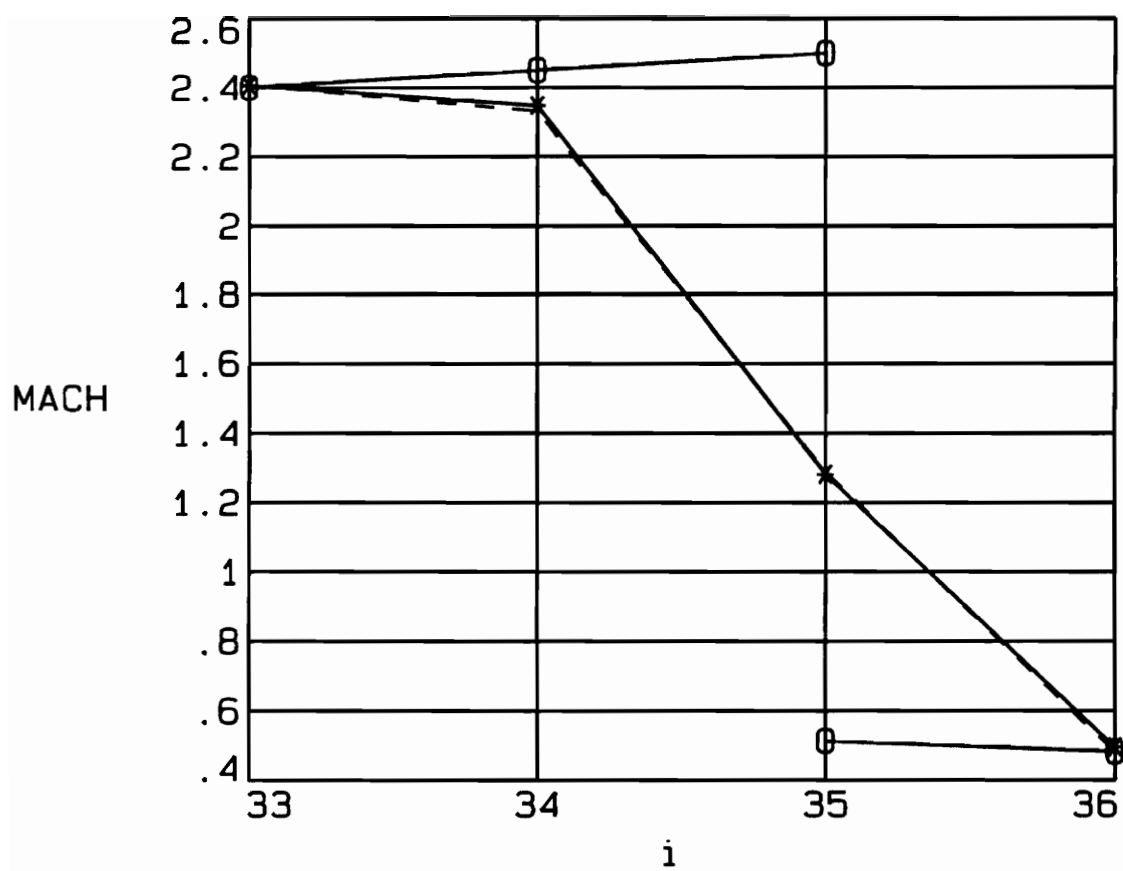


Fig. 5.8 Enlarged shock region for $M_{\text{shock}} = 2.5$, $P_{\text{exit}}/P_{\text{to}} = 0.47101$

0 theoretical
 - 2M formula
 * M&M formula

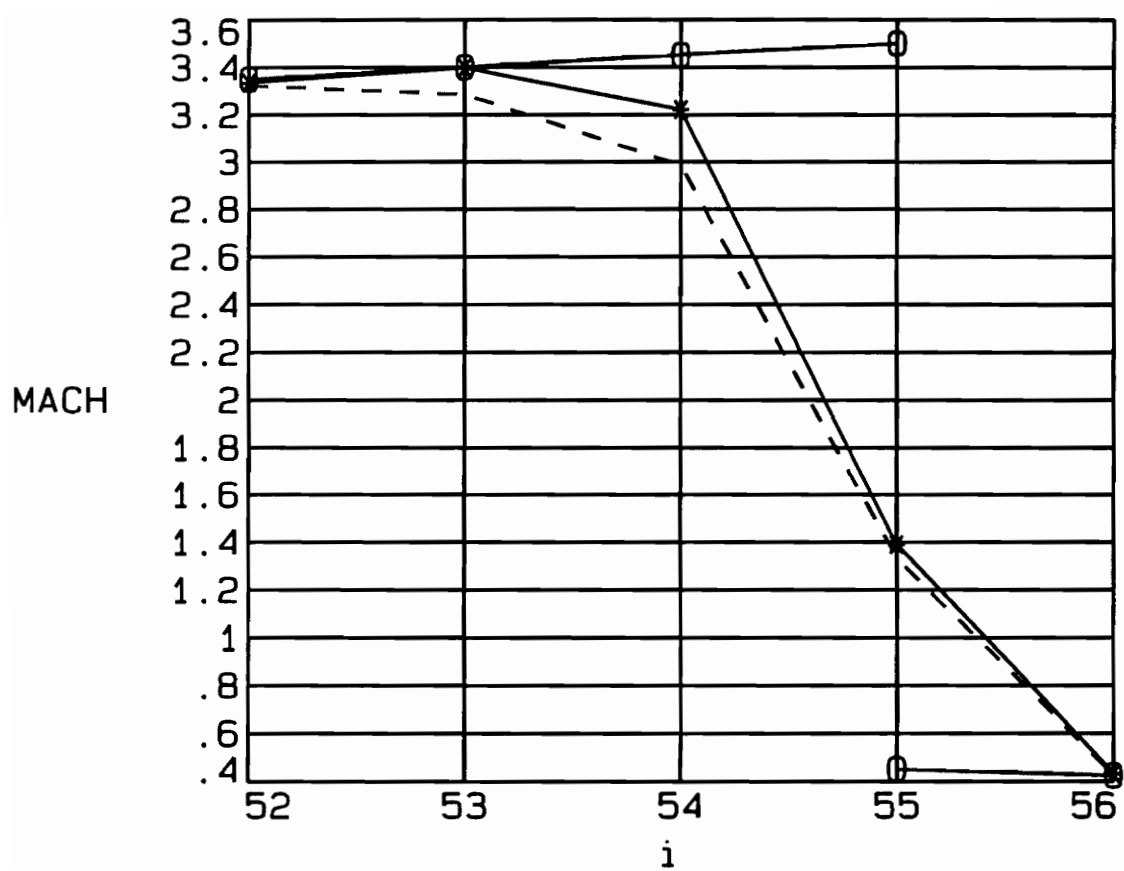


Fig. 5.9 Enlarged shock region for $M_{\text{shock}} = 3.5$, $P_{\text{exit}}/P_{\text{to}} = 0.20285$

0 theoretical
 - 2M formula
 * M&M formula

Table 5.1. Results from the M&M formula and 2M formula compared with theoretical values.

Table 5.1a. Mach number directly upstream / downstream of shock

<u>Pexit/Pto</u>	<u>Theoretical</u>	<u>M&M formula</u>	<u>2M formula</u>
0.86687	1.100/0.912	1.054/0.866	1.073/0.888
0.85	1.267/0.803	1.225/0.774	1.244/0.774
0.80	1.455/0.716	1.411/0.680	1.425/0.701
0.75	1.578/0.676	1.530/0.637	1.549/0.657
0.47101	2.500/0.513	2.406/0.495	2.407/0.481
0.20285	3.500/0.451	3.398/0.433	3.324/0.425

Table 5.1b. Total pressure ratio, Pt, exit / Pt, inlet

<u>Pexit/Pto</u>	<u>Theoretical</u>	<u>M&M formula</u>	<u>2M formula</u>
0.86687	0.99893	0.99891	0.99891
0.85	0.98475	0.98472	0.98472
0.80	0.94339	0.94335	0.94335
0.75	0.90320	0.90318	0.90318
0.47101	0.49901	0.49889	0.49889
0.20285	0.21295	0.21295	0.21295

From Figs. 5.4 - 5.9, the shock appears to be captured with both methods over 3 to 4 grid points, typically centered around the theoretical shock location. Also, both methods calculate similar shock losses, which match the theoretical solutions closely. This is at first surprising since the calculated Mach numbers directly upstream of the shocks are significantly lower than the theoretical values. But, for 1-D flow, the total pressure ratio is basically a measure of how well the transonic flow was modelled in the throat region.

6.0 Oblique Shock Capturing in a Cascade of Wedges

The full 3-D MEFP code is used to test oblique shock capturing in Denton's supersonic staggered wedge cascade [8], shown in Fig. 6.1. It should be noticed from Fig. 6.1 that the suction side of the blade remains flat and the pressure side has two corners. The flow is uniform at the inlet with a Mach number of 1.6 and is parallel to the suction side of the blade. An oblique shock occurs at the leading edge due to the flow turning of 5.727° caused by the wedge. The angle of this shock is at 45° to the incoming flow. The shock is then reflected off the suction side of the lower blade at an angle of 48.2° as shown in Fig. 6.1. It then theoretically cancels at the first corner on the pressure side. At the second corner, a Prandtl-Meyer expansion fan is produced. A third oblique shock is generated at the trailing edge and acts to straighten the pressure side flow. The four regions are labeled with their corresponding Mach numbers, $M_1 - M_4$, in Fig. 6.1. The first two oblique shocks are of primary importance for this test case. The normal Mach numbers and total pressure losses across each shock are given in Table 6.1. It should be noticed that the normal Mach numbers for the three oblique shocks are about the same, $M_n \sim 1.13$, and thus the shocks should theoretically have equal total pressure ratios (losses).

Four different grids were used: 43×22 , 82×22 , 82×42 , and 123×42 in order to check the influence of grid refinement on shock capturing. Figure 6.2 shows the full 43×22 grid, with 43 grid points in the flow direction and 22 grid points in the blade-to-blade (vertical) direction. For the master grid geometry, the variable in the flow direction, A , is assigned a value of -1 at the inlet, 0 at the leading edge, 1 at the first corner, 2 at the second corner, 3 at the

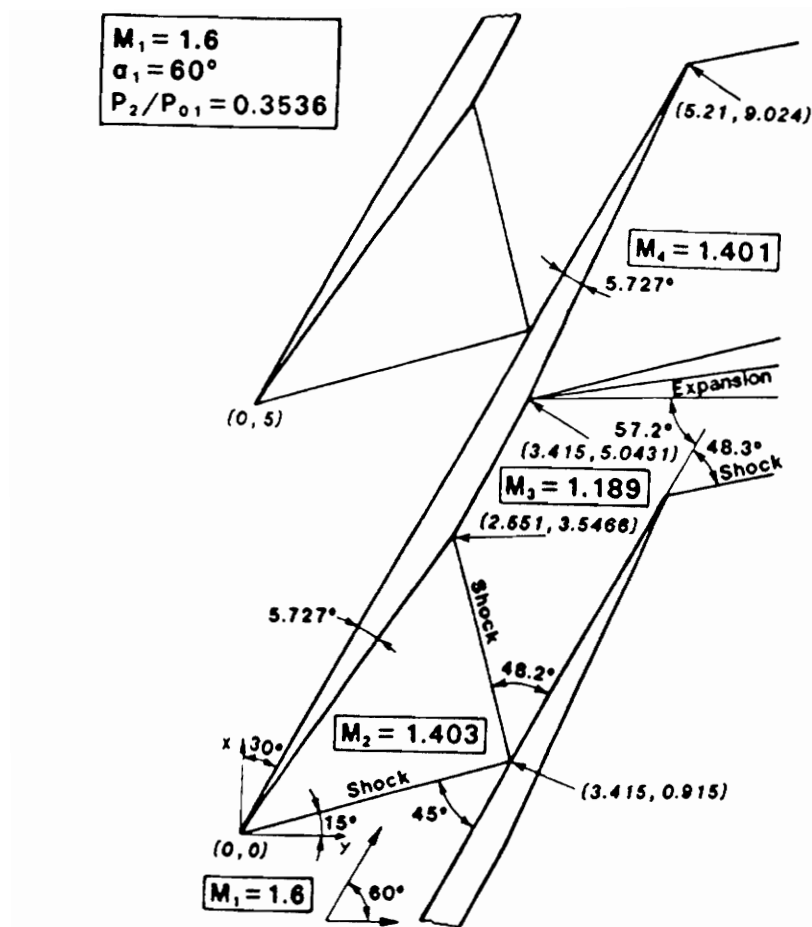


Fig. 6.1 Denton's Cascade of Wedges [8]

Table 6.1 Total and normal Mach numbers and total pressure losses across the oblique shocks

<u>Mach number</u>	<u>Normal Mach Numbers</u>	<u>Pt/Pt₁</u>
M ₁ = 1.6	M _{1n} = 1.13137 M _{2n} = 0.88823	Pt ₂ /Pt ₁ = 0.997702
M ₂ = 1.403	M _{2n} = 1.13399 M _{3n} = 0.88633	Pt ₃ /Pt ₂ = 0.997573 Pt ₃ /Pt ₁ = 0.995281
M ₄ = 1.401	M _{4n} = 1.13382 M _{5n} = 0.88646	Pt ₅ /Pt ₄ = 0.997582 Pt ₅ /Pt ₁ = 0.992874

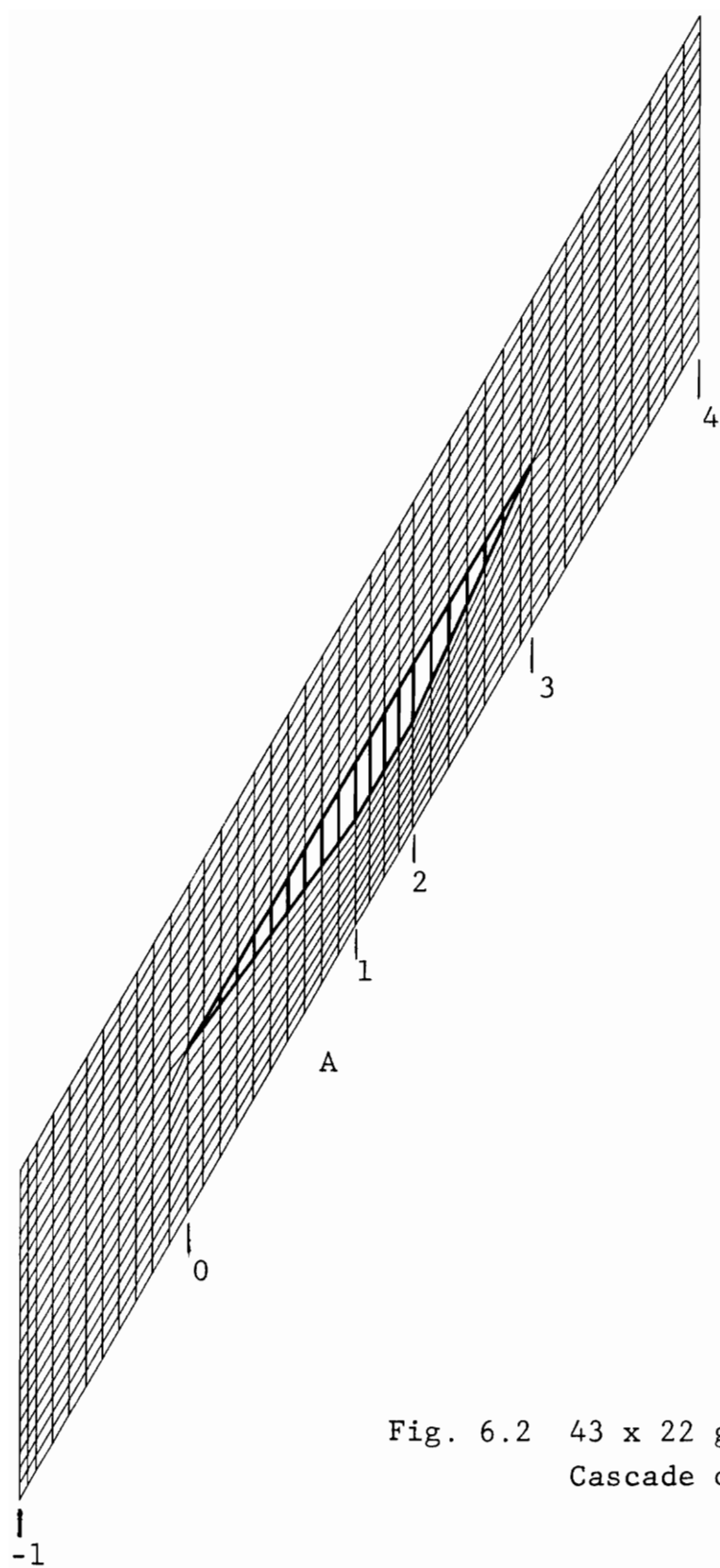


Fig. 6.2 43 x 22 grid for
Cascade of Wedges

trailing edge, and 4 at the exit. The other three grids use the same master geometry. An enlarged plot of the $A = 0$ to $A = 2$ region is shown in Fig. 6.3a for the 43×22 and 82×22 grids. Figure 6.3b is an enlarged plot for the 82×42 and 123×42 grids. In each figure, the theoretical shock locations are sketched to emphasize the shock direction relative to the control volumes and the number of grid points in the shock region. The first shock is diagonal to the control volume whereas the second shock is more parallel to the blade-to-blade grid lines. For the coarse 43×22 grid, the first shock crosses 13 grid lines in the flow direction, while the second shock only crosses 3 grid lines.

The results obtained using the M&M formula are shown in Figs. 6.4 - 6.6. The Mach number and total pressure ratio across the wedge are given in Fig. 6.4a for the 43×22 grid. The corresponding plots for the 82×22 grid, 82×42 grid, and the 123×43 grid are shown in Figs. 6.4b, 6.4c, and 6.4d. As expected, the shocks get sharper with grid refinement. Each of these figures shows a slight expansion, followed by two oblique shocks, an expansion, and a shock off the trailing edge; thus the flow code calculates all of the regions observed in Fig. 6.1.

The regions are most clearly distinguished in Fig. 6.4d which shows the results with the finest grid. The calculated Mach numbers agree quite closely with the theoretical solution. The Mach number upstream of the first shock is about 1.6, falling to just above 1.4 after the first shock, and to just below 1.2 after the second shock. It then rises to about 1.4 following the Prandtl-Meyer expansion.

The total pressure losses across the first two shocks are clearly seen (Fig. 6.4d), while the calculated loss across the trailing edge shock is somewhat smaller. These contours also show errors in total pressure starting just

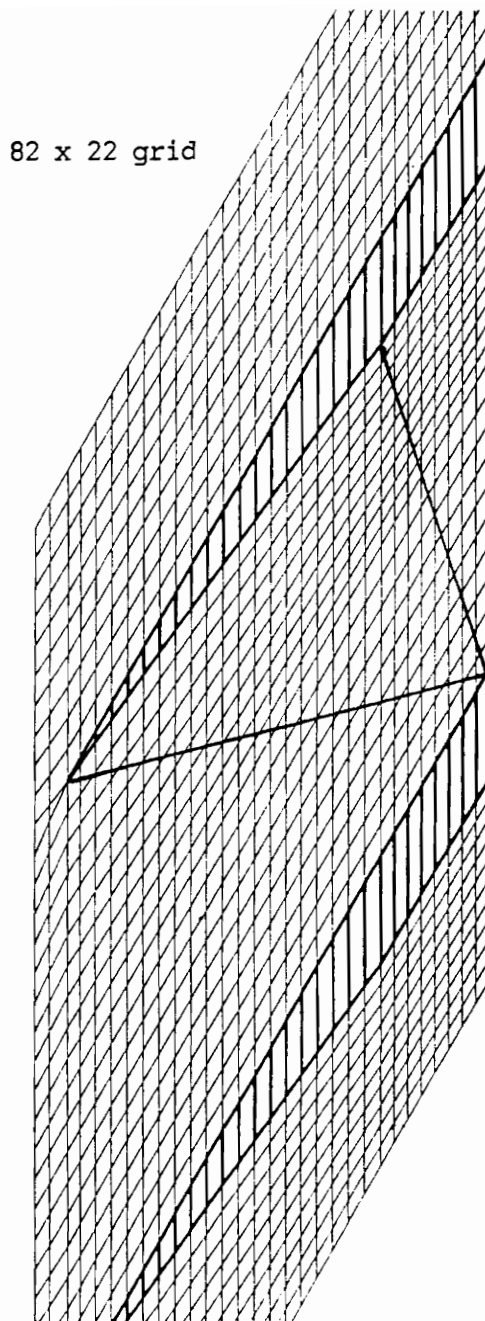
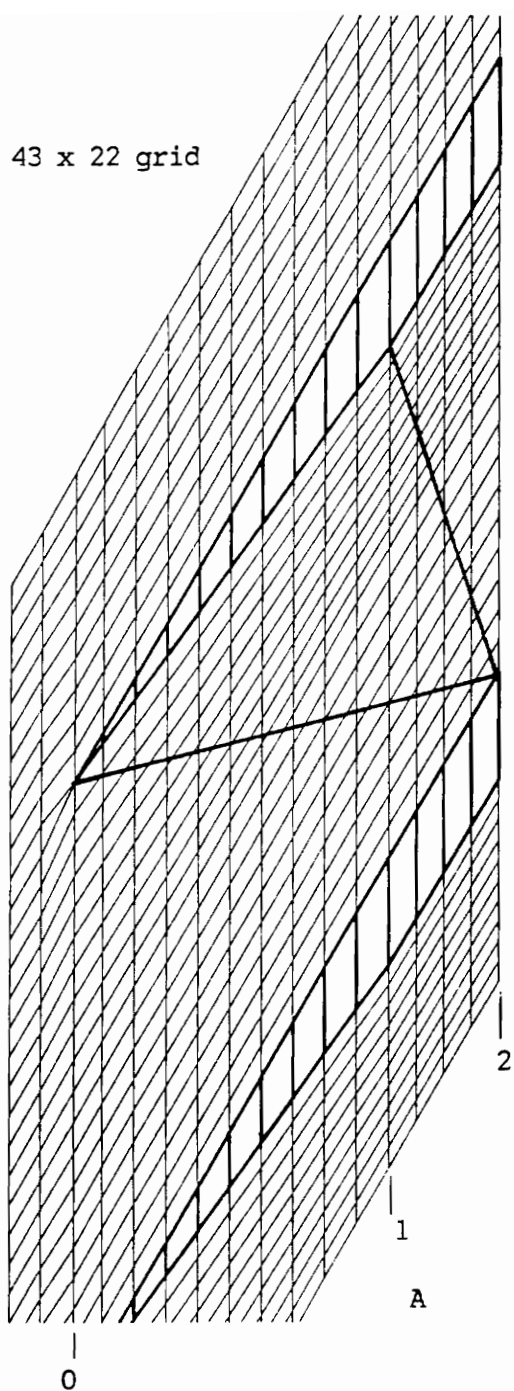
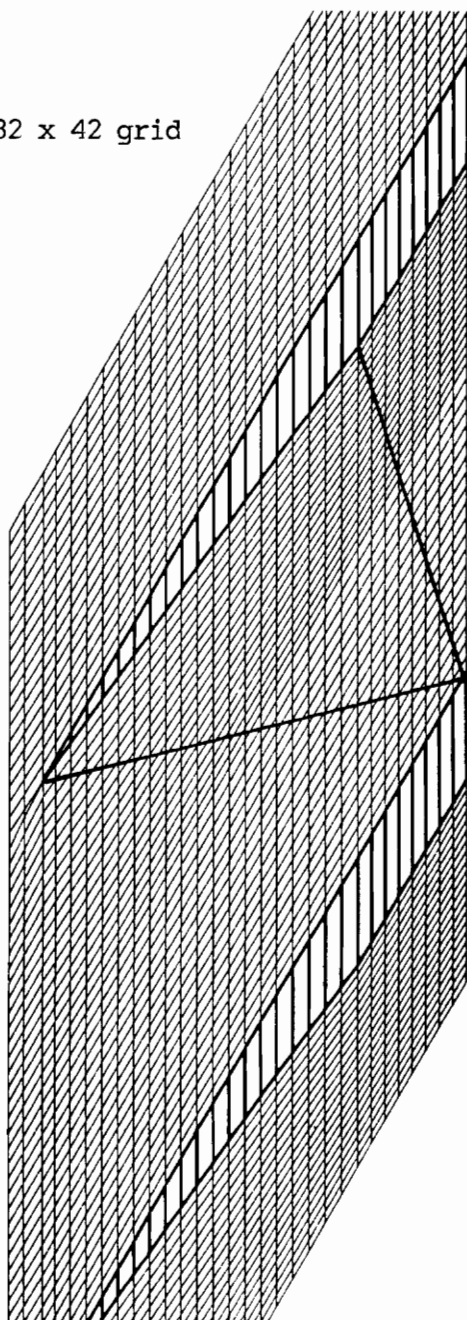


Fig. 6.3a Enlarged oblique shocks region ($A=0$ to $A=2$)
for 43 x 22 and 82 x 22 grids

82 x 42 grid



123 x 42 grid

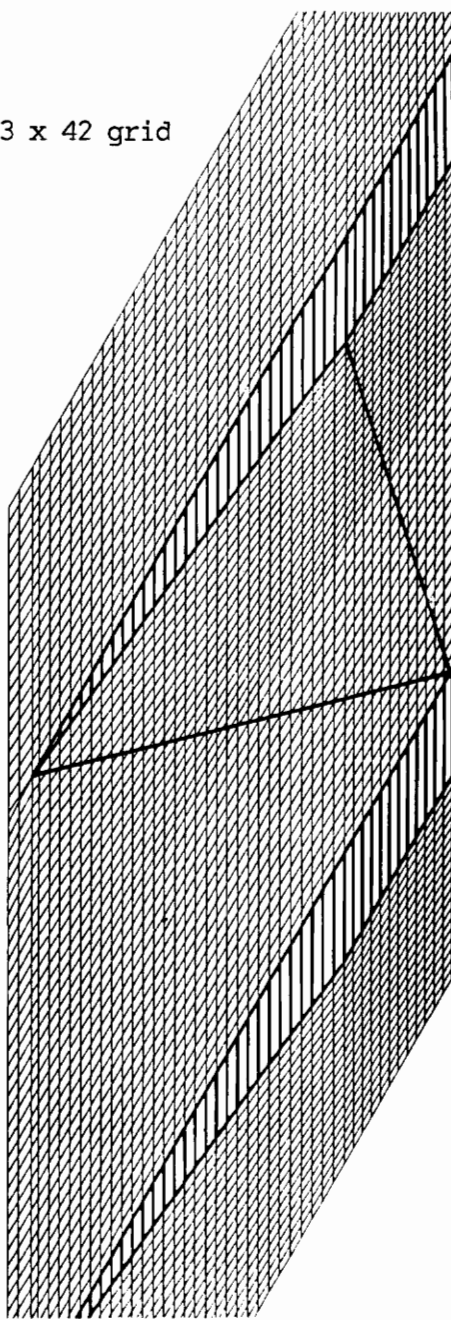


Fig. 6.3b Enlarged oblique shocks region ($A=0$ to $A=2$)
for 82 x 42 and 123 x 42 grids

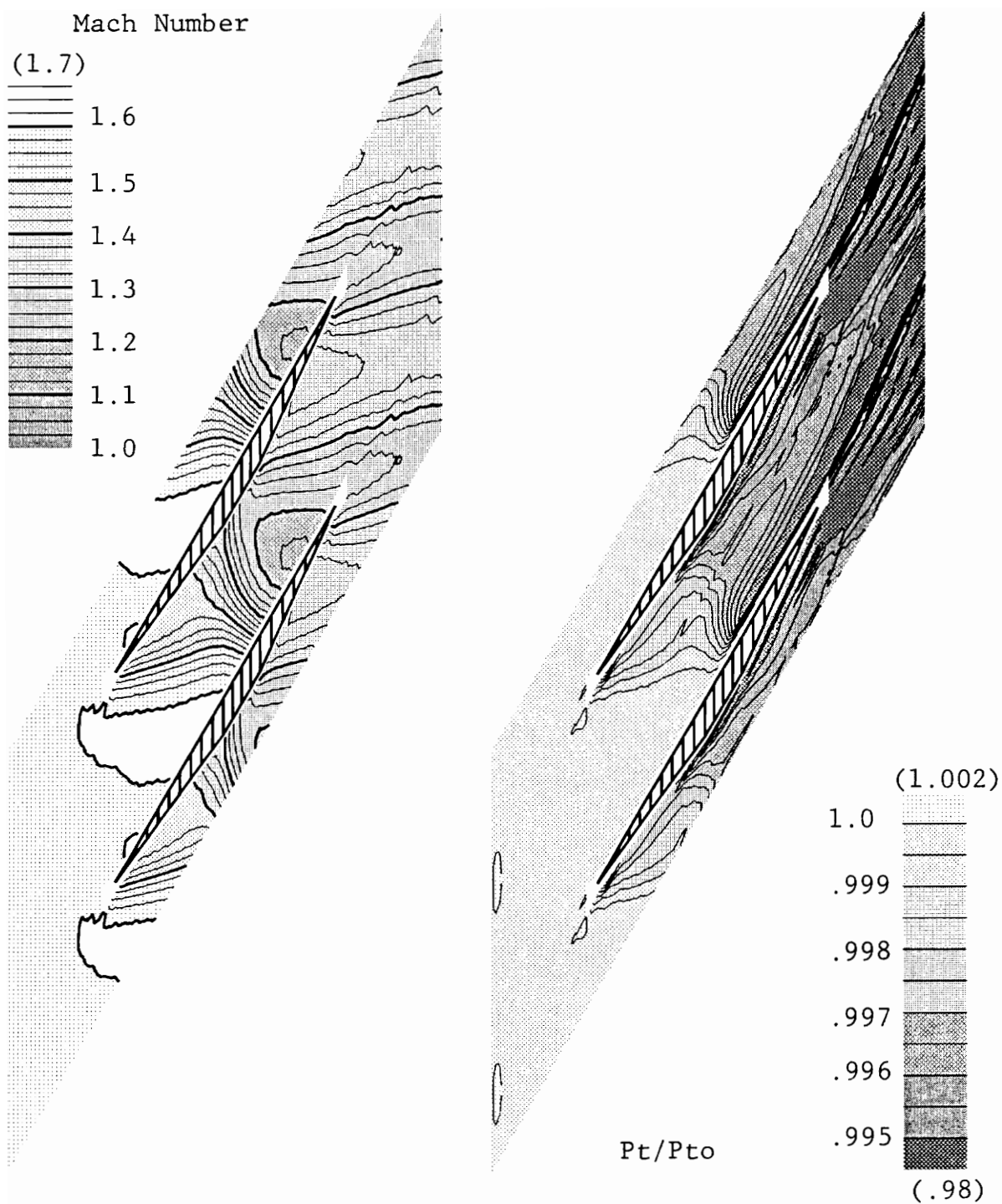


Fig. 6.4a Mach number and Pt/Pto contours
for 43 x 22 grid

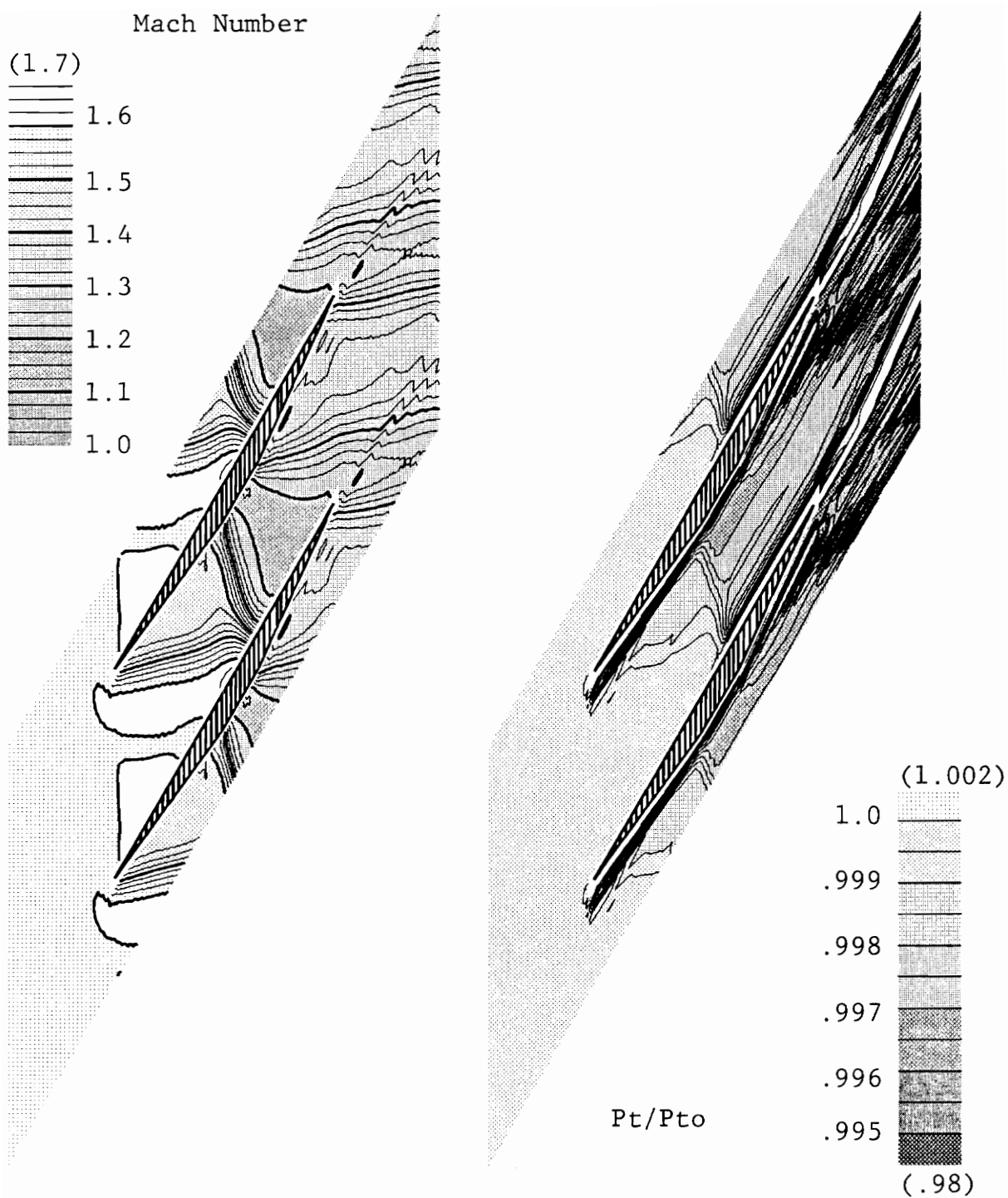


Fig. 6.4b Mach number and Pt/Pto contours
for 82 x 22 grid

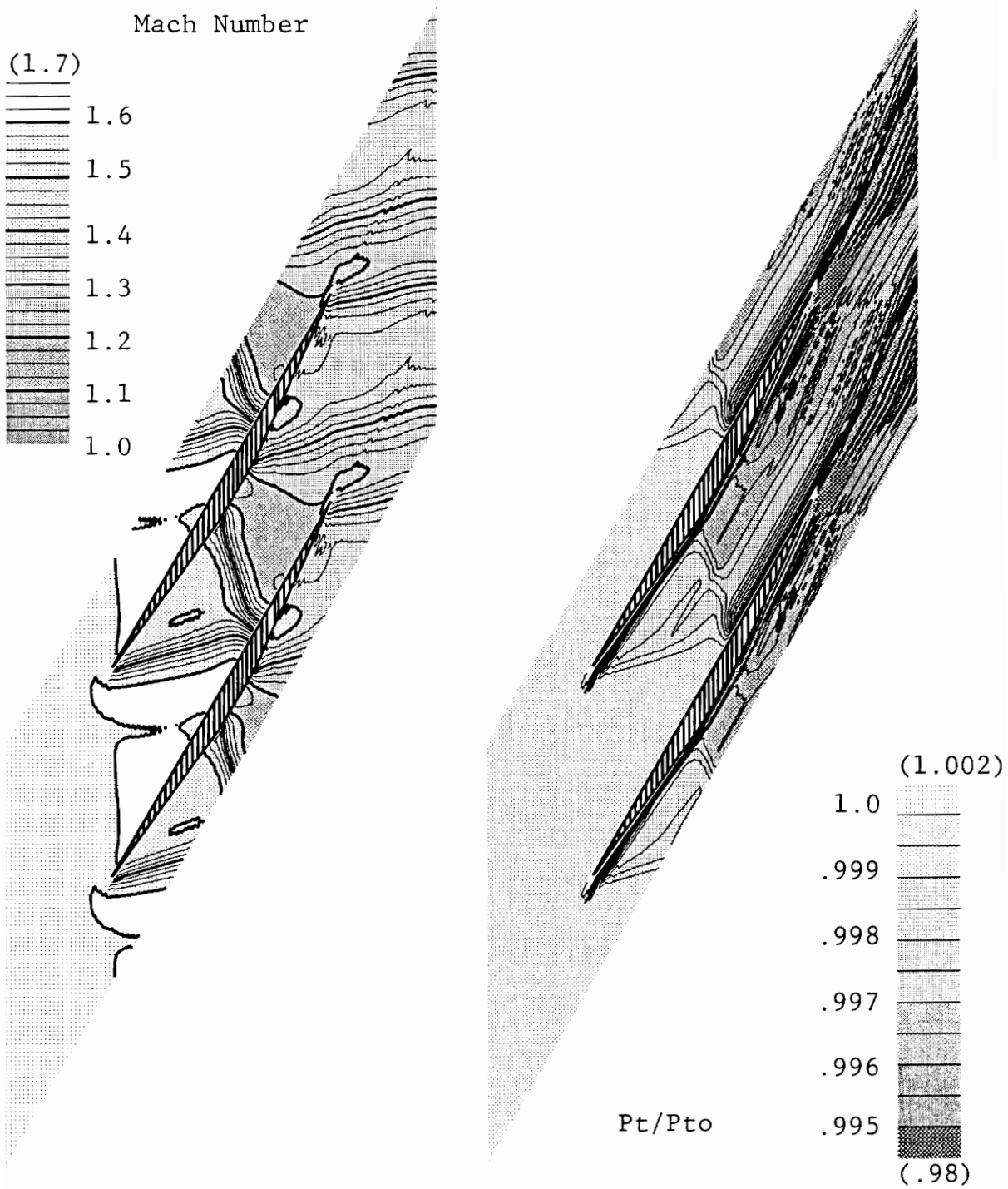


Fig. 6.4c Mach number and Pt/Pto contours
for 82 x 42 grid

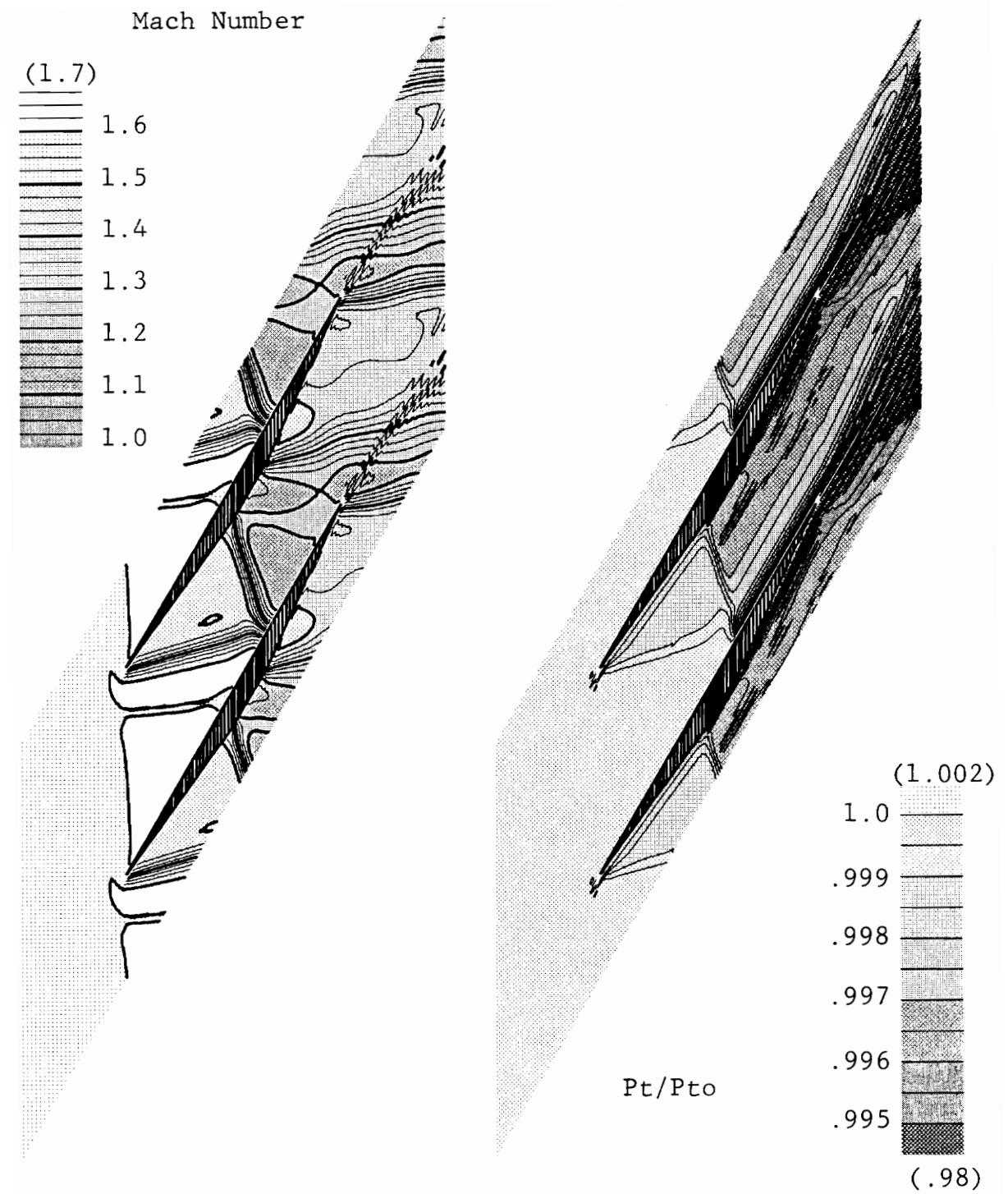


Fig. 6.4d Mach number and Pt/Pto contours
for 123 x 42 grid

upstream of the leading edge of the blade and extending along the pressure surface, and starting near the suction surface after the shock reflection. These errors are associated with discretization errors at the near-wall grid points. There are two probable causes for these errors, the approximations made to run the viscous flow code in inviscid mode, and the handling of the cusped leading edge as very small blunt leading edge with 2 grid points.

Plots of the Mach number and total pressure ratio along the repeating boundary of the 43 x 22 grid are provided in Fig 6.5a and compared with the theoretical values. The corresponding plots for the 82 x 22 grid, 82 x 42 grid, and the 123 x 43 grid are shown in Figs. 6.5b, 6.5c, and 6.5d. From these figures, it is evident that the calculated Mach numbers match the theoretical solution closely. However, it appears that not enough losses are calculated for the first shock while the second shock gets about the right losses, at least for the finest grid. This might be due to the direction of the shocks crossing the control volumes. Since the first two oblique shocks are of primary interest, the discrepancies of total pressure losses at the trailing edge are not considered. Table 6.2 summarizes the Mach numbers and total pressure losses after the first two shocks and the expansion region for each grid case.

Figure 6.6 gives the mass averaged total pressure from the inlet to the trailing edge. At the trailing edge, $A = 3$, the theoretical total pressure ratio is .9953. The 43 x 22 grid gives about 90% of the actual losses while the other cases have only about 70 to 80% of the losses. The order of the curves suggests that the errors in the loss prediction are not a simple function of grid fineness. This level of agreement in predicting the loss within the blade row is reasonable for a cascade with such low losses.

The 2M formula gives results similar to the M&M formula, such that the

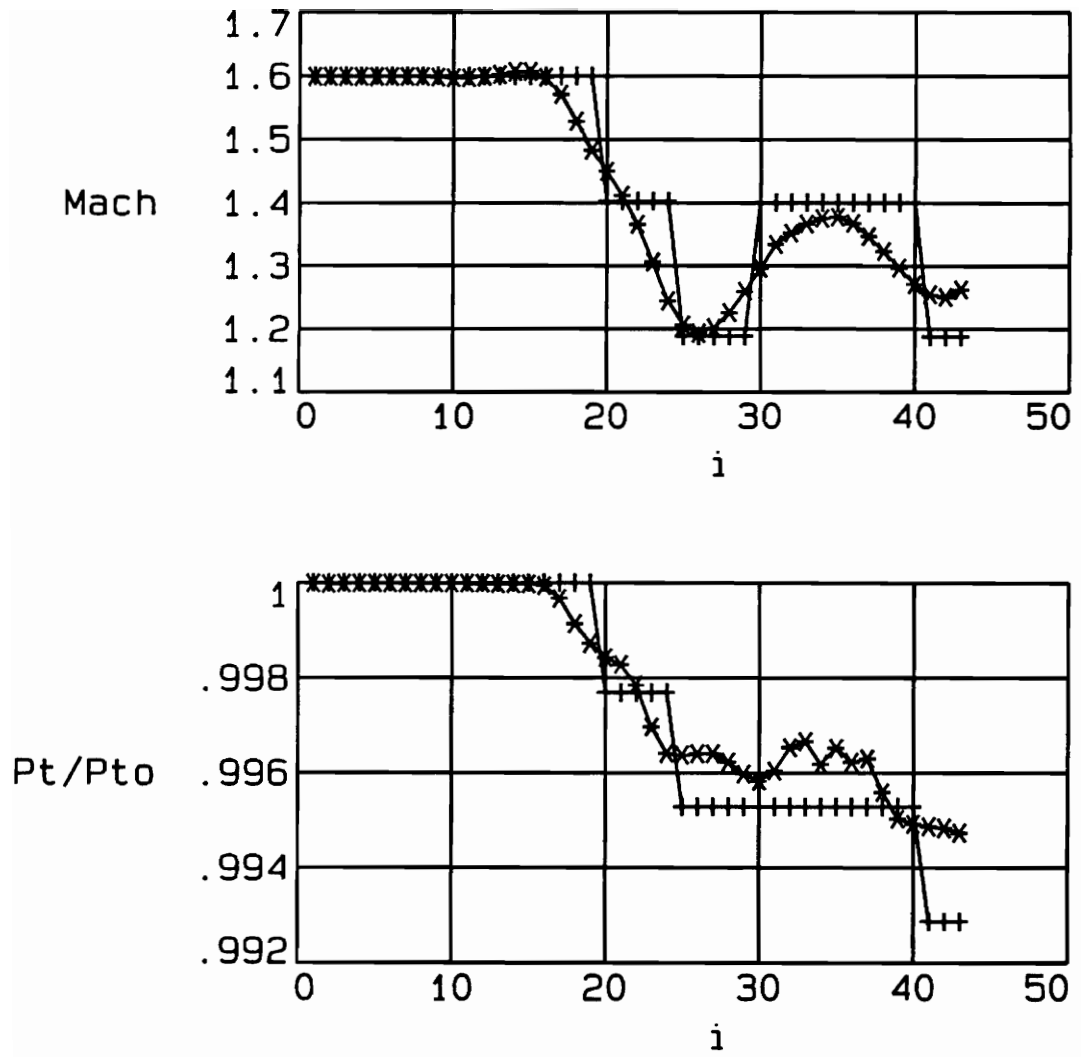


Fig. 6.5a Repeating Boundary Mach number and P_t/P_{t0} distributions for 43 x 22 grid case

- + theoretical solution
- * calculated solution using M&M formula

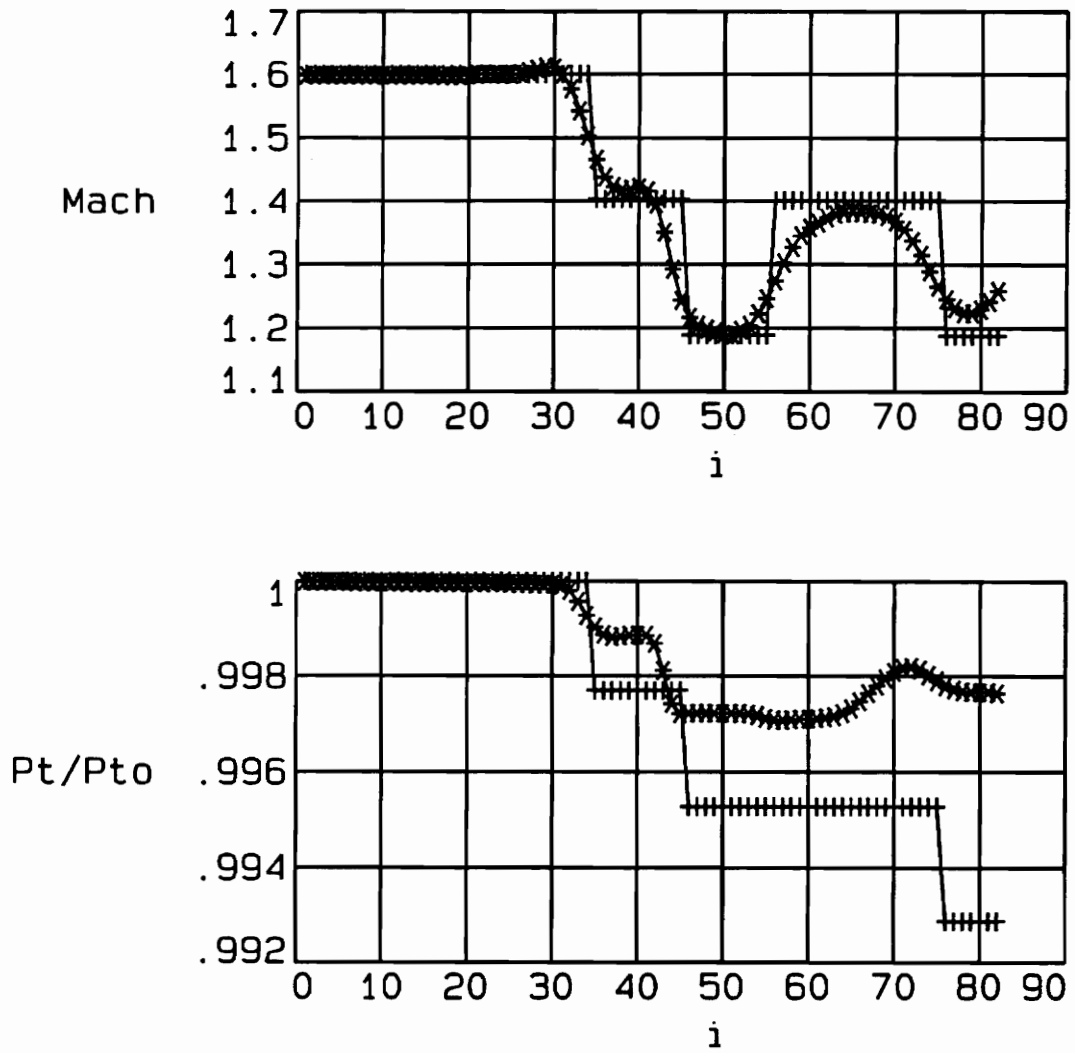


Fig. 6.5b Repeating Boundary Mach number and P_t/P_{t0} distributions for 82 x 22 grid case

- + theoretical solution
- * calculated solution using the M&M formula

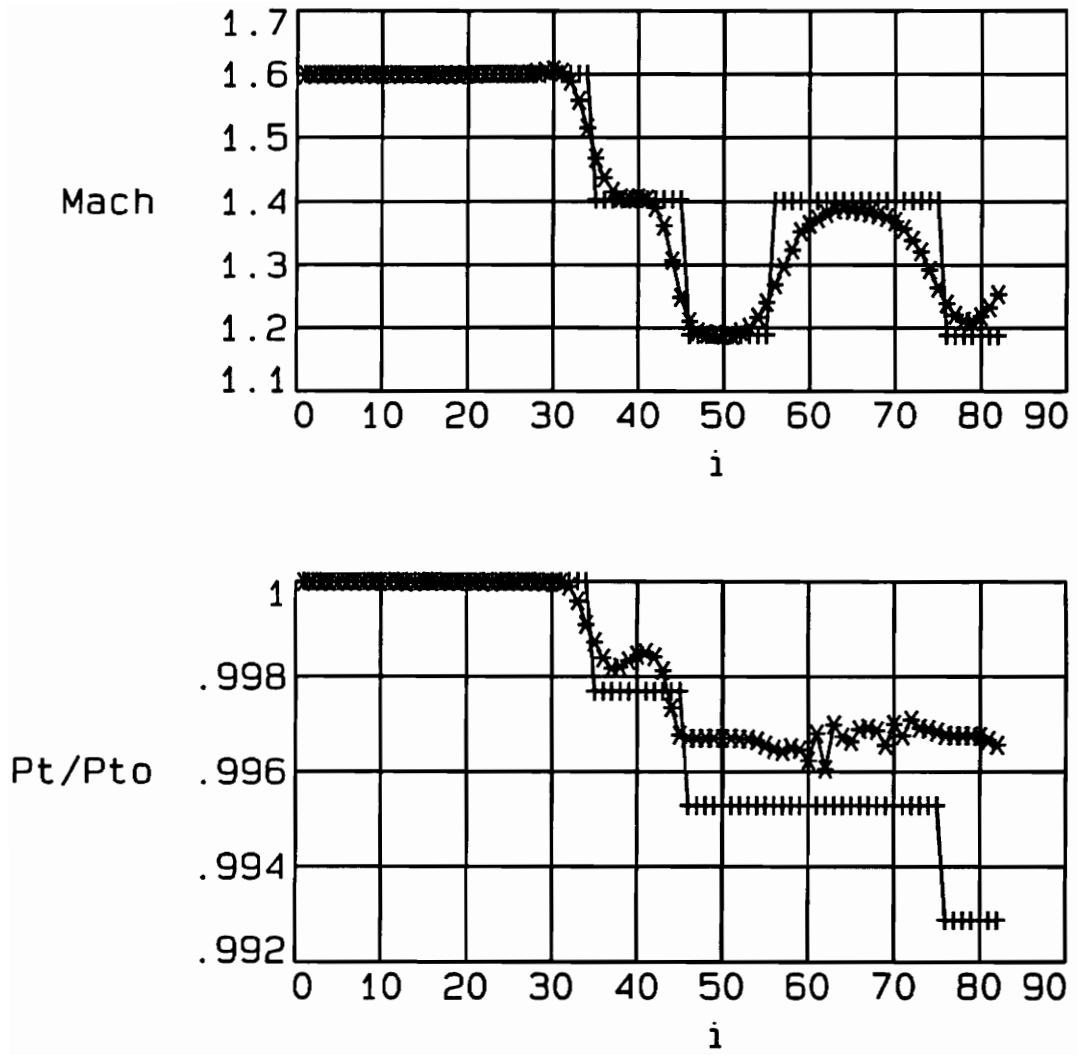


Fig. 6.5c Repeating Boundary Mach number and P_t/P_{t0} distributions for 82 x 42 grid case

- + theoretical solution
- * calculated solution using the M&M formula

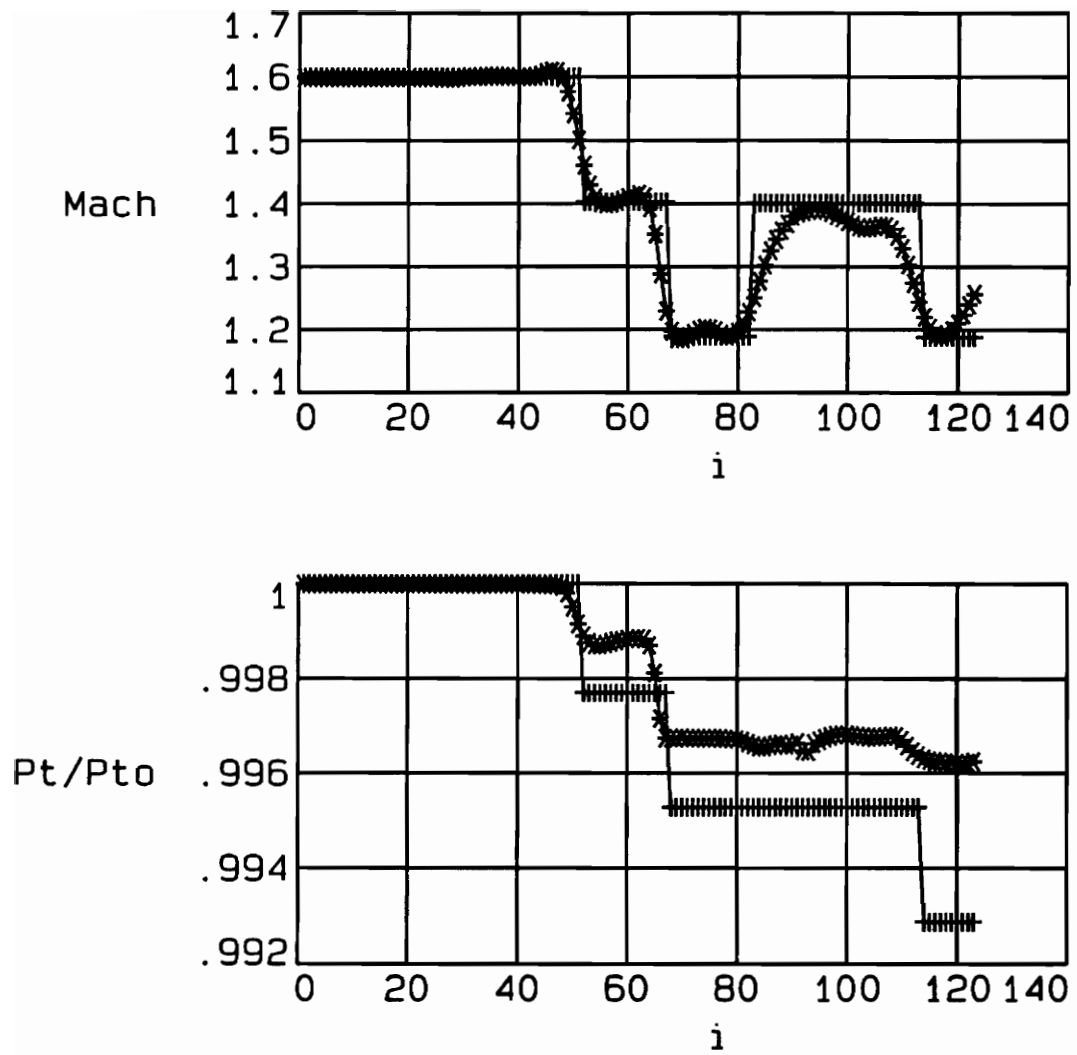


Fig. 6.5d Repeating Boundary Mach number and P_t/P_{t0} distributions for 123 x 42 grid case

- + theoretical solution
- * calculated solution using the M&M formula

Table 6.2 Repeating Boundary Mach Numbers and Total Pressure Losses

		After 1st Shock	After 2nd Shock	Expansion
Grid		Mach Number	Mach Number	Mach Number
43 x 22		1.4505	1.1937	1.3782
82 x 22		1.4179	1.1892	1.3817
82 x 42		1.4043	1.1883	1.3863
123 x 43		1.3987	1.185	1.3717
Ideal		1.403	1.189	1.401
Grid		1 - Pt/Pto	1 - Pt/Pto	1 - Pt/Pto
43 x 22		0.0016	0.0036	0.0035
82 x 22		0.0012	0.0028	0.0027
82 x 42		0.0017	0.0033	0.0034
123 x 43		0.0013	0.0033	0.0032
Ideal		0.0023	0.0047	0.0047

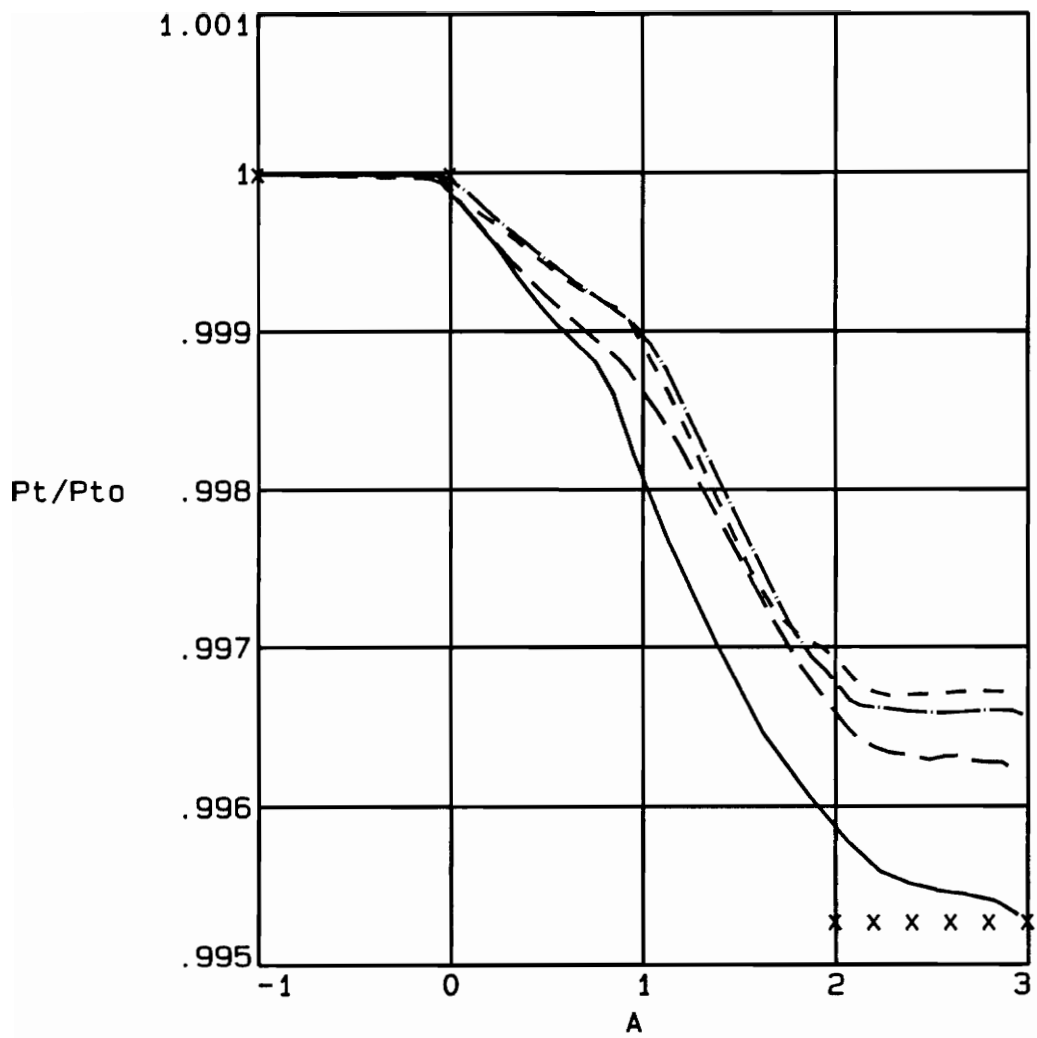


Fig. 6.6 Mass averaged P_t/P_{t0} in flow direction
with $A=0$ (leading edge) and $A=3$ (trailing edge)

—	43 x 22 grid
- - -	82 x 22 grid
- . -	82 x 42 grid
— — —	123 x 42 grid
X X X	theoretical

plots presented above would nearly be identical. However, the 2M formula does calculate a higher a_0 value, which provides a better approximation of the effective pressure (section 4.0). Figure 6.7 shows the increase of a_0 along the repeating boundary for the 82 x 22 grid.

To check the program convergence, the mass flowrate, pressure changes, and velocity changes are graphed with the number of iterations. The mass flowrate, m , and the variation of mass flowrate divided by the mass flowrate, dm/m , are plotted in Fig. 6.8. The mass flowrate remains steady after about 200 iterations for every case except for the 82 x 22 case, which took about 800 iterations to converge. It appears that the dm/m changes decrease over three orders of magnitude after 500 iterations. Figures 6.9 and 6.10 show the maximum and rms pressure changes and the maximum and rms velocity changes with iteration. Again, the property changes decrease over three orders of magnitude after 500 iterations; however, the 82 x 22 case appears to take longer. The 43 x 22 case converges most rapidly with about five orders of magnitude decrease in pressure and velocity changes.

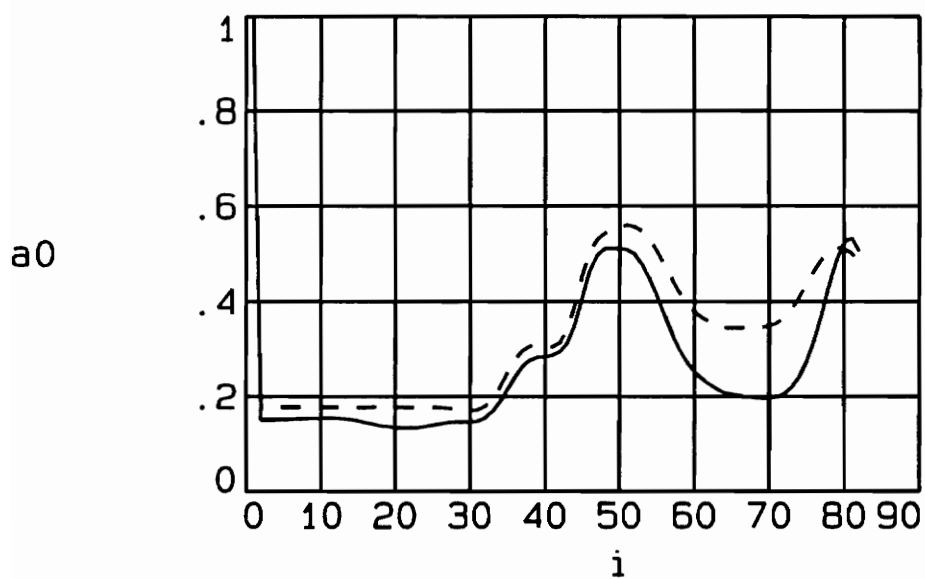


Fig. 6.7 Comparison of a_0 at the repeating boundary for 82 x 22 grid

- - - 2M formula
 _____ M&M formula

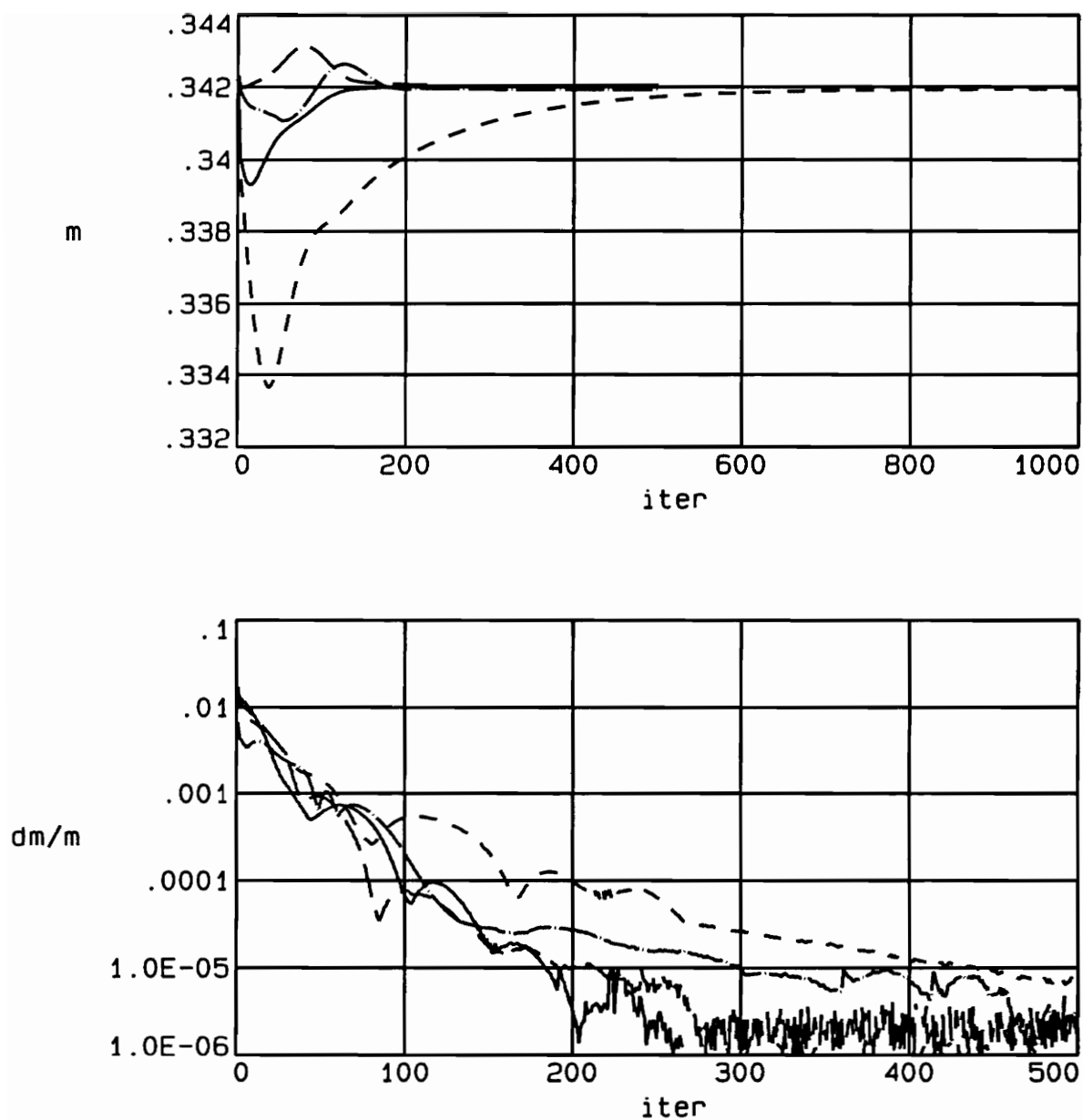


Fig. 6.8 Mass flowrate, m , and change in mass flowrate divided by the mass flowrate, dm/m , versus iteration number.

_____ 43 x 22 grid
 - - - - - 82 x 22 grid
 - - - - - 82 x 42 grid
 - . - . - 123 x 42 grid

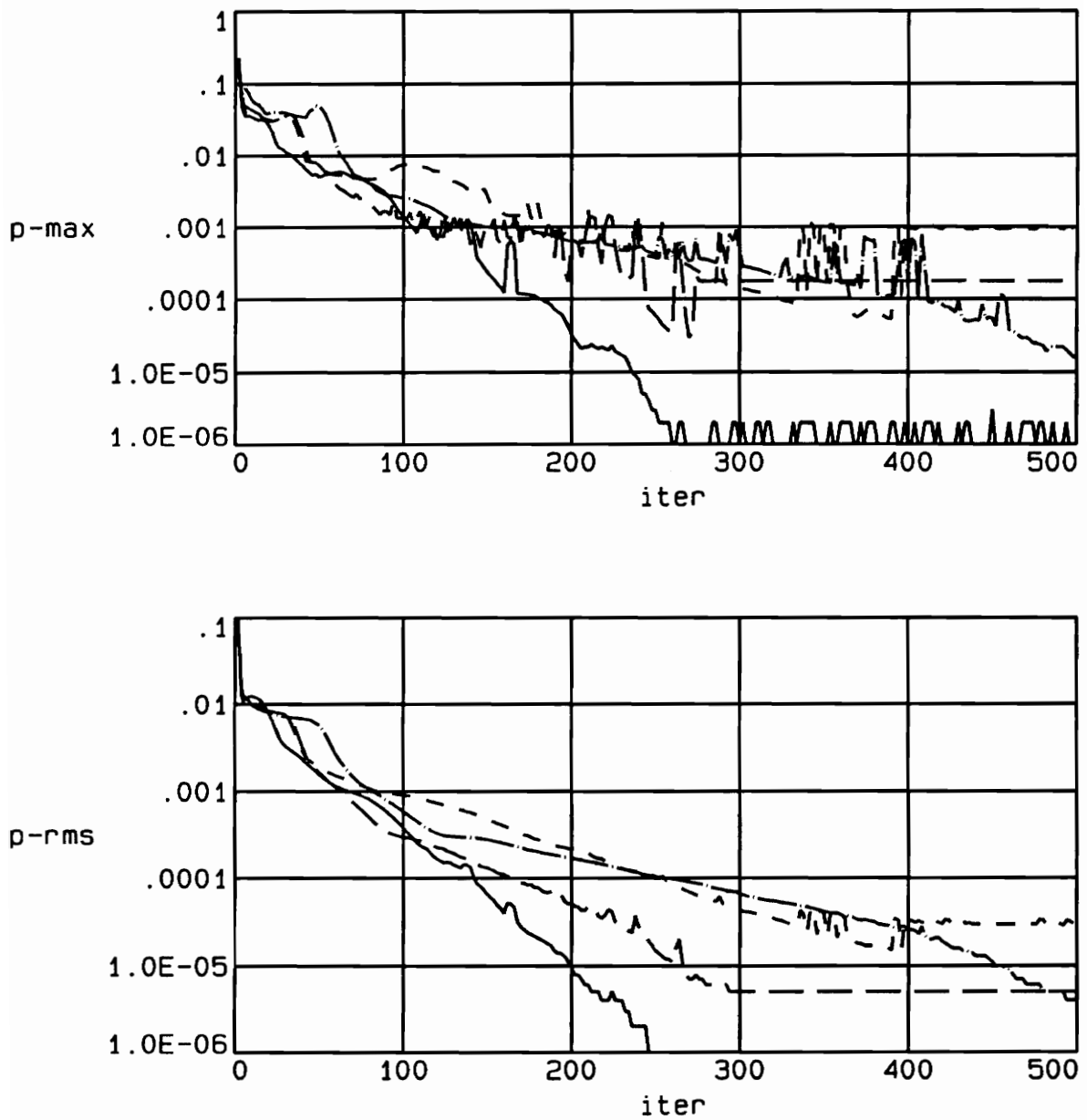


Fig. 6.9 Change in maximum and rms pressure versus iteration number.

————	43 x 22 grid
-----	82 x 22 grid
- . - . -	82 x 42 grid
.....	123 x 42 grid

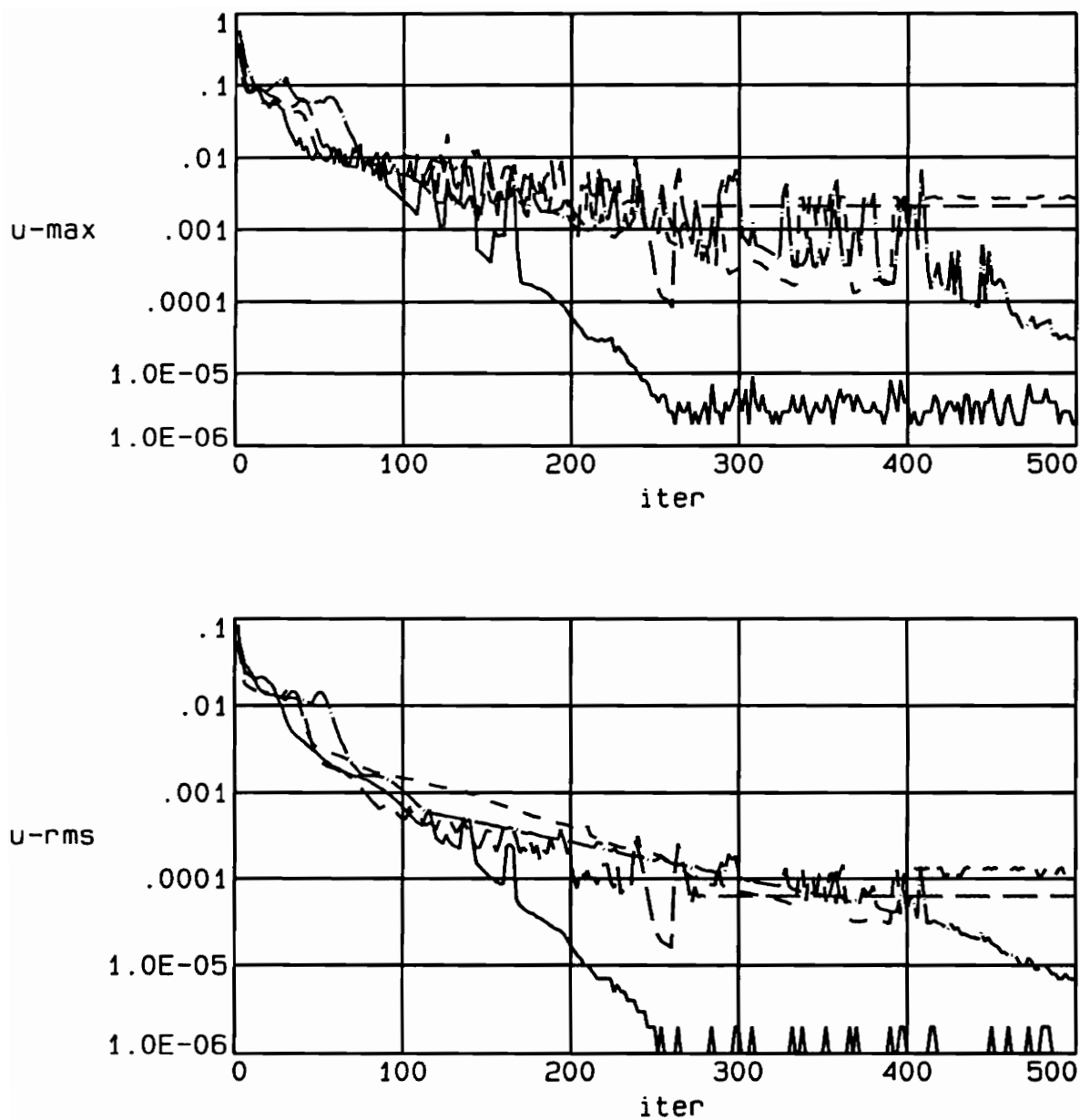


Fig. 6.10 Change in maximum and rms velocity versus iteration number.

————	43 x 22 grid
-----	82 x 22 grid
-----	82 x 42 grid
—.—.—	123 x 42 grid

7.0 L030-4 Transonic Compressor Blade

The full 3-D MEFP code, with the viscous momentum equation (section 2.1), is used for the L030-4 compressor blade test case. The L030-4 is a transonic compressor rotor blade section tested in a cascade wind tunnel at the DFVLR in Cologne, Germany [9]. The turbulent viscosity is evaluated with a one-equation turbulence model, $k^{1/2} - L$. Figure 7.1 shows the compressor blade with a 74×23 grid. The test case was run with an inlet Mach number of 1.1, an exit static pressure $P_2/P_{t0} = 0.68$, and an axial velocity density ratio of 1.18. These conditions gave choked flow with a nearly normal passage shock ending near the trailing edge on the suction surface. The L030-4 is a smooth profile with rounded leading and trailing edges, unlike the cascade of wedges which has sharp corners and cusped leading and trailing edges.

Figure 7.2 shows the calculated Mach number distribution for the 2M and M&M formulae. The darker contour lines are at Mach = 1.0. Although both of the Mach number figures look similar, the 2M formula gives a slightly higher maximum Mach number near the suction surface directly upstream of the passage shock than the M&M formula, 1.60 compared to 1.54. Thus, the 2M formula captures a sharper shock. Figure 7.3 is a comparison of errors in satisfying the perfect gas equation using both formulae. The 2M formula reduces these error regions, particularly at the leading edge and across the shock at the trailing edge.

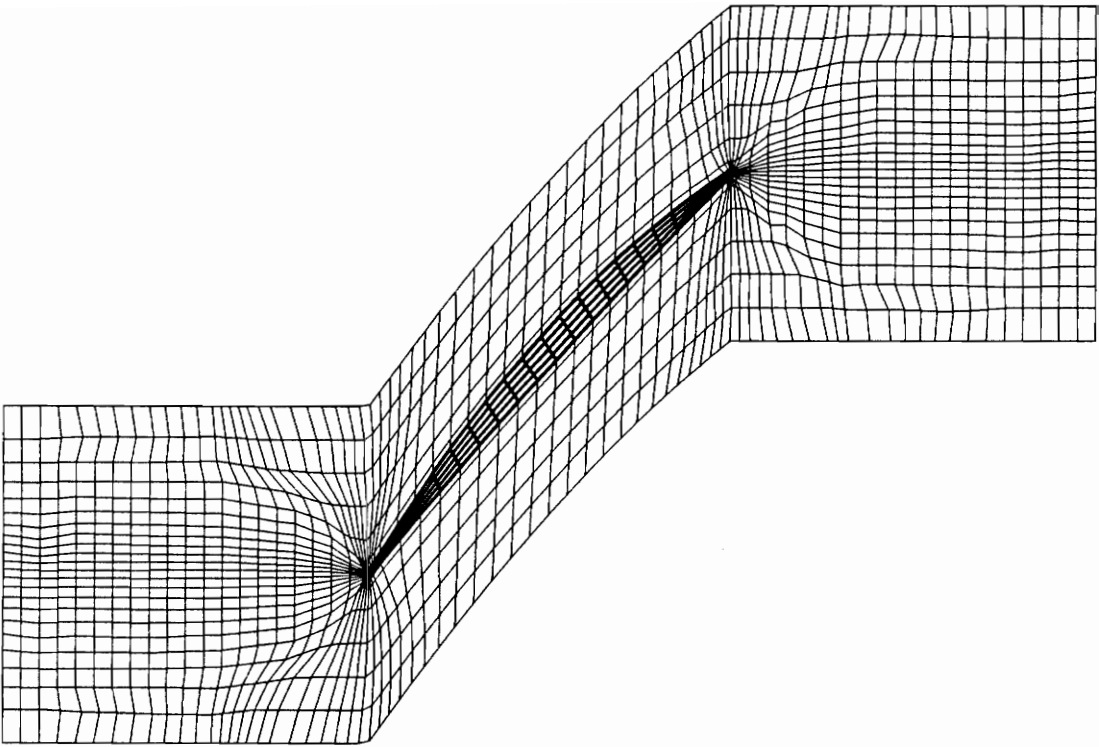
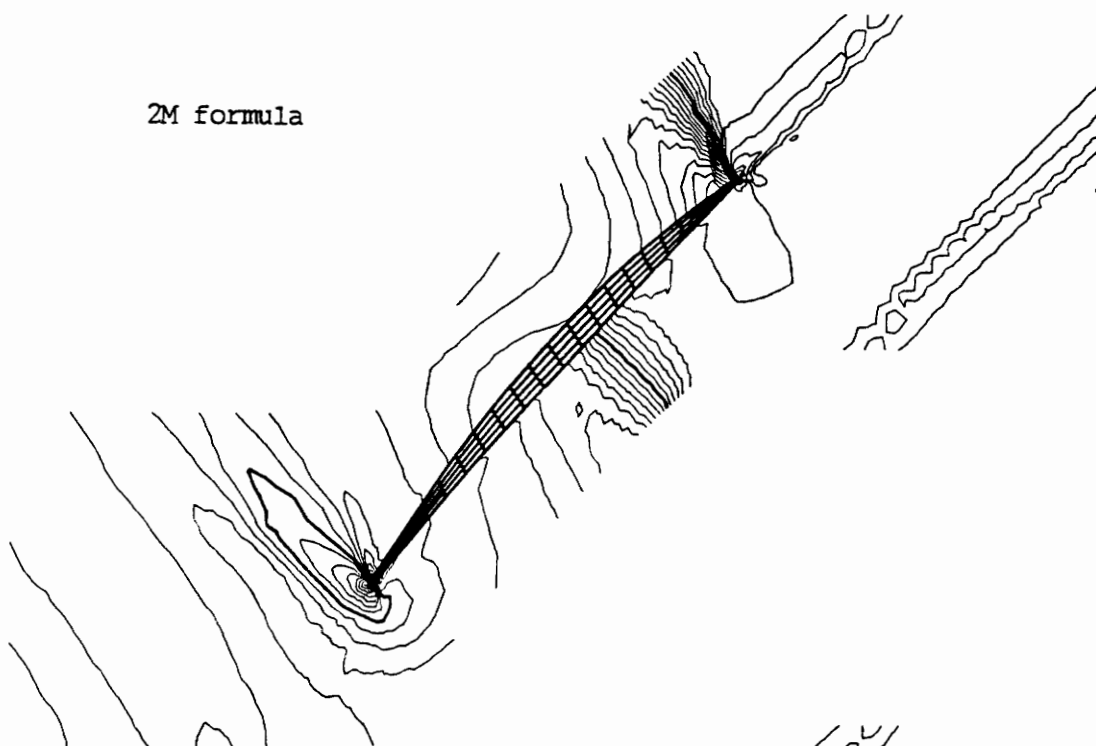


Fig. 7.1 74 x 23 grid for L030-4 compressor blade

2M formula



M&M formula

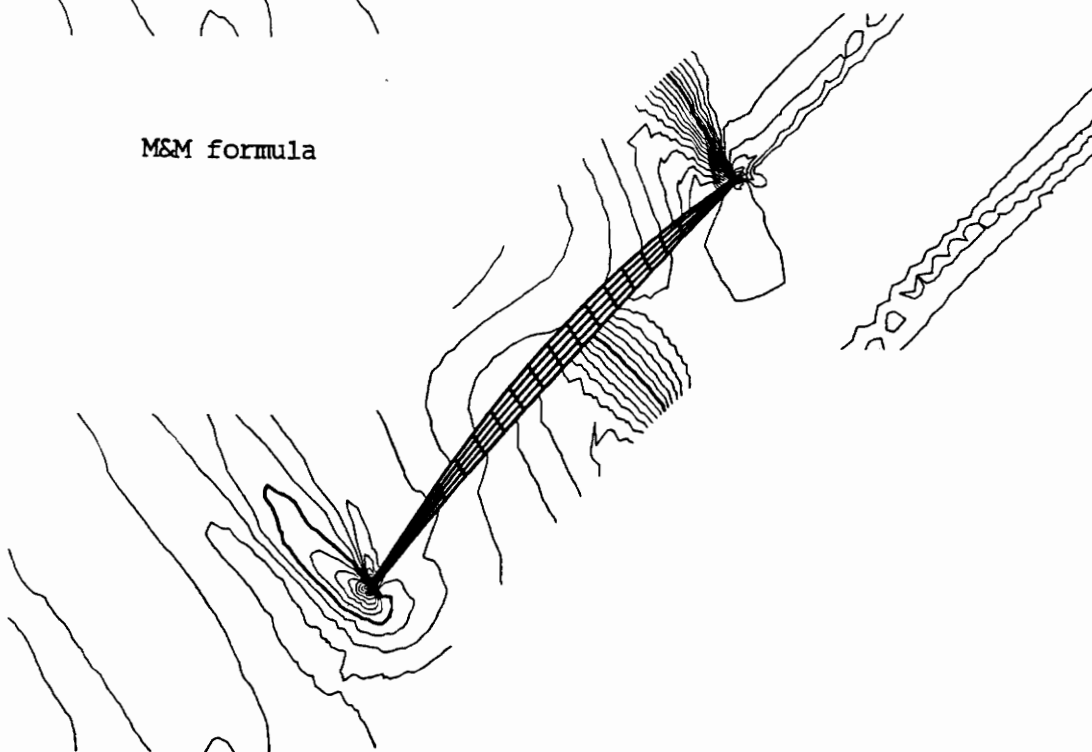


Fig. 7.2 Calculated Mach Number distribution for the 2M and M&M formulae; contour interval = 0.05, the darker contour lines are at Mach = 1.0

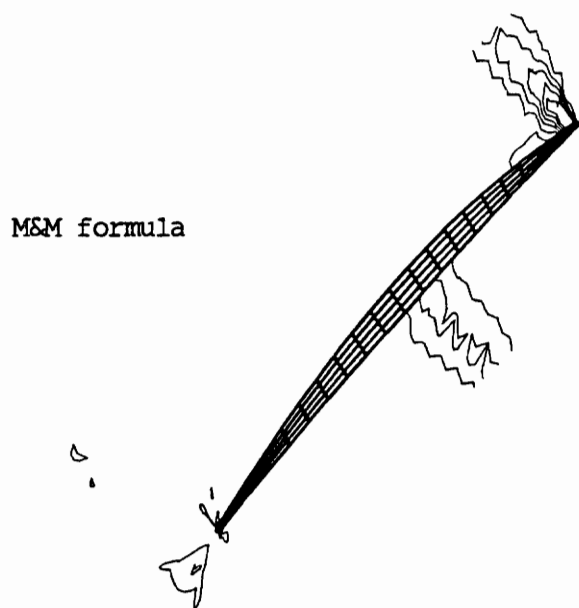
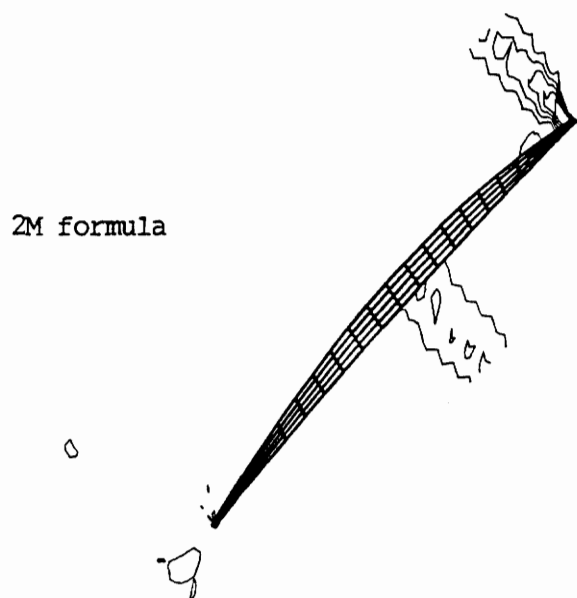


Fig. 7.3 Comparison of the errors in satisfying the perfect gas equation using the 2M and M&M formulae; contours of $P/\rho RT = 0.91$ to 1.09 by $.02$

8.0 Conclusions

In an attempt to improve the shock capturing capabilities of the MEFP pressure correction flow code, a new pressure interpolation method, the 2M formula, is developed. The 2M formula is a two Mach number dependent formula, with Mach numbers M_i and M_{i+1} , whereas the previously used pressure interpolation method, the M&M formula, is a one Mach number dependent formula, using the maximum of M_i and M_{i+1} . Section 4.0 shows the development of the 2M formula with a stability analysis for the effective pressure coefficients, a_0 and a_1 . A 1-D version of the MEFP code is written to help understand the basic numerical procedure and to allow simple testing of the new pressure interpolation formula. This 1-D code is described in Appendix D and summarized in section 3.0.

The 2M formula is compared with the M&M formula for three test cases:

- (1). a 1-D converging-diverging nozzle for several back pressures, giving normal shock strengths of 1.1, 1.267, 1.455, 1.578, 2.5, and 3.5.
- (2). a 2-D supersonic staggered cascade of wedges with oblique shocks with upstream Mach numbers of 1.6, 1.403 and 1.401.
- (3). an L030-4 compressor blade with a round leading edge.

For the nozzle test, the 2M formula appears to capture a sharper shock than the M&M method for weaker shock strengths of 1.0 to 2.0, but does not show any improvement for shocks strengths greater than 2.5. This is due to the M&M formula being second order accurate for all Mach numbers, while the 2M formula is only second order accurate up to a Mach number of 2.2. Both

methods capture the shock over 3 to 4 grid points, typically centered around the theoretical shock location. In addition, both methods calculate shock total pressure losses which match closely with the theoretical losses.

In the cascade of wedges test, four different grids were chosen: 43×22 , 82×22 , 82×42 , and 123×42 , in order to test the oblique shock capturing with grid refinement. Both formulae give similar shock capturing results. The 2M formula however, calculates a slightly higher a_0 value, which provides a better estimate of the effective pressure. The first shock losses are underestimated, but the second shock losses are close to the actual losses, at least for the finest grid. This might be due to the first shock being diagonal to the control volume whereas the second shock is more parallel to the blade-to-blade grid lines. In terms of the mass averaged total pressures, it appears that the 43×22 grid gives about 90% of the actual losses while the other cases calculate only 70 - 80% of the losses. As expected, the oblique shocks sharpened with grid refinement.

For the L030-4 compressor blade case, the errors in satisfying the perfect gas equation due to the pressure interpolation schemes are compared for the 2M and M&M formulae. The 2M formula reduces these errors, particularly at the leading edge and across the shock at the trailing edge. The 2M formula also gives a higher Mach number directly upstream of the shock than the M&M formula, 1.60 compared to 1.54.

Suggestions for further work

(1). The stability analysis can be further developed such that the two Mach number dependent formula is second order accurate for all Mach numbers.

This reanalysis should always capture sharper shocks than the M&M formula, thus further improving the shock capturing capabilities of the MEFP flow code for all shocks.

(2). The method of characteristics can be used to help gain a better understanding of the downstream flow field for the cascade of wedges test.

Appendix A. Denton's other pressure-density schemes [4]

Scheme A

Denton sends the density change to the downstream node, as described in section 2.2, and the pressure is then calculated from the ideal gas equation. A correction factor is used to correct the downwind pressure to a value closer to the true pressure, $P_{A,i}$.

$$P_i = P_{i+1} + CFP_i$$

Now, the pressure correction factor, CFP_i , is approximated as

$$CFP_{i,new} = (1-RF)CFP_{i,old} + (RF)CFP_{i,int.}$$

The relaxation factor, RF , has a typical value of 0.05.

Scheme B

In scheme B, Denton sends the density change to the upstream node because it was noticed that at low Mach numbers, the pressure is closely related to the density. The density change and pressure are now

$$\delta \rho_i = m_{e,i} \delta t / \delta V$$

$$\text{and } P_i = \rho_i R T_i$$

The pressure can be calculated directly from the density without any correction factors. Scheme B is stable for subsonic flows and even reverse flows.

Scheme C

The advantages of schemes A and B were combined such that the density change is sent to the downstream node and a density correction factor is used.

$$\delta\rho_{i+1} = m_{e,i}\delta t/\delta V$$

and

$$P_i = (\rho_{i+1} + CFRO_i)RT_i$$

Again, the density correction factor, $CFRO_i$, is similar to the pressure correction factor

$$CFRO_{i,new} = (1-RF)CFRO_{i,old} + (RF)CFRO_{i,int}.$$

Scheme C is stable for all Mach numbers and has good shock capturing properties; however, it does not permit reversed flow.

A single scheme which would be stable for all Mach numbers and permit reversed flow was desired. After several unsuccessful attempts, Denton developed a linear combination of schemes B and C. The density change is distributed between the upstream and downstream nodes such that

$$\delta\rho_i = \alpha\delta\rho$$

$$\text{and } \delta\rho_{i+1} = (1-\alpha)\delta\rho$$

For Mach numbers less than one, $\alpha = 1$, and for Mach numbers greater than or equal to one, $\alpha = 0$. This distribution of α gave good shock capturing characteristics in 1-D. However, problems occurred in 2-D because of the discontinuity at $M = 1$.

A better approximation for α was found using a linear variation of the Mach number.

$$\alpha = 0.5[1 + (T - T^*)/(T_0 - T^*)]$$

This distribution of alpha allows stability for all Mach numbers and with reverse flow. The pressure is now calculated using the pressures, from schemes B and C, weighted with respect to α .

$$P_i = [\alpha p_i + (1 - \alpha)(p_{i+1} + CFRO_i)]RT_i$$

The solution procedure from this scheme produces overshoots and undershoots across the shock due to a lack in numerical damping.

Appendix B. Truncation Error of Pressure Interpolation Equation [3]

The truncation error of the interpolated pressure used to calculate the density in equation 12 (section 2.2) may be determined using Taylor series analysis. The interpolated effective pressure is given by

$$P_{\text{eff},i+1} = P_i + a_0(P_{i+1} - P_i) + a_1(P_{i+1} - P_{i-1})/2 + a_2(P_{i+1} - P_{i-2})/3$$

where a_0, a_1 , and a_2 are coefficients. To determine the accuracy of the effective pressure, consider the magnitude of $P_{\text{eff},i+1} - P_{i+1}$. With grid spacing h , and expanding about $i+1$,

$$P_{i-2} = P - 3hP' + 9(h^2/2)P'' - O(h^3)$$

$$P_{i-1} = P - 2hP' + 4(h^2/2)P'' - O(h^3)$$

$$P_i = P - hP' + (h^2/2)P'' - O(h^3)$$

$$P_{i+1} = P$$

Therefore,

$$P_{\text{eff},i+1} - P_{i+1} = h(a_0 + a_1 + a_2 - 1)p' - (h^2/2)(a_0 + 2a_1 + 3a_2 - 1)p'' + O(h^3)$$

And if $a_0 + a_1 + a_2 = 1$,

then the difference between P_{eff} and P is of the order of h^2 , so that P_{eff} is a second order accurate approximation for P .

Appendix C. Moore and Moore Pressure Interpolation Schemes [3]

From section 2.2, an effective pressure at $i+1$ was found using Mach number dependent interpolation equations. The density at $i+1$ is then calculated using the effective pressure. Again, the equations are

$$P_{\text{eff},i+1} = P_i + a_0(P_{i+1} - P_i) + a_1(P_{i+1} - P_{i-1})/2 + a_2(P_{i+1} - P_{i-2})/3$$

and $\rho_{i+1} = P_{\text{eff},i+1}/RT_{i+1}$

where a_0, a_1 , and a_2 are coefficients. Three other interpolation methods are possible with these limitations set on the coefficients.

1. If $a_0 = a_1 = a_2 = 0$, an upwind effective pressure interpolation is obtained such that $P_{\text{eff},i+1} = P_i$.
2. If $a_0 = a_1 = 0$ and $a_2 = 1$, a 3-point pressure interpolation procedure occurs where $P_{\text{eff},i+1} = P_i + a_2(P_{i+1} - P_{i-2})/3$.
3. If $a_0 = 1$ and $a_1 = a_2 = 0$, the ideal gas equation occurs, $P_{\text{eff},i+1} = P_{i+1}$.

Appendix D. 1-D version of MEFP

Appendix D gives a full description of the 1-D version of MEFP. A summary of this code is outlined in section 3.0.

1.1 Background

This program was written in order to capture a shock in a 1-D converging-diverging nozzle and analyze the effects of Mach number and pressure losses across the shock. The solution method used in this program is similar to the MEFP transonic calculation procedure, such that discretized forms of the momentum and continuity equations are satisfied. These equations make use of an effective density at a point, calculated from the perfect gas equation with an interpolated static pressure. A pressure interpolation method is used to determine an effective pressure. The Mach number, static and total pressures are calculated across the shock for a fixed inlet stagnation pressure and an exit pressure. Exit pressure ratios, P_{exit}/P_0 , of 0.75, 0.80, and 0.85 were used for comparison. A constant total temperature was assumed for the calculations.

In order to make the equations in the program dimensionless, the following variables were defined as shown below.

$$P = P/P_0$$

$$T = T/T_0$$

$$\rho = \rho/\rho_0$$

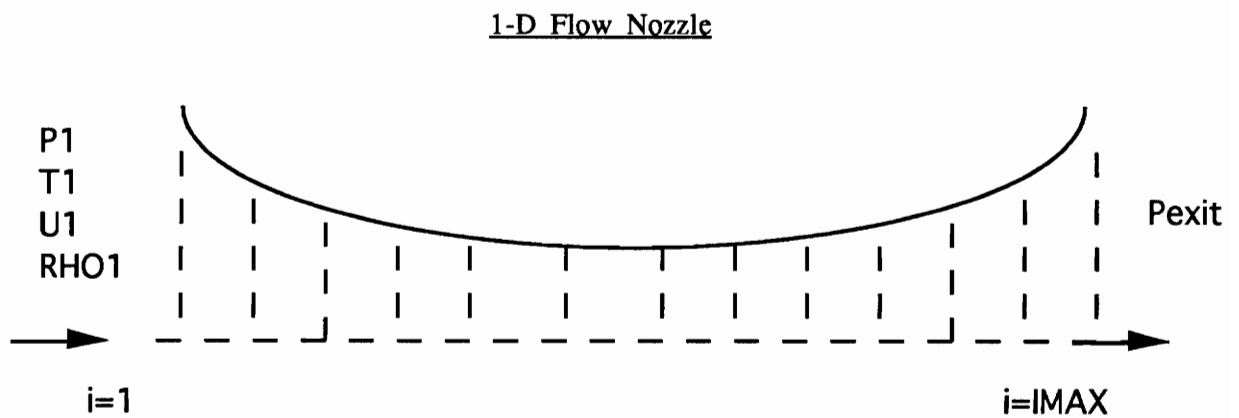
$$\gamma = 1.4$$

$$R = 1.0$$

$$C_p = 3.5$$

1.2 Initialization of Flow Variables

The Mach number, area, pressure, temperature, velocity, and density are initialized in subroutine initial. An inlet Mach number of 0.8 and exit Mach number of 1.8 was used. A change in Mach number, DM, of 0.025 was chosen to obtain 40 grid steps across the converging-diverging nozzle. The areas are determined from an isentropic relation to the Mach number.



For $i= 1, IMAX$

$$M_i = M_1 + (i-1)DM$$

$$A_i = (1/M_i) \left[\left(1 + \frac{(\gamma - 1)}{2} M_i^2 \right) / \left(\frac{\gamma + 1}{2} \right) \right]^{(\gamma + 1) / 2(\gamma - 1)}$$

The initial pressure, temperature, and velocity at the nozzle's inlet and exit are calculated from isentropic relations.

$$P_1 = \left[1 + \frac{(\gamma - 1)}{2} M_i^2 \right]^{-\gamma / (\gamma - 1)}$$

$$T_1 = P_1^{[(\gamma - 1) / \gamma]}$$

$$U_1 = [2C_p(1 - T_1)]^{0.5}$$

$$P_{IMAX} = P_{exit}$$

$$T_{IMAX} = P_{IMAX}^{[(\gamma - 1) / \gamma]}$$

$$U_{IMAX} = [2C_p(1 - T_{IMAX})]^{0.5}$$

A linear relationship is used to initialize pressure and velocity along the nozzle. The density is calculated from the perfect gas equation.

For $i = 1, \text{IMAX}$

$$P_i = P_1 + [P_{\text{IMAX}} - P_1][(I-1)/(\text{IMAX}-1)]$$

$$U_i = U_1 + [U_{\text{IMAX}} - U_1][(I-1)/(\text{IMAX}-1)]$$

$$T_i = 1 - U_i^2/2C_p$$

$$M_i = [5(1/T_i - 1)]^{0.5}$$

$$\rho_i = P_i/T_i$$

1.3 Velocity Updated from Continuity

The mass flowrate is calculated at the nozzle inlet. The velocity is then updated from this flowrate in subroutine fixcont.

$$m = \rho_1 U_1 A_1$$

$$U_i = m/[\rho_i A_i] \quad \text{For } i = 2, \text{IMAX}$$

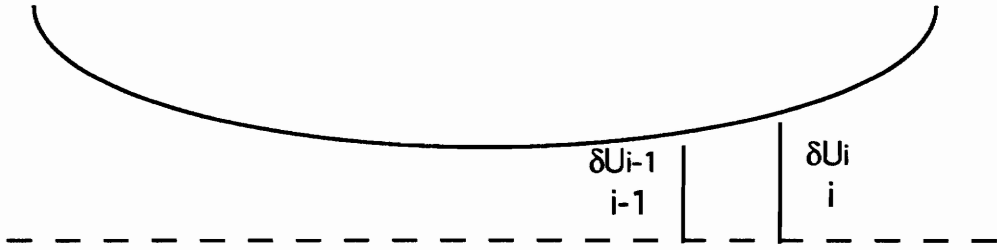
1.4 Momentum Equation

The one dimensional form of the momentum equation, $\rho U [\delta U / \delta x] = -\delta P / \delta x$, is discretized to the form,

$$0.5[\rho_i U_i + \rho_{i-1} U_{i-1}][\delta U_i - \delta U_{i-1}] = -P_i + P_{i-1} - 0.5[\rho_i U_i + \rho_{i-1} U_{i-1}][U_i - U_{i-1}].$$

This discretized equation can be written as $AM_i \delta U_i + AU_i \delta U_{i-1} = BMOM_i$. It is assumed that $\delta U_{i-1} = 0$, so that $\delta U_i = BMOM_i / AM_i$. The change in velocity, δU_i , is used to update velocity, which is described in section 1.7 of this appendix .

Momentum



$$AM(1) = \rho_1 U_1$$

Then subroutine inlet is called to update the inlet velocity.

For $i = 2, IMAX$

$$RU = 0.5[\rho_i U_i + \rho_{i-1} U_{i-1}]$$

$$AM_i = RU$$

$$AU_i = -RU$$

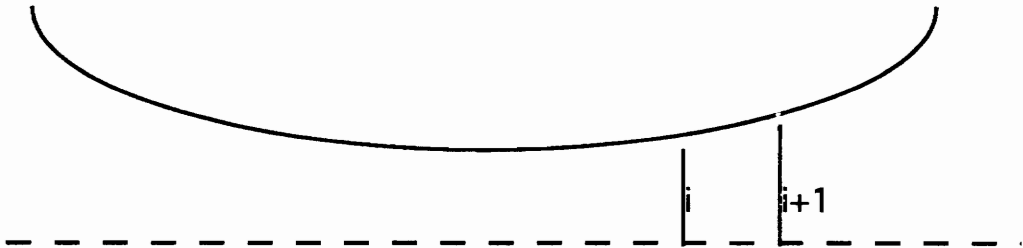
$$BMOM_i = -P_i + P_{i-1} - RU[U_i - U_{i-1}]$$

1.5 Pressure Correction Equations

The left hand side of the discretized continuity equation

$APU_i \delta P_{i-1} + APM_i \delta P_i + APD_i \delta P_{i+1} = BCONT_i$ is calculated in subroutine lhscont.

Continuity



The pressure correction equations are formed by substituting $\delta U_i = (\delta P_{i-1} - \delta P_i)/AM_i$ and $\delta \rho_i = \delta P_{i-1}/RT_i$ in the continuity equation $[\rho_{i+1}\delta U_{i+1} + U_{i+1}\delta \rho_{i+1}]A_{i+1} - [\rho_i\delta U_i + U_i\delta \rho_i]A_i = -\rho_{i+1}U_{i+1}A_{i+1} + \rho_iU_iA_i$.

For $i = 1, \text{IMAX}-1$

$$CDUI = \rho_i A_i / AM_i$$

$$CDUID = \rho_{i+1} A_{i+1} / AM_{i+1}$$

$$CDRI = U_i A_i / T_i$$

$$CDRID = U_{i+1} A_{i+1} / T_{i+1}$$

$$APU_i = -CDUI - CDRI$$

$$APM_i = CDUI + CDUID + CDRID$$

$$APD_i = -CDUID$$

At $i=1$, $\delta U_1 = -\delta P_1/AM_1$ and $\delta \rho_1 = \delta P_1/RT_1$ since there is not an upstream point; therefore, APU , APM , and APD at the nozzle inlet are defined as:

$$APU(1) = 0.0$$

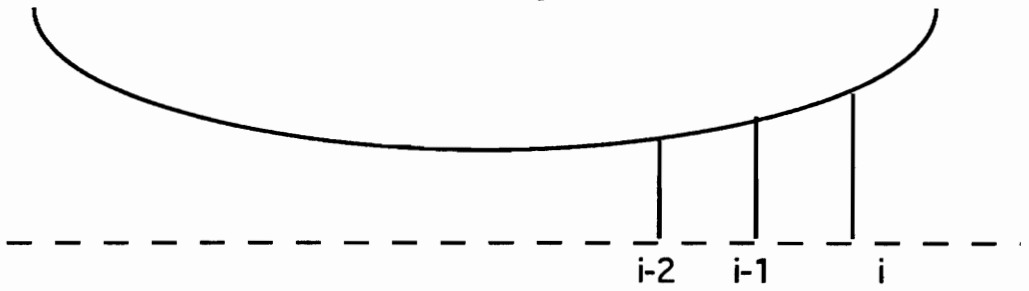
$$APM(1) = CDUI + CDUID + CDRID - CDRI$$

$$APD(1) = -CDUID$$

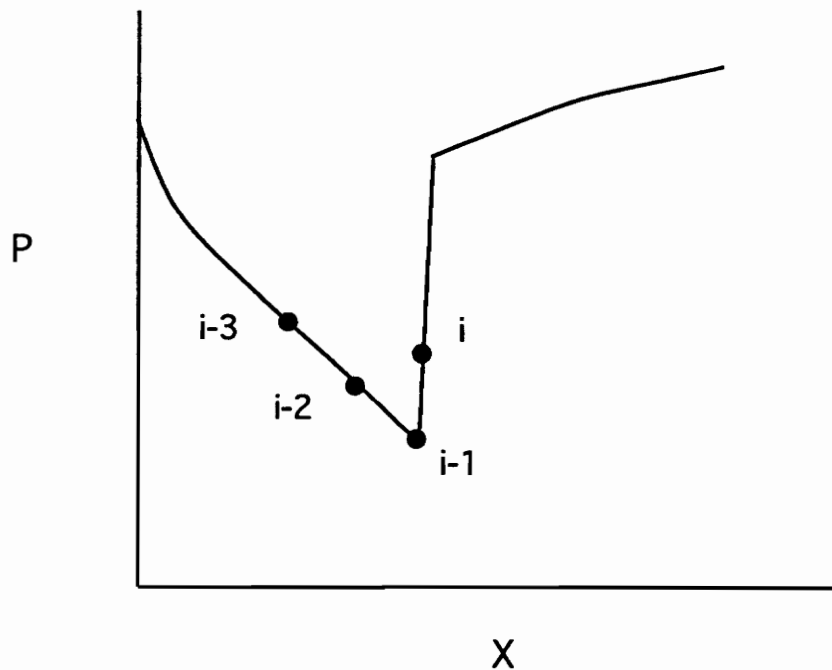
1.6 Update Density using Interpolated Pressure

The density is updated from the perfect gas equation using an interpolated pressure in subroutine gasrho.

Pressure Interpolation



The effective pressure is calculated using AZ , $A1$, and $A2$ in the form $P_{eff_i} = P_{i-1} + AZ_i[P_i - P_{i-1}] + A1_i[P_i - P_{i-2}]/2 + A2_i[P_i - P_{i-3}]/3$. However, the coefficients $A1$ and $A2$ are only used if the pressure difference associated with each coefficient is a positive contribution to evaluating P_i from P_{i-1} . For example, if $[P_i - P_{i-1}]$ is positive and $[P_i - P_{i-3}]$ is negative as shown in the figure below, the coefficient $A2$ would not be used.



Using the **M&M formula**, the coefficient **AZ** is calculated from the maximum Mach number of the point evaluated, M_i , and one point upstream, M_{i-1} .

For $i = 1, \text{IMAX}$

$$T_i = 1 - U_i^2/2C_p$$

$$M_i = [5(1/T_i - 1)]^{0.5}$$

$$\text{AMMAX} = M_i$$

$$\text{IF } (\text{AMMAX} < M_{i-1}) \text{ AMMAX} = M_{i-1}$$

$$\text{AZ}_i = 0$$

$$\text{A1}_i = 4/\text{AMMAX}^2$$

IF ($\text{AMMAX} < 2.0$) **THEN**

$$\text{AZ}_i = (0.8/3)[4/\text{AMMAX}^2 - 1]$$

IF ($\text{AZ}_i > 1$) $\text{AZ}_i = 1$

$$\text{A1}_i = 1 - \text{AZ}_i$$

The **2M formula** is an alternative method to solve for the effective pressure coefficients. The numbers next to the **AZ** and **A1** coefficients below are equation numbers used from section 3.0.

For $i = 1, \text{IMAX}$

$$T_i = 1 - U_i^2/2C_p$$

$$M_i = [5(1/T_i - 1)]^{0.5}$$

$$\text{AZ}(1) = 1.$$

$$\text{A1}(1) = 1.$$

For $i = 1, \text{IMAX}$

$$g = 1.4$$

add = 0.075

$M_i = M_i + \text{add}$

$M_p = M(\text{MIN0}(i+1, \text{IMAX})) + \text{add}$

$A = gM_p + 1/M_p + 1/M_i - gM_i$

$B = .5gM_p + 2/M_p + 1/M_i - gM_i$

If $A > 0$

$AZ_{22i+1} = 1 + 1/(gM_p^2) + 1/(gM_pM_i) - M_i/M_p$

$A1_{i+1} = 1$

If $B > 0$

$AZ_{29i+1} = 4/(3gM_p^2) + 2/(3gM_pM_i) - 2M_i/(3M_p) + 1/3$

$AZ_{i+1} = \text{AMIN1}(AZ_{22i+1}, AZ_{29i+1})$

$A1_{i+1} = 1.$

ENDIF

IF $B \leq 0$

$AZ_{i+1} = 0.$

$A130_{i+1} = 2 + 4/(gM_p^2) + 2/(gM_pM_i) - 2M_i/M_p$

$A1_{i+1} = a130_{i+1}$

ENDIF

ENDIF

If $A \leq 0$

$AZ_i = 0$

$AZ_{i+1} = 0$

$A123_i = (gM_p + 1/M_p + 1/M_i)/(gM_i)$

$A133_{i+1} = (gM_p + 2/M_p + 1/M_i)/(gM_i + 0.5gM_p)$

$A135_i = (gM_p + 2/M_p + 1/M_i)/(gM_i + 0.5gM_p)$

$A1_i = \text{AMIN1}(A123_i, A135_i, A1_i)$

$A1_{i+1} = A133_{i+1}$

ENDIF

If $AZ_i > 1$ $AZ_i = 1$

If $AZ_i > 0$ $A1_i = 1 - AZ_i$

For both formulae, the M&M and 2M, the variable C1 is calculated to determined if the coefficient A1 is to be used. The variable C2 is calculated only for the M&M formula to determine if the coefficient A2 is to be used. The coefficient A1 is used only if C1 is positive and A2 is used only if C2 is positive. The equations below are used for the M&M formula and are applicable to the 2M formula with A2 = 0.

For i = 2, IMAX

$$Pe_{ff_i} = P_{i-1} + AZ_i[P_i - P_{i-1}]$$

$$\text{IF } i > 2 \quad C1 = [P_i - P_{i-1}][P_i - P_{i-2}]$$

$$\text{IF } C1 > 0.0 \quad Pe_{ff_i} = Pe_{ff_i} + A1_i[P_i - P_{i-2}]/2$$

$$A2_i = 1 - AZ_i - A1_i$$

ELSE

$$A2_i = 1 - AZ_i$$

ENDIF

$$\text{IF } i > 3 \quad C2 = [P_i - P_{i-1}][P_i - P_{i-3}]$$

$$\text{IF } C2 > 0.0 \quad Pe_{ff_i} = Pe_{ff_i} + A2_i[P_i - P_{i-3}]/3.$$

The effective pressure is bounded by P_i and P_{i-1} .

$$Pe_{ff_i} = \text{AMAX1}(Pe_{ff_i}, \text{AMIN1}(P_i, P_{i-1}))$$

$$Pe_{ff_i} = \text{AMIN1}(Pe_{ff_i}, \text{AMAX1}(P_i, P_{i-1}))$$

$$\rho_i = Pe_{ff_i}/T_i$$

1.7 Update Velocity using Momentum

In subroutine unew, the velocity is updated such that $U_i = U_i + \delta U_i$. The momentum equations are solved assuming $\delta U_{i-1} = 0$.

$$U_i = U_i + BMOM_i / AM_i$$

For i = 2, IMAX

1.8 Calculating Continuity Errors

The right hand side of the discretized pressure correction equation (continuity) is calculated in subroutine rhscont.

$$BCONT_i = -\rho_{i+1}U_{i+1}A_{i+1} + \rho_i U_i A_i \quad \text{For } i = 1, IMAX-1$$

1.9 Solve for Pressure Corrections

In subroutine solvepc, a corrected pressure is calculated using a tri-diagonal matrix algorithm.

For $i = 1, IMAX-1$

$$APM_i = APM_i - APU_i APD_{i-1}$$

$$APD_i = APD_i / APM_i$$

$$BCONT_i = [BCONT_i - APU_i BCONT_{i-1}] / APM_i$$

$$PC_{IMAX} = 0$$

For $II = 1, IMAX-1$

$$PC_i = BCONT_i - APD_i PC_{i+1} \quad \text{where } i = IMAX - II$$

1.10 Update Density, Velocity, and Pressure from Corrected Pressure

The density is updated using the corrected pressure in subroutine rhopc.

$$\rho_1 = \rho_1 + PC_1 / T_1$$

$$\rho_i = \rho_i + PC_{i-1} / T_i \quad \text{For } i = 2, IMAX$$

The velocity is updated using the corrected pressure in subroutine upc.

$$U_i = U_i + (PC_{i-1} - PC_i) / AM_i \quad \text{For } i = 1, IMAX$$

The pressure is updated using the corrected pressure in subroutine addpcp.

$$P_i = P_i + PC_i \quad \text{For } i = 1, \text{IMAX}$$

1.11 Recalculate Mass Flowrate and Velocity

The inlet velocity is recalculated using the new inlet static pressure, and a total pressure, $P_t = 1$, in subroutine inlet.

$$U_1 = [(1 - P_1^{(\gamma-1)/\gamma})2C_p]^{0.5}$$

The mass flowrate is recalculated at the nozzle inlet using the new inlet velocity, U_1 . The velocity is then updated from this flowrate in subroutine fixcont.

$$m = \rho_1 U_1 A_1$$

$$U_i = m / [\rho_i A_i] \quad \text{For } i = 2, \text{IMAX}$$

1.12 Average Values for Convergence

At the end of every other iteration, the current density, velocity, and pressure are averaged with values from the previous iteration and then used for the next iteration. This procedure is in subroutine average and helps the program converge.

$$\rho_i = 0.5[\rho_i + \rho_{OLD_i}] \quad \text{For } i = 1, \text{IMAX}$$

$$U_i = 0.5[U_i + U_{OLD_i}]$$

$$P_i = 0.5[P_i + P_{OLD_i}]$$

REFERENCES

1. Wendt, J.F., Computational Fluid Dynamics, Springer-Verlag, 1992.
2. Moore, J., Moore, J.G., "Shock Capturing and Loss Prediction for Transonic Turbine Blades Using a Pressure Correction Method," IX International Symposium on Air Breathing Engines, Athens, Greece, September 1989.
3. Moore, J., and Moore, J.G., "Shock Capturing Using Pressure Interpolation," Turbomachinery Research Group Report No. JM/86-1, Mechanical Engineering Department, Virginia Polytechnic Institute and State University, 1986.
4. Denton, J.D., "An Improved Time Marching Method for Turbomachinery Flow Calculation," ASME Paper 82-GT-239.
5. Moore, J.G., "Pressure Correction Calculation Procedures for 3-D Viscous Flow," ASME Short Course on 3-D Flows in Turbomachinery Blade Rows, Orlando, FL, June 1991.
6. Denton, J.D., "A Method of Calculating Fully Three Dimensional Inviscid Flow Through Any Type of Turbomachinery Blade Row," ASME Short Course on 3-D Flows in Turbomachinery Blade Rows, Phoenix, AZ, March 1983.
7. Moore, J., Moore, J.G., and Nicholson, S., "Thermodynamic Evaluation of Transonic Compressor Rotors Using the Finite Volume Approach," Turbomachinery Research Group Report No. JM/87-4, Mechanical Engineering Department, Virginia Polytechnic Institute and State University, 1987.
8. Denton, J.D., Hirsch, Ch., and Meauze, G., "Analytical Test Cases for Cascades," Test Cases for Computation of Internal Flows in Aero Engine Components, Working Group 18, AGARD Advisory Report No. 275, AGARD 1990.
9. Schreiber, H.A., Starken, H., "Experimental Cascade Analysis of a Transonic Compressor Rotor Blade Section," ASME Paper 83-GT-209.

Vita

The author was born on July 1st, 1970 in Yonkers, New York, but spent most of his life in Greenville, South Carolina. In August 1988, he graduated from Mauldin High School, where he was active in the National Honor Society and played on the tennis team. He enrolled at Clemson University in August 1988 and obtained a Bachelor of Science degree in Mechanical Engineering in December 1992. During his undergraduate studies, he completed one year of cooperative education (co-op) experience with Dow Chemical. In January 1993, he entered Virginia Polytechnic Institute and State University, where he obtained a Master of Science degree in Mechanical Engineering in December 1993. The title of his master's thesis was "Development of a New Shock Capturing Formula for Pressure Correction Methods" with Dr. John Moore as his advisor. The author is a member of ASME, NSPE, Tau Beta Pi, Golden Key National Honor Society, and is registered as an Engineer-In-Training in South Carolina.

Gjay Kumar Gupta